2009

Micro-Fabricated Hydrogen Sensors Operating at Elevated Temperatures

Chi Lu
University of Kentucky, clu2@uky.edu

Abstract of Dissertation

Chi Lu

The Graduate School

University of Kentucky

2009

Micro-Fabricated Hydrogen Sensors Operating at Elevated Temperatures

---

Abstract of Dissertation

A dissertation presented to the Faculty of the Graduate School of the University of Kentucky in Partial Fulfillment of the Requirements for the Degree of Doctor of Philosophy in the College of Engineering at the University of Kentucky.

By

Chi Lu

Lexington, KY

Director: Zhi Chen, Professor of Electrical and Computer Engineering
Lexington, Kentucky
2009

Abstract of Dissertation

Micro-Fabricated Hydrogen Sensors Operating at Elevated Temperatures

In this dissertation, three types of microfabricated solid-state sensors had been designed and developed on silicon wafers, aiming to detect hydrogen gas at elevated temperatures. Based on the material properties and sensing mechanisms, they were operated at 140°C, 500°C, and 300°C. The MOS-capacitor device working at 140°C utilized nickel instead of the widely-used expensive palladium, and the performance remained excellent. For very-high temperature sensing (500°C), the conductivity of the thermally oxidized TiO_2 thin film based on the anodic aluminum oxide (AAO) substrate changed 25 times in response to 5 ppm H_2 and the response transient times were just a few seconds. For medium-high temperatures (~300°C), very high sensitivity (over 100 times' increment of current for H_2 concentration at 10 ppm) was obtained through the reversible reduction of the Schottky barrier height between the Pt electrodes and the SnO_2 nano-clusters. Fabrication approaches of these devices included standard silicon wafer processing, thin film deposition, and photolithography. Materials characterization methods, such as scanning electron microscopy (SEM), atomic force microscopy (AFM), surface profilometry, ellipsometry, and X-ray diffractometry (XRD), were involved in order to investigate the fabricated nano-sized structures. Selectivities of the sensors to gases other than H_2 (CO and CH_4) were also studied. The first chapter reviews and evaluates the detection methodologies and sensing materials in the current research area of H_2 sensors and the devices presented this Ph.D. research were designed with regard to the evaluations.

Keywords: hydrogen sensor, elevated temperature, silicon wafer, thin film, micro-fabrication.

Chi Lu
October 27, 2009

Micro-Fabricated Hydrogen Sensors Operating at Elevated Temperatures

By

Chi Lu

Zhi Chen, Ph.D.
Director of Dissertation

Stephen Gedney, Ph.D.
Director of Graduate Studies

October 27, 2009
Date

Rules for use of Dissertations

Unpublished dissertations submitted for the Doctor's degree and deposited in the University of Kentucky Library are as a rule open for inspection, but are to be used only with due regard to the rights of the authors. Bibliographical references may be noted, but quotations or summaries of parts may be published only with the permission of the author, and with the usual scholarly acknowledgements.

Extensive copying or publication of the dissertation in whole or in part also requires the consent of the Dean of Graduate School of the University of Kentucky.

Dissertation

Chi Lu

The Graduate School

University of Kentucky

2009

Micro-Fabricated Hydrogen Sensors Operating at Elevated Temperatures

---

Dissertation

A dissertation presented to the Faculty of the Graduate School of the University of Kentucky in Partial Fulfillment of the Requirements for the Degree of Doctor of Philosophy in the College of Engineering at the University of Kentucky.

By

Chi Lu

Lexington, KY

Director: Zhi Chen, Professor of Electrical and Computer Engineering
Lexington, Kentucky
2009

Acknowledgments

This Ph.D. research was supported by the Department of Energy (DE-FG02-00ER4582 and DE-FG26-04NT42171), National Science Foundation (ECS-0609064 and EPSCOR0447479), and Army Research Laboratory (W911NF-04-2-0023).

The author appreciates Dr. Zhi Chen's guidance through all the research.

The author is very grateful to Dr. J. Todd Hastings, Dr. Vijay P. Singh, and Dr. Fuqian Yang for frequently answering questions from the author for his Ph.D. research.

The author remembers the training and help from the late Mr. George Spiggle forever.

The author would like to thank Mr. Zhifang Fan for his help in photolithography; Ms. Jing Guo for her help in the ellipsometry measurement; Mr. Vijaysree Karre for her help in using the profiler; Mr. Bing Hu, Ms. Jingyuan Yao, Mr. Brian Wajdyk, and Dr. Xinghua Sun for their help in the AFM; Dr. Young-Sik Song and Mr. Jun Fang for their help in the SEM; Dr. Ye Sun, Mr. Wenzhong Li, and Ms. Lei Wang for their help in the XRD; Mr. Kandaba Rakish and Mr. Raghu Mangu for providing the Sn evaporation source; Mr. Mark Crain, Ms. Ana Kieswetter, and Mr. Joseph Lake in their help in the clean room works in the Center for Micro/NanoTechnology, University of Louisville.

Table of Contents

List of Figures

Chapter 1 - Introduction

1.1 The significance of H_2-sensing study:

Discovered by Henry Cavendish in 1766 and then named by Antoine Lavoisier a few years later [1], hydrogen gas has been used by the human kind for many decades. Although artificially produced H_2 was primarily used in aviation as the floatation gas for balloons and Zeppelins in the first one and half centuries after the discovery, nowadays gaseous hydrogen exploited by the society are mostly found in the fuel cells, which are emerging as a kind of promising clean energy source in the 21st century [2]. Nowadays, industries, such as the coal fire power plants and oil refineries, use large amount of H_2 at high temperatures while H_2 is an explosive gas (e.g., back to the age of the Zeppelins, the crash of the Hindenburg airship in 1937 in Manchester, New Jersey cost 36 lives [3]), detecting hydrogen with trace concentrations at elevated temperatures are applied extensively in industries and society.

Besides of portability, cheapness, sensitivity, and rapidity, durability at high-temperatures is an indispensable requirement for any materials/structures involved in the sensors demanded for H_2 fuel cells. In our research, the sensors are additionally required to operate in oxygen-free environments.

Based on hydrogen sensors in commercial markets and scientific literatures, several detection methodologies and numerous sensing materials have been developed by

researchers. The next three sections will present a brief review and evaluation to the methods and materials, as well as presenting the fundamental ideas of this research based on the review and evaluation. Since the aim of the research is to develop on-chip sensors based on semiconductor technologies and microelectromechanical systems (MEMS), only solid-state hydrogen sensors will be involved in the review. Non-solid-state hydrogen sensors, such as the bulky flame ionization detector, thermal conductivity sensor, and nuclear magnetic resonance (NMR) sensor, are not the objects of this Ph.D. research.

1.2 Methodologies of detection:

Based on the fundamental approaches of detection, solid-state gas sensors can be roughly divided into four major types: optic, acoustic (piezoelectric), electrochemical, and electric. Optic sensors record the optical signals resulting from the change in volume, reflection/distinction intensity, refractive index, or color of the sensing material (e.g., palladium) due to the adsorption of gas molecules [4]. In acoustic sensors, the signal is generated from the variation of the characteristics, such as wavelength, phase, and attenuation, of certain microwave (usually surface acoustic wave (SAW)) owing to the mass change of the sensing material [5]. Currently, a large amount of devices belonging to the two types mentioned above is developed upon micro-machined cantilevers [6] due to the low-cost and easiness of fabrication in large arrays.

Although a lot of optic and acoustic sensors in literatures possess high sensitivities and quick responses to H_2, three major disadvantages prevent them from being widely used as durable, portable, and economy gas detectors at high temperatures. First, the fabrication is complicated by the three-dimensional structures involved, such as the cantilever. Second, the requirement of light or wave source and detector enlarges the size of the overall equipment, as well as increasing the cost. Finally, and the most important, these two types of sensors have little compatibility with high-temperature applications, due to the sophisticated structure of the sensor, the extremely-temperature-dependence of the optic and piezoelectric properties of the sensing materials, and the vulnerability of the auxiliary components (light or wave source and detector).

The sensing mechanism of an electrochemical H_2 sensor is very close to the principle of a hydrogen fuel cell. The current in the solid-state electrolyte, which comprises the body of the sensor, is primarily carried by the oxidized state of the hydrogen gas in the ambient, the proton [7]. Gas concentrations are measured based on the electrochemical reactions occurring on the electrodes and/or at the electrode/solid-state electrolyte interface. While this type of sensors usually works at high-temperature in order to enhance the proton mobility in the solid-state electrolyte, the low detection limits are always quite high. For H_2 concentration at ppm levels, the protonic current is too low to be differentiated from noises. Also, the large size is a drawback of many electrochemical sensors due to the requirement of reference gas chambers.

Therefore, the last type mentioned in the first paragraph, the electric sensor, seems to be the best candidate so far for detection of low-concentration H_2 at elevated temperatures.

"Electric sensor" is just a coined term for expediency. A sensor is called "electric" if and only if the signal results directly from the reversible change of certain electronic properties of the sensing material, such as resistance (or conductance), capacitance, inductance, or any field-effect characteristics (e.g., the capacitance-voltage (C-V) relationship of an MOS (metal-oxide-semiconductor) device). This kind of gas or humidity sensors was divided into two or three major types in reported reviews [4-5, 8] based on their sensing principles. Most of presented electric hydrogen gas sensors can be grouped into two kinds of devices: resistors and field-effect devices. Up to now, few hydrogen sensors have been reported based on the variation of capacitance or inductance (the C-V sensors do not account for this category but belong to the field-effect devices), although they are considered as a major kind of detectors for humidity [8].

Fig. 1-1 shows the fundamental sensing principle of a MOS capacitor. H_2 molecules adsorb on the gate metal surface and then dissociate in to hydrogen atoms ($H_2 \leftrightarrow 2H$), which diffuse in the metal, reaching the metal/oxide interface. Finally, the hydrogen atoms form a dipole layer at the metal/insulator (SiO_2) interface and an electric field is generated, pointing from the gate to the silicon. Thus, the flat band voltage becomes more negative and the C-V curve of the MOS capacitor is shifted to the left (assuming the semiconductor is p-type silicon). Elevated H_2 concentration causes higher dipole density at the metal/SiO_2 interface and therefore larger C-V shift. If the H_2 concentration returns

to zero, the dissolved hydrogen will be released from the gate metal and the C-V curve regains the original shape.

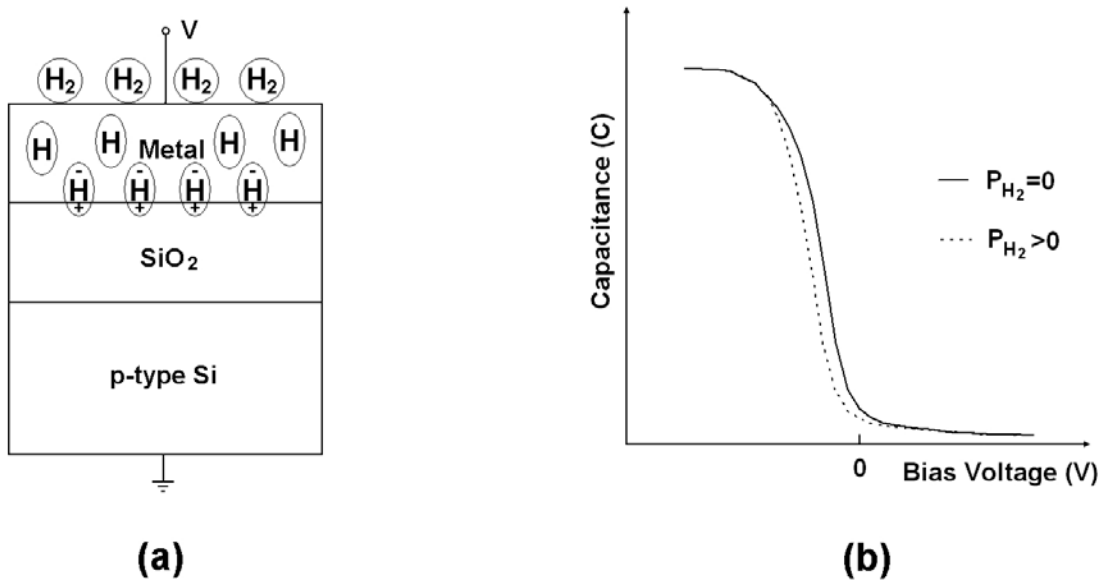

Fig. 1-1 Sensing principle of a typical hydrogen-sensitive MOS capacitor. (a) Device scheme and the formation of a dipole layer of hydrogen atoms at the metal/SiO_2 interface. (b) Shift of the C-V curve due to the introduction of H_2.

Since the first MOS capacitor H_2 sensor reported in the 1970s [9], similar devices have been frequently reported. The SiO_2 layer beneath the metal gate in Fig. 1-1 (a) can be replaced by other insulators and therefore a metal-insulator-semiconductor (MIS) device is formed, while SiO_2 grown from the silicon wafer (also the substrate of the device) usually holds the smallest leakage current density. Also, the silicon in Fig. 1-1 (a) can be replaced by other kinds of semiconductors as required by the measurements [9] (will be discussed in details in the next section).

The sensing mechanism and electrical characteristics of another major type of field-effect H_2 sensors, the Schottky diode [10], is shown in Fig. 1-2. A Schottky junction is formed at the metal/semiconductor interface. To simplify the problem, no bias voltage is applied to the device on both energy band diagrams (Fig 1-2 (a) and (b)). In other words, the Schottky junction is always at the flat band. In vacuum or certain inert ambient (e.g., Ar, N_2), the barrier height is the subtraction of the electron affinity of the semiconductor (χ) from the work function of the metal (Φ, assuming $\Phi>\chi$). Upon the introduction of H_2, a process similar to the one described in the last few paragraphs (the MOS capacitor) occurs. H_2 molecules adsorbed on the metal surface and dissociate into hydrogen atoms (H), diffusing into the metal bulk and reaching the metal/oxide interface. The work function of the metal thin layer in proximity to the interface is therefore reduced by the donation of electrons from the atomic hydrogen (Fig 1-2 (b)). As a result, the barrier height of the Schottky junction is lowered down. With bias voltages are applied (Fig. 1-2 (c)), the current under either forward or reverse bias increases due to the reduction of the Schottky barrier height. Higher concentration of H_2 results in further reduction of the

barrier height, and therefore larger current under certain bias voltage. The reduction of the barrier height must always be reversible as long as the sensor is within its life-time.

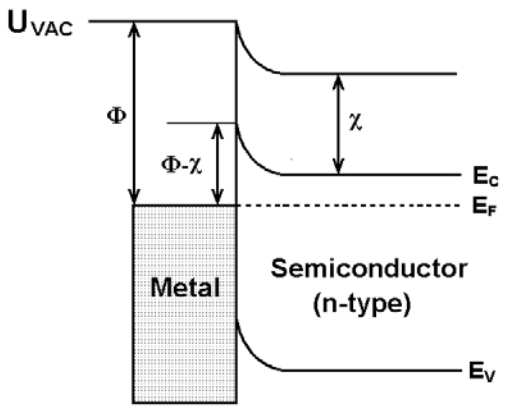
U VAC
Φ
Φ-χ
χ
E C
E F
Metal
Semiconductor
(n-type)
E V

(a)

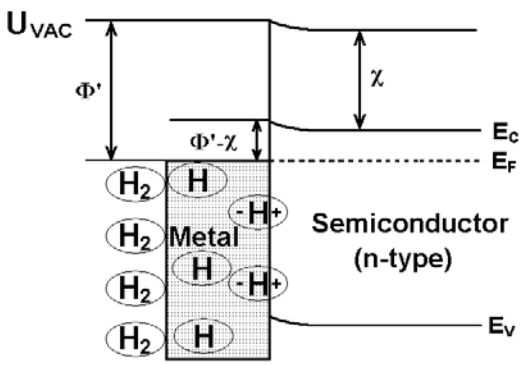
U VAC
Φ'
Φ'-χ
χ
E C
E F
H2
H
-H+
Metal
Semiconductor
(n-type)
E V

(b)

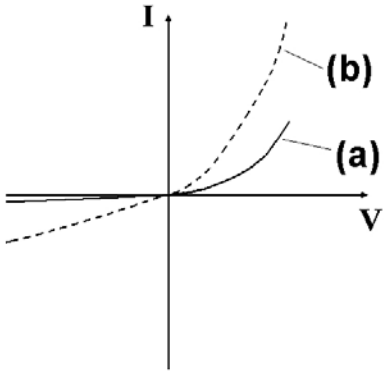
I
(b)
(a)
V

(c)

Fig. 1-2 Energy band diagrams at the flat band and current-voltage (I-V) curves of a metal/n-type semiconductor interface (a Schottky junction). The metal is assumed to be quite thin (e.g., nanometers) in order to neglect the variation of work function along the direction normal to the interface. (a) In vacuum or certain inert ambient. (b) After exposure to H_2. (c) I-V curves of the device when bias voltages are applied. The solid line represents the I-V curve in vacuum or certain inert ambient (in the case of Fig. 1-2 (a)); the dashed line stands for the I-V curve in the presence of H_2 (in the case of Fig. 1-2 (b)). U_{VAC} is the energy in the vacuum level. E_c, E_F, and E_V represent the energies at the conduction band, the Fermi level, and the valence band of the semiconductor, respectively.

The reduction of the barrier height in Fig. 1-2 can be also attributed the atomic hydrogen dipoles formed at the metal/semiconductor interface (see Fig. 1-2 (b)). Since these dipoles build up an electric field pointing to the semiconductor, the electrons in the bulk semiconductor are attracted to the interface, and the depletion of the semiconductor in proximity to interface is therefore partially neutralized. On the other hand, the C-V shift of the MOS capacitor in Fig. 1-1 can be also ascribed to the reduction of the work function of the thin layer of the metal gate close to the metal/oxide interface due to the donor effect of the dissolved hydrogen. These two descriptions (dipole formation at the interface and reduction of metal work function) for the sensing mechanisms of field-effect devices are actually equivalent [11].

Since the C-V shift is generated by the dissolving and dissociation of H_2 in the gate metal, metals with high hydrogen solubility and exceptional capability to dissociate H_2 into single atoms, are expected to be good candidate for the MOS sensors. These metals will be discussed in details in the next section.

The principle of resistor-based H_2 sensor is apparent simple: the conductivity of the sensing material changes (reversibly in most cases) with the H_2 concentration. However, detailed mechanisms are different from one material to another. We will introduce the physical and chemical properties of the most frequently reported sensing materials for H_2 in the next section, and the mechanisms of resistivity variation of these materials upon H_2 introduction will be discussed in details.

1.3 Sensing materials:

A sensing material (or sensitizer) for H_2 is a substance that changes its physical and/or chemical properties with regarding to the variation of H_2 concentration in the ambient, and the resulting changes can be converted into recordable signals. The primary interaction between the sensing material and the H_2 in the ambient is surface adsorption. Therefore, the specific surface area (or surface morphology) of the sensing material always have a significantly effect on the amount of hydrogen adsorbed, and therefore on the sensing characteristics.

Almost all of the reported sensing materials for solid-state H_2 sensors can be divided into two groups: metals (including alloys) and metal oxides (including composite or doped oxides).

Palladium (Pd) is used or at least involved in most of the reported studies of H_2 sensors. It is the best hydrogen-dissolving material that absorbs up to 900 times of its own volume of H_2 at room temperature [12]. As a result of the reversible hydrogen dissolving, the conductivity of Pd deceases due to the formation of PdH_x ($x<1$), while detailed information about the formation and properties of this unstable metal hydride remains not quite clear [12-13]. Since the response (resistance change) of bulk palladium to hydrogen is slow and acceptable response speeds can only be acquired at high H_2 concentrations, Pd is always used as the gate metal of MOS sensors; the sensing principle is not the conductivity change but the C-V shift as demonstrated in Fig. 1-1. Hydrogen MOS

sensors based on Pd and commercial semiconductor wafers were exhaustively studied in the past three decades by researchers [9, 14] due to their great compatibility to the semiconductor industry.

In the last few years, significant improvements of the performance of resistive Pd sensors have been achieved by the using of nanostructures, on which response times as short as less than 100 ms were demonstrated [15-16]. Nonetheless, resistive H_2 sensors based on Pd nanomaterials are still research-level techniques, whereas the Pd-MOS devices had become mature enough to be applied in industries [9]. Furthermore, few Pd-based resistive sensors were reported to operate at above room temperature due to the oxidation of Pd (will discussed again in the next paragraph).

Although Pd is the preferred sensing material for H_2, two major drawbacks remain. First, it is expensive, the price was around 30 $/g in 2008 and once reached about 100 $/g in 2001 [17]. Although a single sensor uses little palladium, considerable amount is consumed in mass production. Another drawback is the chemical reactivity. While Pd is usually regarded as a stable metal in air, it is oxidized at elevated temperatures (as tested in our group, 45 nm-thick Pd thin layer became non-conductive and the metallic luster disappeared after N_2 annealing at 250°C for 2h due to the small leakage of air into the system) and therefore rarely used in sensors of any type working above 300°C.

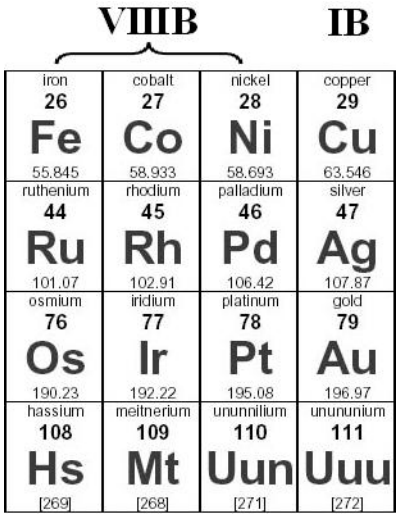

Fig. 1-3 Elements locally close to Pd in the periodic table.

In the periodic table (Fig. 1-3), nickel (Ni), a low-cost metal with the average price of about only 15 ¢/g in 2008 [18], is located just above Pd and expected to have similar chemical and physical properties to the former. In Chapter 3, we will study the sensing characteristics and principles of H_2 sensors based on MOS capacitors with Ni gate. In Fig. 1-3, it also can been that ruthenium (Ru), osmium (Os), rhodium (Rh), iridium (Ir), palladium (Pd), and platinum (Pt) are proximally located in the table and all belong to the VIII Group. Researchers in chemistry, physics, and mineralogy have found out that all these six elements share similar chemical and physical properties and their minerals are likely to occur together in nature [19]. The capabilities to absorb and dissociate H_2, which are in common among these elements, have been applied in chemical catalysis from many years. Despite of the similarity in chemistry, the resistance to oxidation of Pt or Ir is much better than that of Pd. Therefore, for high-temperature hydrogen-sensing (e.g., over 300˚C), Pt and Ir have been used as substitutes for Pd and shown good performance [9]. Since this dissertation is focused on H_2-detection at elevated temperatures, Pt will be used in the devices in Chapter 4 as electrodes for resistive sensors and Chapter 5 as the metal terminal for Schottky-diode-based sensors.

For high-temperature field-effect devices, the stability or durability of the metal materials is just a part of the problems. Traditional Si or GaAs wafers will become conductors at the temperatures over 300˚C due their narrow band gaps (less than 1.5 eV). Therefore, semiconductors with wide band gaps (>3.0 eV), such as silicon carbide (SiC), diamond (C), tin dioxide (SnO_2), titanium oxide (TiO_2), are applied in the MOS- and Schottky-diode-based H_2 sensors [9, 20]. However, the intimidating prices of SiC or diamond

wafers keep this kind of single-crystal materials from being widely applied. Therefore, wide-band-gap polycrystalline metal oxides (SnO_2, TiO_2, ZnO) are more economy choices for field-effect H_2 sensors operating at high temperatures despite of their high-density of defects. Sensors based on Pt/SnO_2 Schottky junctions will be developed and studied in Chapter 5.

As discussed above, besides of being used in field-effect devices, Pd films are also reported as H_2-sensitive resistors. However, Pd is not durable at very high temperatures. To fabricate high-temperature H_2-sensitive resistors, another major group of resistive sensing materials, the metal oxides, are utilized. According to the reported studies in the recent half century [5, 21-22], the majority of metal oxide-based hydrogen sensors works in oxygen-rich atmospheres (e.g., air) and the mechanism is that the adsorbed H_2 molecules alleviate or even eliminate the depletion caused by O_2 adsorbed prior to the hydrogen (as shown in Fig. 1-4). The resistance at the grain-grain boundary, and therefore of the overall device, is reduced as a result of the alleviation of the oxygen depletion. The major drawback of this type of sensors is that oxygen must be presented in the ambient in order to "sensitize" the surface of the metal oxides.

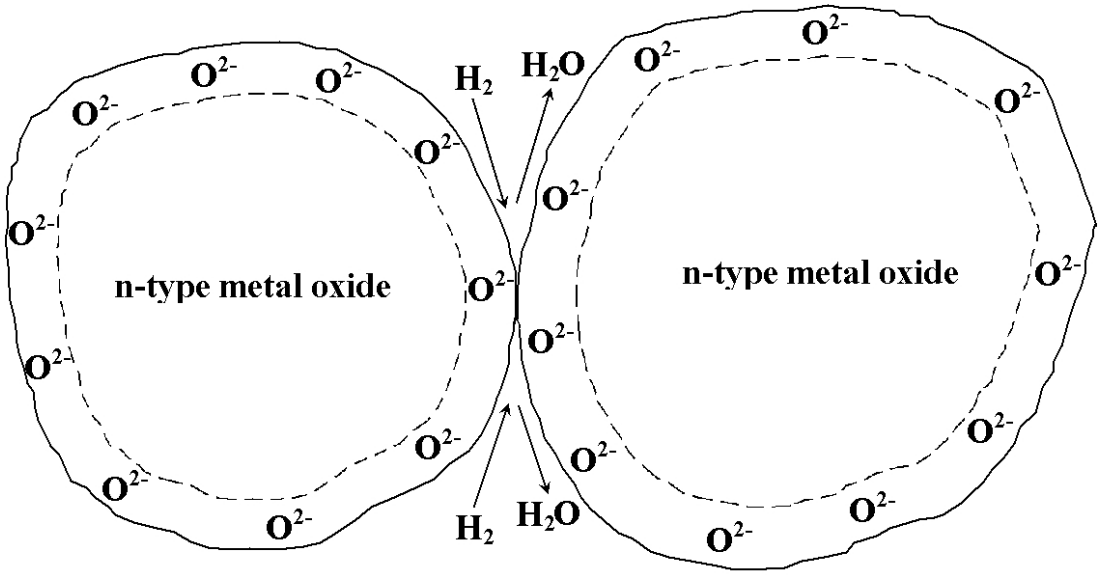
n-type metal oxide
n-type metal oxide
O^{2-}
H_2
H_2O
H_2
H_2O

(a)

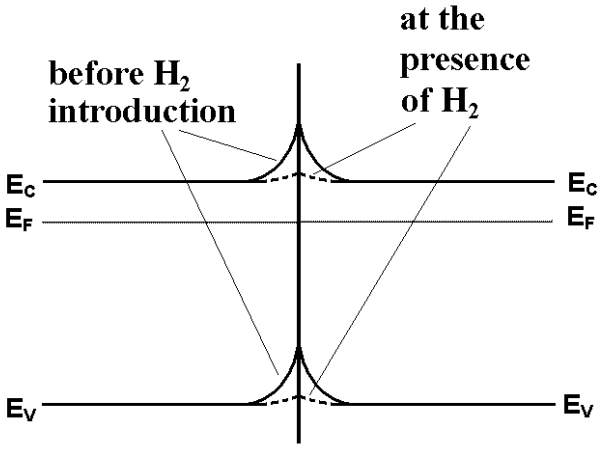
before H_2 introduction
at the presence of H_2
E_C
E_F
E_V
E_C
E_F
E_V

(b)

Fig. 1-4 Oxygen depletion quenched by hydrogen absorbing of an n-type material (e.g. SnO_2). (a) Oxygen depletion regions (between the dashed line and the grain surface) in two neighboring grains of an n-type metal oxide and the release of oxygen due to adsorption of H_2 on the surface (water formation). (b) Change in the energy band diagram at the grain-grain boundary due to H_2 adsorption. E_c, E_F, and E_V represent the energies at the conduction band, the Fermi level, and valence band of the metal oxide, respectively.

Although devices operated in air constitute the dominant party of metal oxide-based resistive H_2 sensors, a different sensing mechanism has been reported and studied for H_2 detection without the necessity of pre-adsorption of O_2 on the oxide surface [23, 24]. In this mechanism, the dissolved and dissociated hydrogen (mostly in the form of single atoms) spills out from the catalytic metal electrodes or metal particle dopants (e.g., Pt or Pd) to the surface of the metal oxide thin or thick film and then chemically adsorbed at the interstitial positions in the oxide lattice structure. Via this chemisorption, partial electron charge is transferred from the spilt hydrogen to the metal oxide. If the oxide is n-type, the resistance will drop. Different from the metal oxide-based sensors dependent on the reduction of energy barrier at the grain-grain boundaries due to the removal of pre-adsorbed oxygen, the fundamental sensing principle of this kind of devices is the elevation of the Fermi level of the metal oxide (assuming n-type) through the partial electron charge transfer from the split hydrogen, as shown in Fig. 1-5.

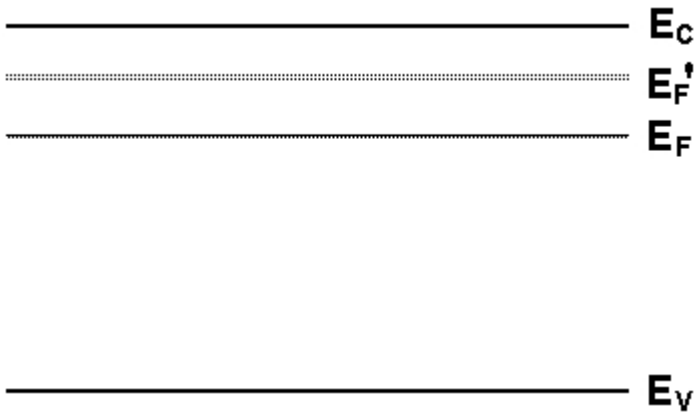

Fig. 1-5 Elevation of the Fermi level of an n-type metal oxide due to the partial electron charge transfer from the chemisorbed hydrogen that spills out of the Pt or Pd attached to the metal oxide. E_c, E_F, and E_v represent the energies at the conduction band, the Fermi level, and valence band of the metal oxide, respectively. E_F' is the elevated Fermi level energy owing to the partial electron charge transfer.

This "partial electron charge transfer" effect was initially studied in chemical catalysis [25]. Until now, most of the hydrogen-sensing studied in this domain are based on Pt-TiO_2 systems [23, 24]. TiO_2 thin film resistive sensors with Pt as electrodes will be developed and studied in Chapter 4 and the sensing principle is proposed to be the partial electron charge transfer resulting from this effect.

1.4 Summary of the designs:

As discussed in the past two sections, commercial [26] and experimental microfabricated H_2 sensors based on different detection approaches and materials can be summarized in the hierarchical organization chart in Fig. 1-6. Electric sensors will be chosen as objects for this Ph.D. research due to their high-sensitivity, low-cost, simplicity, and compatibility to high-temperature applications. Since material compatibility is the primary concern for designing hydrogen sensors operating at elevated temperatures, platinum will be used as the electrodes for the devices operating at above 200°C owing to both of its chemical stability and competence in dissolving and dissociating H_2. Low-cost SnO_2 thin films will be synthesized to fabricate H_2-sensitive Pt/SnO_2 Schottky diodes for applications at the temperature around 300°C (Chapter 5). In Chapter 4, resistive TiO_2 thin films with Pt electrodes will be prepared for sensing H_2 at the temperature as high as 500°C. MOS capacitors with Ni gates will also be developed for hydrogen detection at medium temperatures (e.g., 140°C) due to the low-cost of nickel.

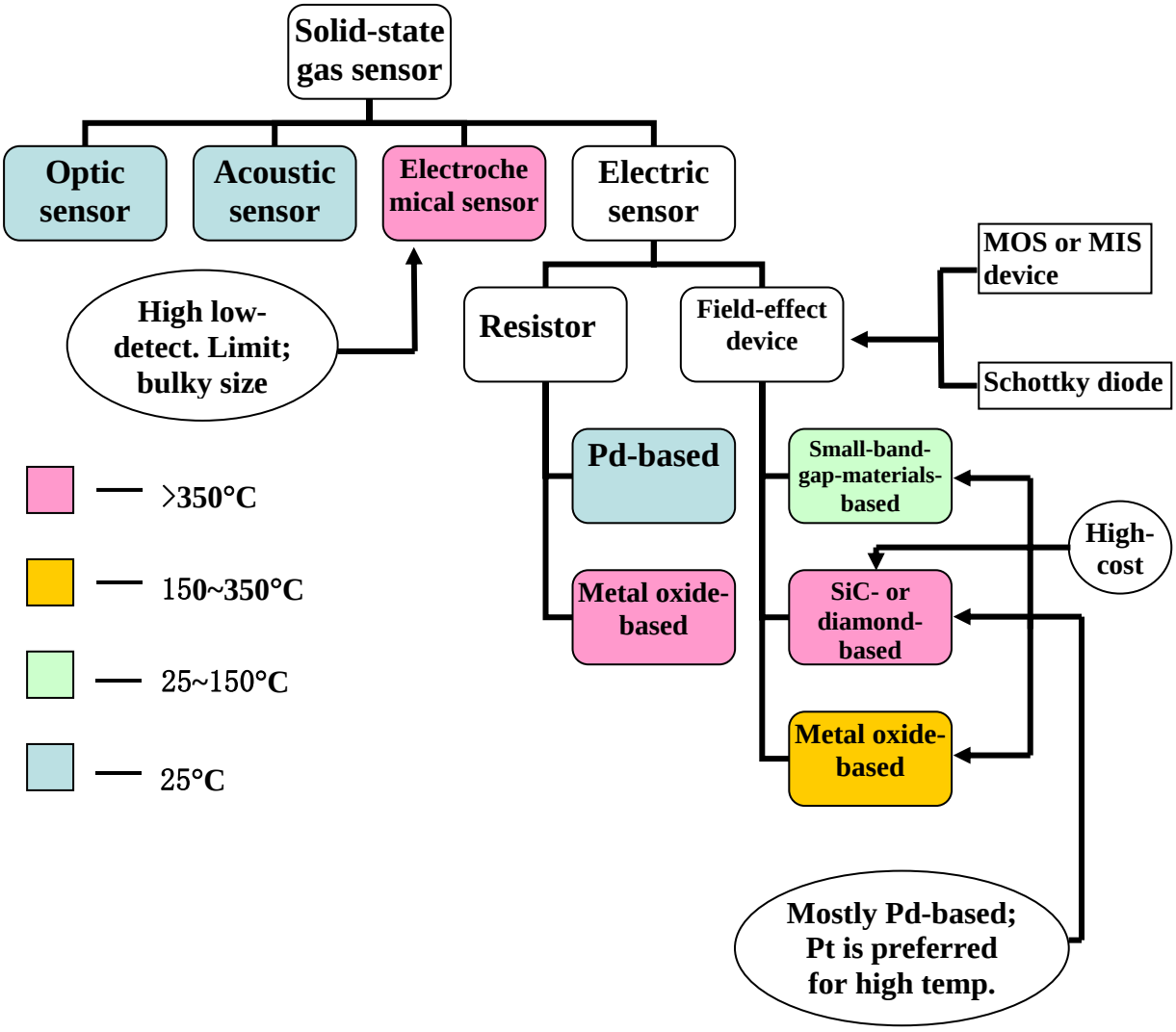

Fig. 1-6 Hierarchical organization chart of solid-state hydrogen gas sensors with respect to the compatibility to operating temperatures. The maximum tolerable temperature ranges for the devices are marked in different colors.

References for Chapter 1:

[1] A. Stwertka, A Guide to the Elements, 2nd Edition, Oxford University Press, New York, NY, 2002.

[2] National Research Council and National Academy of Engineering, The Hydrogen Economy: Opportunities, Costs, Barriers, and R&D Needs, National Academies Press, Washington, DC, 2004.

[3] R. Archbold, Hindenburg: An Illustrated History, Toronto: Viking Studio/Madison Press, Toronto, Canada, 1994.

[4] S. Capone, A. Forleo, L. Francioso, R. Rella, P. Siciliano, J. Spadavecchia, D. S. Presicce, A. M. Taurino, Solid state gas sensors: state of the art and future activities, Journal of Optoelectronics and Advanced Materials 5 (2003) 1335-1348.

[5] P. T. Moseley, Solid state gas sensors, Meas. Sci. Technol. 8 (1997) 223-237.

[6] K. M. Goeders, J. S. Colton, L. A. Bottomley, Microcantilevers: Sensing chemical interactions via mechanical motion, Chem. Rev. 108 (2008) 522-542.

[7] G. Korotcenkov, S. D. Han, J. R. Stetter, Review of electrochemical hydrogen sensors, Chem. Rev. 109 (2009) 1402–1433.

[8] Z. Chen, C. Lu, Humidity sensors: a review of materials and mechanisms, Sensor Letters 3 (2005) 274-295.

[9] I. Lundström, H. Sundgren, F. Winquist, M. Eriksson, C. Krantz-Rülcker, A. Lloyd-Spetz, Twenty-five years of field effect gas sensor research in Linköping, Sensors and Actuators B 30 (2007) 247-262.

[10] G. Korotcenkov, Metal oxides for solid-state gas sensors: What determines our choice? Materials Science and Engineering B 139 (2007) 1-23.

[11] J. Janata, R. J. Huber (Ed.), Solid State Chemical Sensors, Academic Press, New York, NY, 1985.

[12] D. R. Lide (Ed.), CRC Handbook of Chemistry and Physics, Internet Version 2008, <http://www.hbcpnetbase.com>, CRC Press, Boca Raton, FL, 2008.

[13] N. Lopez, Z. Lodziana, F. Illas, M. Salmeron, When Langmuir is too simple: H_2 dissociation on Pd (111) at high coverage, Physical Review Letters 93 (2004) 146103/1-146103/4.

[14] C. Christofides, A. Mandelis, Solid-state sensors for trace hydrogen gas detection, J. Appl. Phys. 68 (1990) R1-R30.

[15] F. Favier, E. C. Walter, M. P. Zach, T. Benter, R. M. Penner, Hydrogen sensors and switches from electrodeposited palladium mesowire arrays, Science 293 (2001) 2227-2231.

[16] T. Xu, M. P. Zach, Z. L. Xiao, D. Rosenmann, U. Welp, W. K. Kwok, G. W. Crabtree, Self-assembled monolayer-enhanced hydrogen sensing with ultrathin palladium films, Appl. Phys. Lett. 86 (2005) 203104/1-203104/3.

[17] Kitco Inc., Monthly Palladium Chart, Retrieved 08/25, 2009.

[18] London Metal Exchange, Primary Nickel Price Graph, Retrieved 08/25, 2009.

[19] D. C. Harris, L. J. Cabri, Nomenclature of platinum-group-element alloys: review and revision, The Canadian Mineralogist 29 (1991) 231-237.

[20] K. Potje-Kamloth, Semiconductor junction gas sensors, Chem. Rev. 108 (2008) 367-399.

[21] N. Barsan, D. Koziej, U. Weimar, Metal oxide-based gas sensor research: How to? Sensors and Actuators B 121 (2007) 18-35.

[22] G. Korotcenkov, The role of morphology and crystallographic structure of metal oxides in response of conductometric-type gas sensors, Materials Science and Engineering R 61 (2008) 1-39.

[23] U. Roland, R. Salzer, T. Braunschweig, F. Roessner, H. Winkler, Investigations on hydrogen spillover: Part 1 - Electrical conductivity studies on titanium dioxide, J. Chem. Soc., Faraday Trans. 91 (1995) 1091-1095.

[24] O. K. Varghese, D. Gong, M. Paulose, K. G. Ong, E. C. Dickey, C. A. Grimes, Extreme changes in the electrical resistance of titania nanotubes with hydrogen exposure, Adv. Mater. 15 (2003) 624-627.

[25] Jr. W. C. Conner, G. M. Pajonk, S. J. Teichner, Spill over of sorbed species, in: D. D. Eley, H. Pines, P. B. Weisz (Ed.), Advances in Catalysis, Academic Press, NY, New York, 1986, vol. 34, 1-74.

[26] W. Buttner, Today's commercial hydrogen sensors, DOE Hydrogen Sensor Workshop, April 4, 2007.

Chapter 2 - Technologies and approaches

2.1 Device fabrication:

Since all the sensors in this Ph.D. research use silicon wafers as substrates, conventional silicon wafer processes, including RCA cleaning and oxidation, were applied in the sensor fabrication. Fig. 2-1 (a) and (b) show the clean bench for RCA cleanings and the tube furnace for oxidations (Linderburg Blue HTF55347C). The role of the RCA cleaning is to remove contaminants and the native oxide on the silicon wafer; detailed procedures are described in handbooks [1]. Thermal oxidations for silicon wafers were performed at high temperatures in flowing O_2, and the thickness of the resulting SiO_2 is dependent on both the temperature and the time [2]. Thicknesses of thermally grown SiO_2 films in this research were determined by a J. A. Woollam M-2000V spectroscopic ellipsometer (Fig. 2-1 (c)).

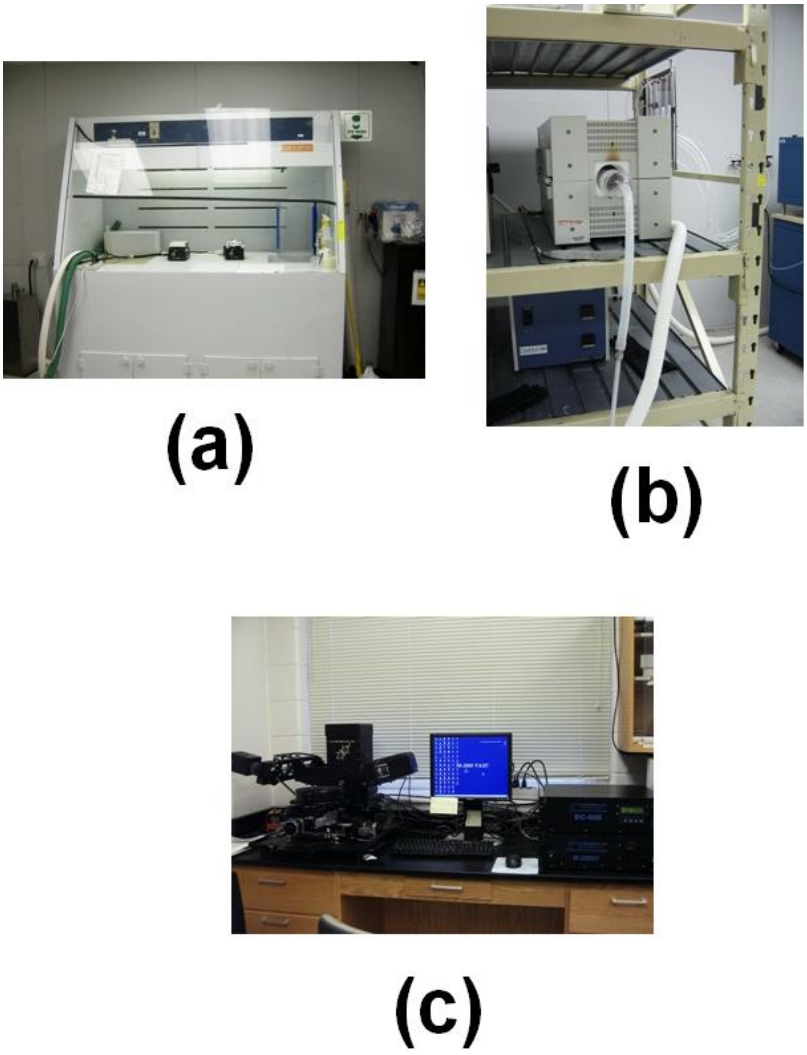

Fig. 2-1 Major equipments for the silicon wafer processes. (a) Clean bench for RCA cleanings. (b) Oxidation furnace. (c) Ellipsometer.

Photolithography was used to define patterns on the samples [3]. Four major steps are involved in the photolithography: photoresist (PR) coating, baking, exposure, and developing. Fig. 2-2 shows the spin coater to disperse the PR, the hot plate to bake the coated thick layer of the PR, the mask aligner for exposure, and the solvent hood for pre-cleaning of the device samples and developing the pattern, as well as for the lift-off process following the thin film deposition (see next paragraph). A microscope was used to inspect the quality of the photolithography (also shown in Fig. 2-2).

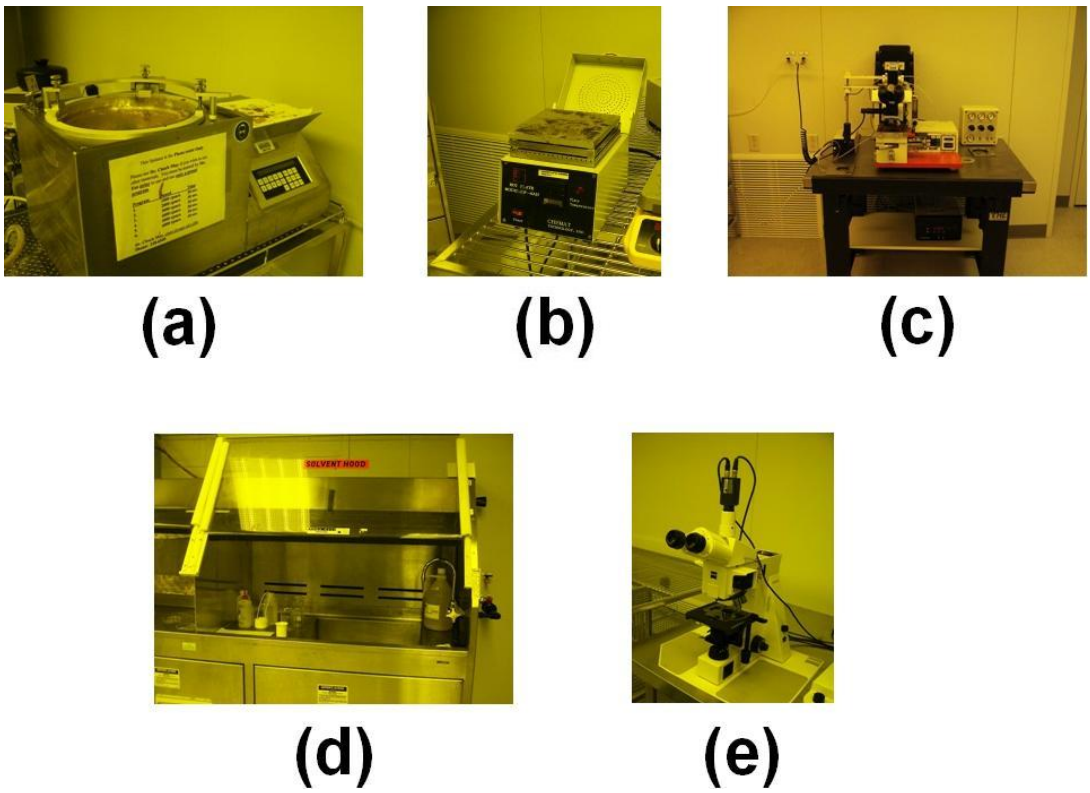

Fig. 2-2 Major equipments for the photolithography. (a) Spin coater (CEE 100). (b) Hot plate (CHEMAT Technology KW-4AH). (c) Mask aligner (Karl Suss 100UV002). (d) Solvent hood. (e) Microscope (Carl Zeiss 181549).

Thin film deposition techniques, including electron beam (e-beam) evaporation and sputtering, were applied to fabricate tens of angstroms to a few microns of metal layers on the samples (non-metal materials can be also deposited by these techniques while in this research only metals are deposited). The principles of e-beam evaporation and sputtering can be found out in textbooks [3]. Lift-off processes, in which the exposed or unexposed PR (depending on whether the PR is positive or negative) beneath the deposited metal films is dissolved so that the metal layer on top is stripped off, were carried out as long as patterns were required on the samples. Heating and ultrasonic cleaning may be needed to accomplish the lift-off. The microscope in Fig. 2-2 was used to inspect the quality of the lift-off. Thicknesses of the deposited films were determined and calibrated by a stylus profiler.

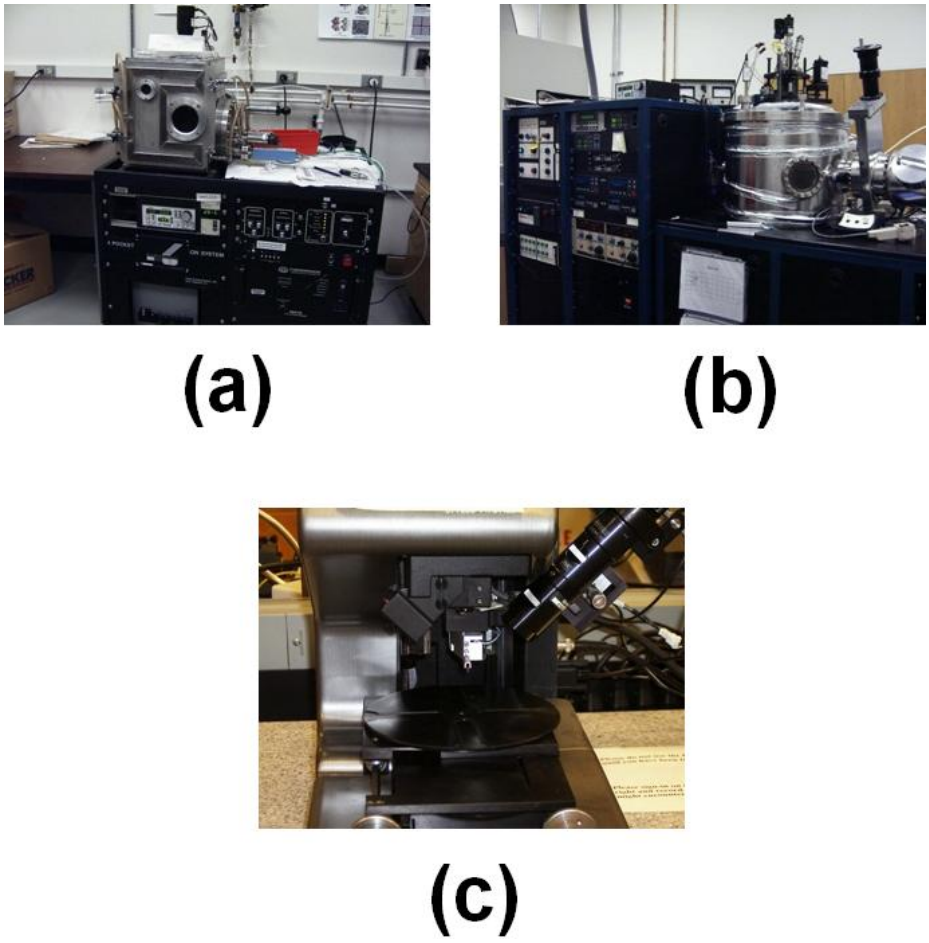

Fig. 2-3 Major equipments for the thin film deposition. (a) Torr International EB-4P Series electron beam evaporator. (b) AJA International ATC2000 sputtering system. (c) Dektak 6M stylus profiler.

2.2 Characterization of materials and structures:

The material/structure characterization included the investigation of morphologies of the sample surfaces and the determination of crystal phases of the synthesized films. A scanning microscope (Hitachi S-4300) and an atomic force microscope (TI A-35) were used to study the surface morphologies and the crystal phases are determined by an X-ray diffractor (Siemens D500). The principles of scanning microscopy (SEM), atomic force microscopy (AFM), and X-ray diffractometry (XRD) can be found out in textbooks [4-5].

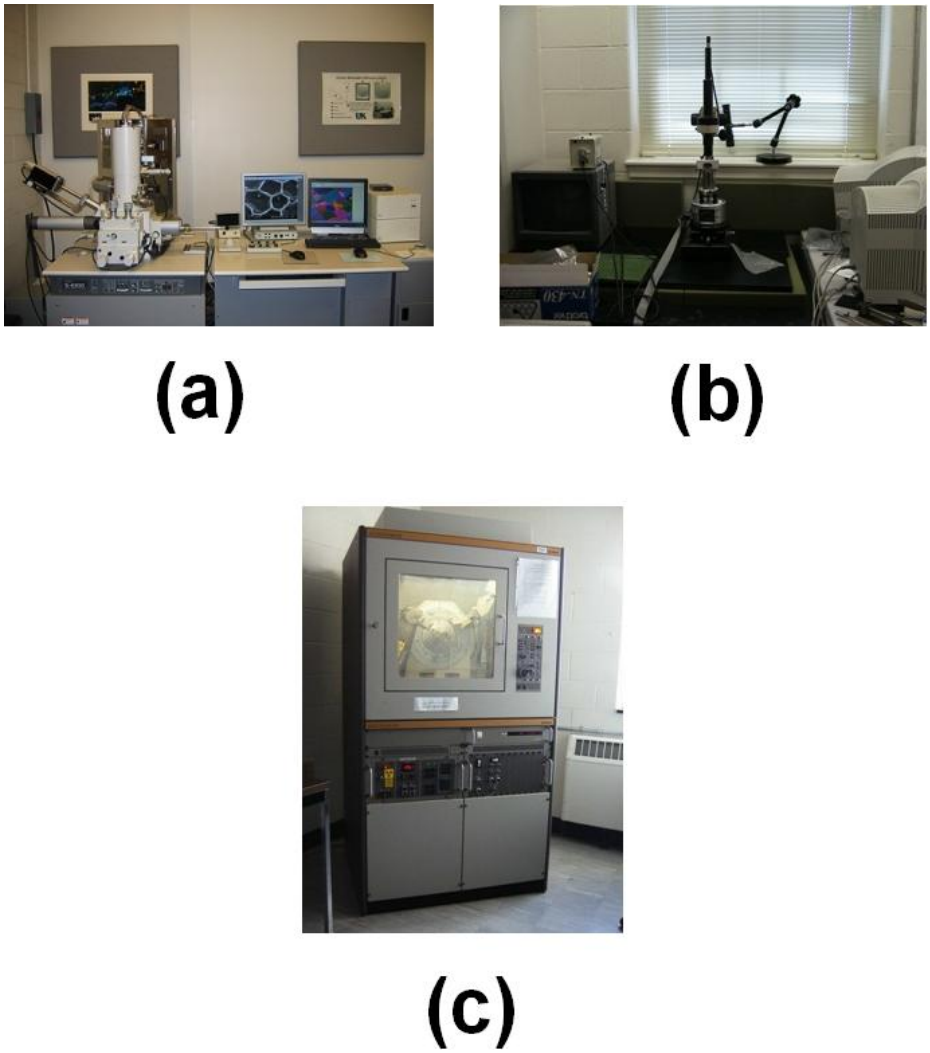

Fig. 2-4 Major equipments for the material/structure characterization. (a) Hitachi S-4300 scanning microscope (Copyright 2009, Electron Microscope Center, University of Kentucky). (b) TI A-35 atomic force microscope. (c) Siemens D500 X-ray diffractor.

2.3 Measurement of gases:

A Barnstead International F21100 tube furnace with adjustable operating temperatures was used as the testing chamber for H_2 and the assumed cross-sensitive gases, such as CO and CH_4. Commercial gas tanks (purchased from Scott-Gross) were connected to the furnace tube via a multi-input single-output gas flow meter. The concentration of the tested gas was prepared by mixing the tested gas with the background gas. Both nitrogen and air were used as the background gas. To prepare concentrations below 1000 ppm, commercial tanks filled with pre-mixed low-concentration H_2 or CO (e.g., 1000 ppm) were utilized. The total flow rate was set to over 1 liter/min in order to minimize the resident time of the whole system. The overall gas measurement system is shown in Fig. 2-5.

Fig. 2-5 Gas measurement system.

Additionally, a special cap for the quartz tube in the furnace was made in the Glassware Shop, Department of Chemistry, University of Kentucky. This cap, as shown in Fig. 2-6, is equipped with three tungsten rods piercing through the glass without any orifices. The sealed penetration was attained by thrusting the tungsten rods into the half-melted glass and then cooling the glass down. The major advantage of using this special cap is that the testing chamber (inside the tube) is excellently physically separated from but electrically connected to the outside.

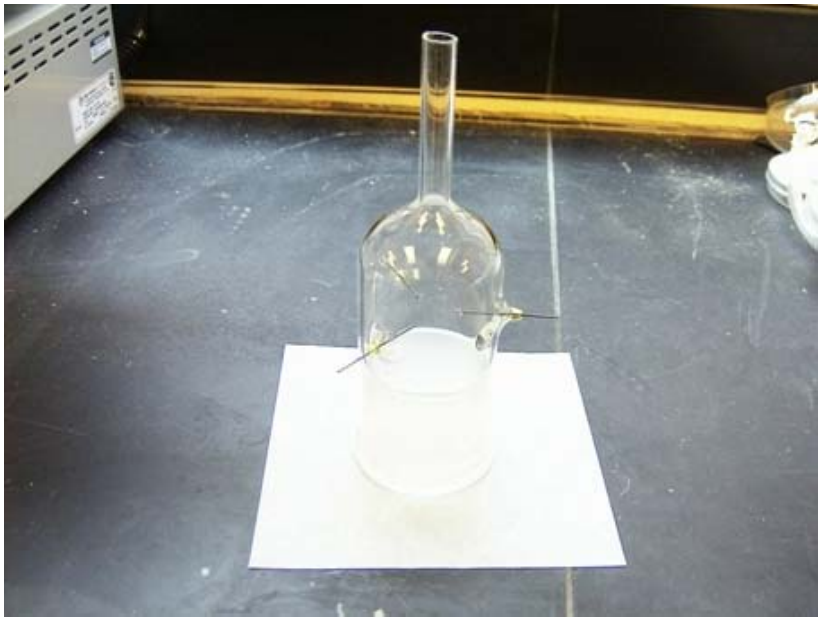

Fig. 2-6 Lab-made cap of the quartz tube with tungsten rods piercing through.

References for Chapter 2:

[1] K. A. Reinhardt, W. Kern, Handbook of Silicon Wafer Cleaning Technology, 2nd Edition, William Andrew Publishing, Norwich, NY, 2008.

[2] R. C. Jaeger, Introduction to Microelectronic Fabrication, 2nd Edition, Prentice Hall, Upper Saddle River, NJ, 2001.

[3] S. A. Campbell, The Science and Engineering of Microelectronic Fabrication, 2nd Edition, Oxford University Press, New York, NY, 2001.

[4] M. Mulder, Basic Principles of Membrane Technology, 2nd Edition, Kluwer Academic Publishers, New York, NY, 1996.

[5] C. Giacovazzo, H. L. Monaco, G. Artioli, D. Viterbo, G. Ferraris, G. Gilli, G. Zanotti, M. Catti, Fundamentals of Crystallography, 2nd Edition, Oxford University Press, New York, NY, 2002.

Chapter 3 - Hydrogen sensors based on $Ni/SiO_2/Si$ MOS capacitors

3.1 Introduction:

Since hydrogen fuel cells are emerging as a promising clean energy source in the 21st century, detecting and monitoring of hydrogen leakage will be applied extensively in industries and society. Hydrogen MOS sensors based on palladium (Pd) sensing were widely studied in the past three decades by numerous researchers [1-4]. The adsorbed and dissolved hydrogen atoms form a dipole layer at the Pd/insulator (mostly silicon oxide) interface and the work function of the Pd gate is decreased [1, 5, 6]. Although palladium (Pd) is well-known for sensing of hydrogen, nickel (Ni), an element in the same group in the periodic table as the former, is also good at adsorbing and dissolving hydrogen and has been used for hydrogen storage or batteries for many years [7, 8]. When hydrogen molecules dissociate on nickel surface and diffuse in the metal bulk, some nickel-hydrogen compounds are formed under certain conditions [9-11]. Comparing with the expensive palladium, hydrogen sensors based on nickel have an advantage of low cost in large-scale manufacturing. Up to now, there are no reports on nickel-based hydrogen-sensing devices using MOS structures.

In this paper, we report a novel Ni-based hydrogen sensor using the $Ni/SiO_2/Si$ MOS structure. We present experimental results of the performance of the sensor and discuss the possible sensing mechanism.

3.2 Experimental:

Conventional fabrication processes for silicon MOS capacitors were used. A thin silicon oxide layer of 14.4 nm was grown on a regular (100) p-type wafer, following a standard RCA cleaning. A nickel film with a thickness of 500 Å was deposited on the silicon oxide by argon plasma sputtering and patterned by photolithography. The size of the Ni-covered area was 5×5 mm^2. At a fixed frequency (100 kHz), the capacitance was measured as the d.c. bias (gate voltage) was scanned from accumulation to strong inversion. The capacitance-voltage (C-V) measurements were carried out at hydrogen concentrations of 50 ppm, 100 ppm, 200 ppm, 500 ppm, and 1000 ppm, obtained by diluting hydrogen in pure nitrogen or synthetic air. The response/recovery measurements for hydrogen concentrations at 100 ppm, 200 ppm, and 1000 ppm were carried out by keeping the bias voltage at a constant value (-0.4 V) and monitoring the capacitance as a function of time. All the data were collected by using an HP4192 Impedance Analyzer with an a.c. testing signal of 100 kHz frequency at 140˚C.

3.3 Results and discussion:

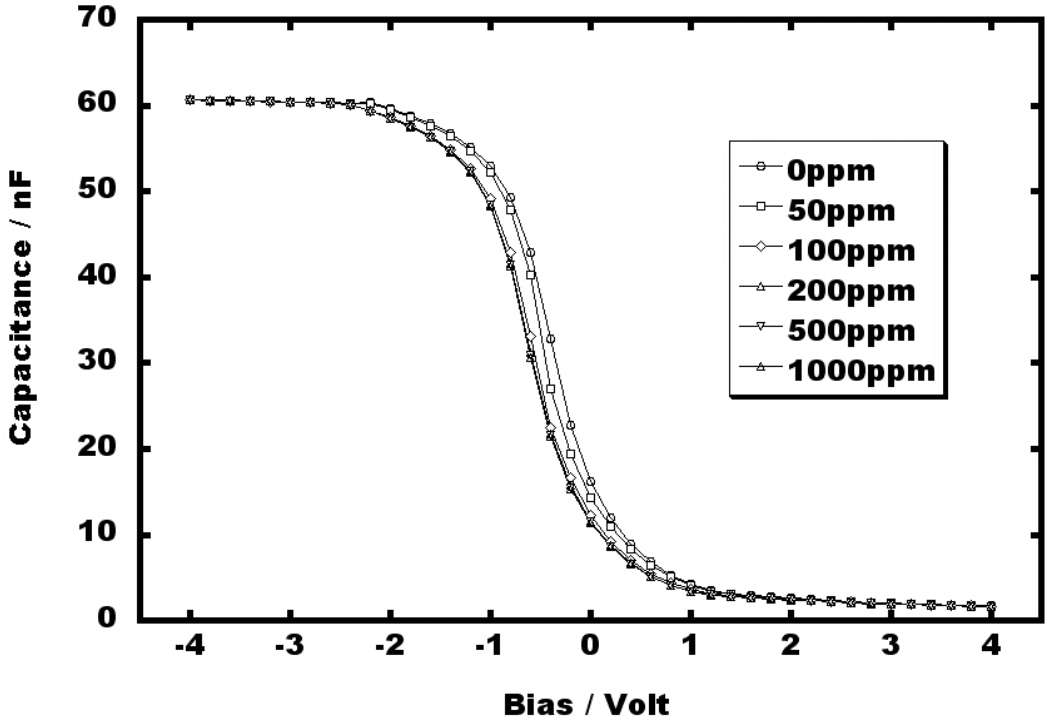

Fig. 3-1 C-V curves at different bias voltages for various H_2 concentrations diluted by nitrogen.

Fig. 3-1 shows C-V curves of the Ni/SiO_2/Si MOS capacitor in different hydrogen concentrations. It can be seen that exposure of the sensor to higher hydrogen concentrations causes a shift of the whole C-V curve to a more negative voltage. The hydrogen-induced shift of C-V curves is similar to that of the palladium MOS sensors, which was attributed to the reduced work function of the gate caused by the formation of a polarized hydrogen atom layer at the Pd/SiO_2 interface [12-13]. The variation of sensor response to the bias voltage is shown in Fig. 3-2. For a certain bias voltage, the response (R) is defined as:

$$R = 100\% \times \frac{\Delta C}{C} \qquad (3\text{-}1)$$

where C is the capacitance in pure nitrogen; ΔC is the change in capacitance at a certain hydrogen concentration. From Fig. 3-2, it is observed that the highest response always occurs at the same bias voltage (-0.4 V) for all concentration levels and the response increases with the H_2 concentration.

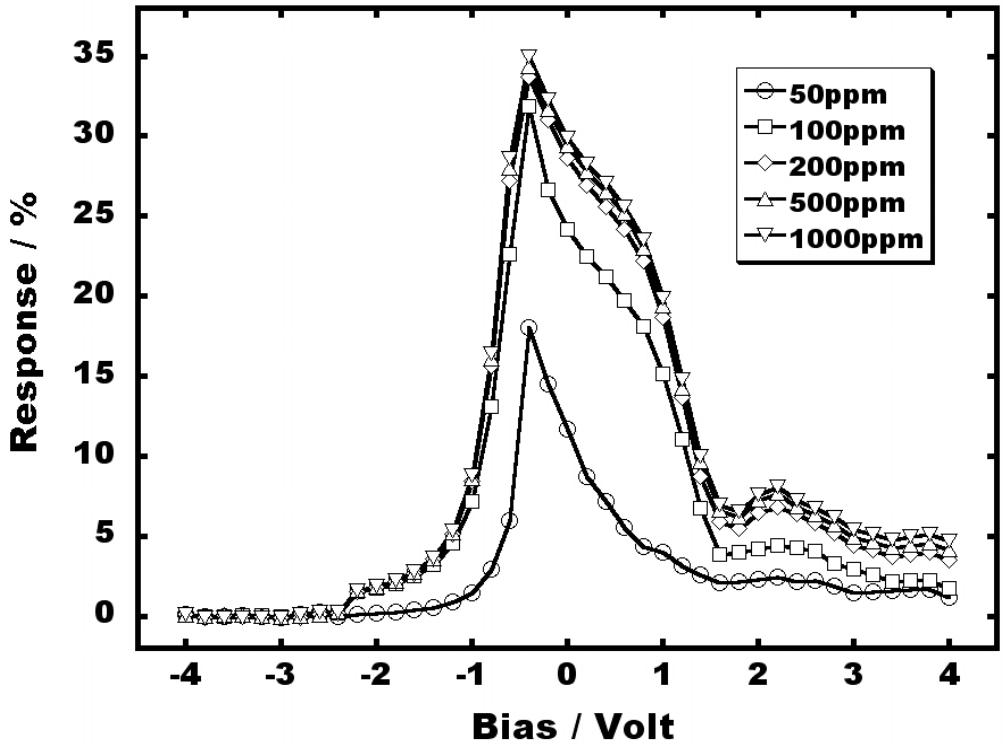

Fig. 3-2 Response as a function of bias voltage (in nitrogen).

By replotting the data at bias=-0.4 V, the response as a function of the hydrogen concentration is shown in Fig. 3-3. It can be seen that the response is reduced substantially by changing the carrier gas from nitrogen to synthetic air. Lofdahl et al. [14] has observed that at a hydrogen concentration of 250 ppm, the response of a Pt-MOS sensor was very small in air although increased considerably in nitrogen. This difference in response was ascribed to the existence of oxygen, which caused a high hydroxyl formation rate on the Pt surface. The cause of reduction of response of the presented Ni-MOS sensor in the presence of oxygen might be similar to those of the Pt-MOS sensor, while further research is necessary to investigate the principles.

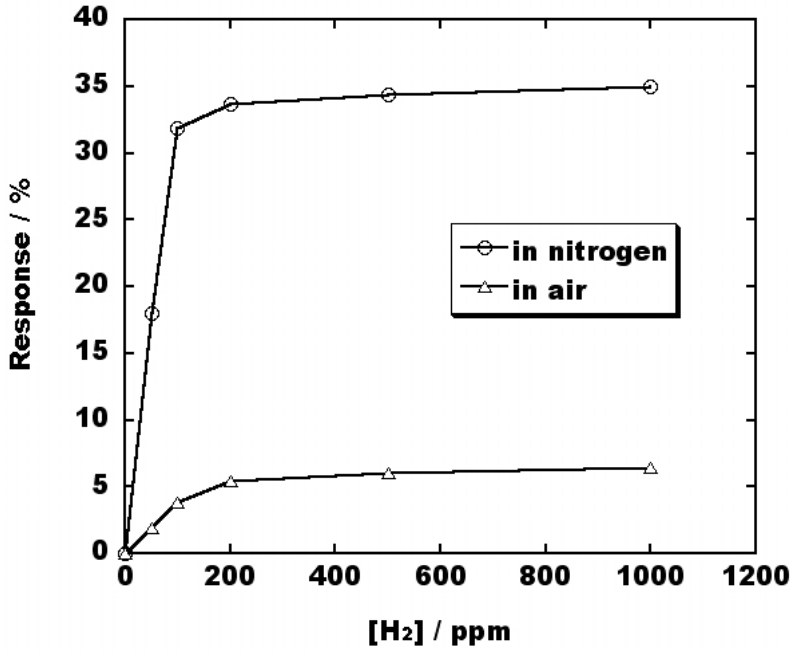

Fig. 3-3 Dependence of the highest response on the hydrogen concentration (bias voltage = -0.4 V).

According to Fig. 3-3, it is plausible to use the Langmuir isotherm model to explain the adsorption/desorption mechanism of dissolved hydrogen at the metal/SiO_2 interface in nitrogen ambient, similar to those proposed for palladium devices [15, 16]. The Langmuir isotherm model assumes that, on a given interface, there are a fixed and evenly distributed number of active sites for a certain kind of gaseous specie to be adsorbed; and one active site can only adsorb one molecule or atom.

As long as equilibrium is established, the solid-state concentration of atomic hydrogen in the nickel thin layer will be proportional to the hydrogen partial pressure in the gaseous ambient. If we assume that the Ni/SiO_2 interface has a fixed number of active sites, the dissolved hydrogen coverage (θ) on this interface, at equilibrium, will be functionally related to the hydrogen gas concentration, whose square root is proportional to the solid-state concentration of hydrogen atoms in nickel, as presented in several references [1, 14, 17-19],

$$K \times [H_2]^{\frac{1}{2}} = \frac{\theta}{1-\theta} \tag{3-2}$$

where K is a constant associated with the temperature. It is reasonable to assume that the hydrogen coverage on the Ni/SiO_2 interface is proportional to the change of the capacitance, because the hydrogen atoms trapped at the interface can be considered as polarized dipole charges [13-14, 19-21]. At the maximum coverage (θ = 1), at which all of the active sites are occupied by the dissolved atomic hydrogen, the change of the capacitance or the response (R) should reach the maximum. Therefore the relationship between the response and the hydrogen coverage (θ) can be established as:

$$R = \frac{\Delta C}{C} = k \times \theta \tag{3-3}$$

and $$R_{max} = \frac{\Delta C_{max}}{C} = k \tag{3-4}$$

where ΔC is the change of the capacitance and k is a constant that is equal to the maximum response. R_{max} is found to be about 35%, corresponding to 1000 ppm hydrogen, at which the response to hydrogen is nearly saturated. Use R/R_{max} to represent θ, we have

$$K \times [H_2]^{\frac{1}{2}} = \frac{\frac{R}{R_{max}}}{1 - \frac{R}{R_{max}}} \tag{3-5}$$

In Fig. 3-4, the experimental data in nitrogen are plotted using the above equation and a good linearity is obtained. This means that the proposed Langmuir isotherm model is in agreement with our experimental data. However, the fact that the regression line is not passing zero might be an indication that some hydrogen molecules could be consumed during the diffusion inside the nickel layer, e.g., by the formation of nickel-hydrogen compounds. The data for hydrogen concentrations larger than 500 ppm are not plotted in Fig. 3-4, because R is quite close to R_{max}, leading to a large computation error as shown in Eq. (3-5).

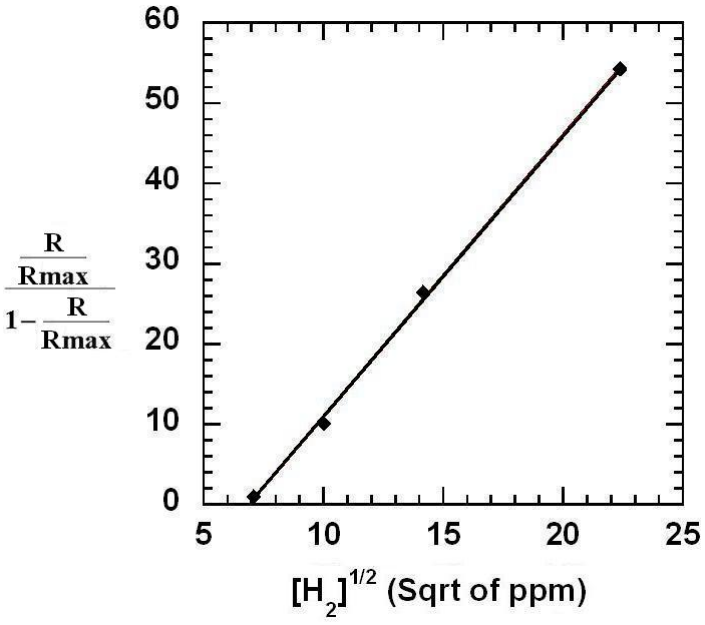

Fig. 3-4 Dependence of the highest response on the hydrogen concentration, replotted to fit the Langmuir isotherm model (bias voltage = -0.4 V, in nitrogen).

Fig. 3-5 shows response/recovery transients of the sensor at the bias voltage of -0.4V and hydrogen concentrations of 100 ppm, 200 ppm, 1000 ppm in pure nitrogen. The response times for reaching 50% peak values (t50%) for hydrogen gases are 23 s from 0 ppm to 100 ppm, 37 s from 0 ppm to 200 ppm, and 44 s from 0 ppm to 1000 ppm, while recovery times are 160 s from 100 ppm to 0 ppm, 270 s from 200 ppm to 0 ppm, and 630 s from 1000 ppm to 0 ppm. The transient curve of 50 ppm H_2 is very close to that of 100 ppm, and the response/recovery times of 500 ppm are in between of those of 200 ppm and 1000 ppm. To avoid confusion, the response/recovery curves for 50 ppm and 500 ppm are therefore omitted in Fig. 3-5.

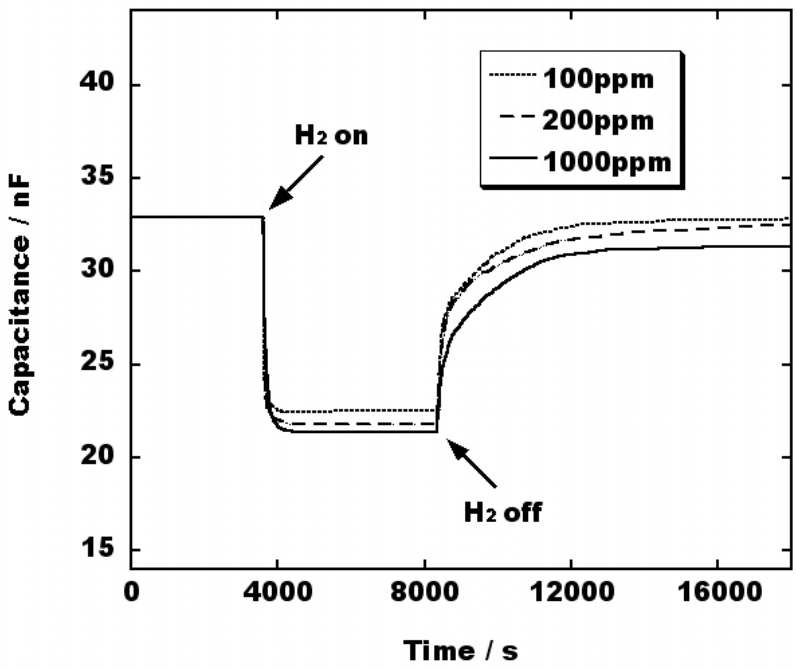

Fig. 3-5 Response/recovery transients at different hydrogen concentrations (bias voltage = -0.4 V, in nitrogen).

Response/recovery becomes slow as hydrogen concentrations increase. For all the concentrations, the recovery is much slower than the response. The response/recovery of our Ni sensors is very similar to that of palladium sensors reported [5, 15]. It was also reported that the dissolved hydrogen atoms diffused through the thin oxide layer and trapped at the Si/SiO_2 interface [5, 22-23]. Removal of the atomic hydrogen depends on the sorption or trapping energy, resulting in slow recovery. At high H_2 concentrations, a large amount of hydrogen atoms are chemisorbed or trapped in the MOS structure, and therefore the removal takes longer time.

The device performance at room temperature (25˚C) was also investigated. However, both the response and recovery required more than half an hour to reach or retreat to 50% peak values (the recovery time ($t_{50\%}$) was found out to be as long as about 2 h as the ambient was switched from 100 ppm H_2 to pure N_2). Very slow transients at room temperature had been reported in MOS capacitors with Pd-gates long time ago [1], and can be ascribed to the reduced diffusivity of hydrogen in nickel and the decreased dissociating rate of H_2 into H at lower temperatures.

Two more MOS capacitors with the Ni gate thicknesses of 30 nm and 100 nm respectively were also fabricated using the same procedure described in the Section 3.2. The responses (as defined in Eq. (3-1)) of devices with three different gate thicknesses to 200 ppm H_2 at the bias voltage of -0.4 V were shown in Fig. 3-6. According the result it can be concluded that within the range of 30 to 100 nm of the thickness of the Ni gate, the response is not likely to vary significantly. The insignificant influence of gate metal

thickness on device response to H_2 was also verified by previous Pd- , Pt-, and Ir-MOS studies [14]. However, thick gates waste nickel while very thin gates are liable to be damaged (e.g., the 30 nm-thick Ni in this report was much easier to be scratched than the thicker ones). Therefore, moderate gate thickness is preferable.

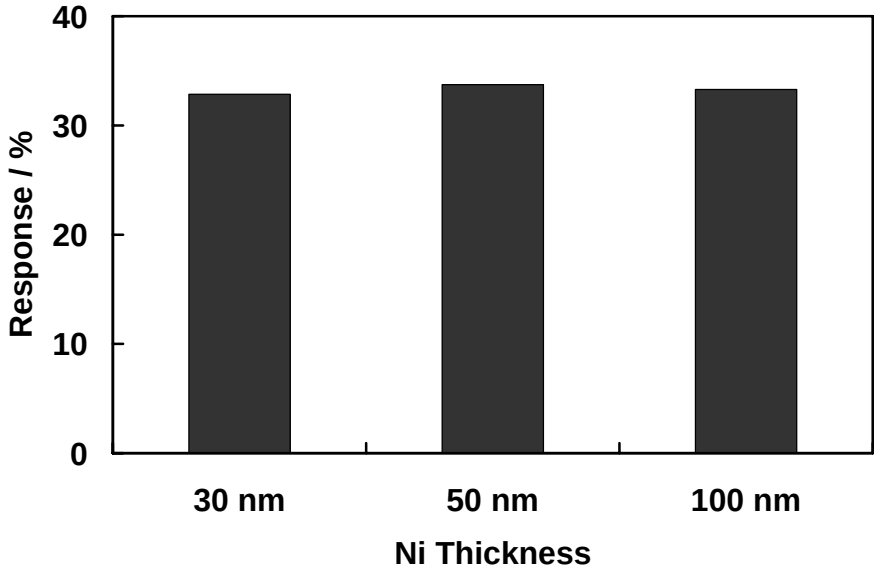

Fig. 3-6 Ni thickness vs. response (ΔC/C) to 200 ppm H_2 at 140˚C. Bias voltage = -0.4 V.

3.4 Conclusions:

A novel hydrogen sensor based on Ni/SiO_2/Si MOS capacitors were fabricated and characterized at hydrogen concentrations ranging from 50 ppm to 1000 ppm at an operating temperature of 140 ˚C. The highest response occurs at the same bias voltage (-0.4 V) for all the concentration levels measured and is about 18% at 50 ppm in nitrogen ambient. The response/recovery time of the Ni-based sensors is similar to that of the Pd-based hydrogen sensors. The proposed model based on the Langmuir isotherm is in good agreement with our experimental data. Influences of operating temperature and gate metal thickness on the device performance were also studied. The low-cost nickel-based hydrogen sensors showed the same sensing capability as Pd-based ones, suggesting that it is a promising low-cost alternative for hydrogen sensing in oxygen-free environments.

Reference for Chapter 3:

[1] I. Lundstrom, S. Shivaraman, C. Svensson, L. Lundkvist, A hydrogen-sensitive MOS field-effect transistor, Appl. Phys. Lett. 26 (1975) 55-57.

[2] H. E. Prakasam, F. Serina, C. Huang, G. W. Auner, L. Rimai, S. Ng, R. Naik, Palladium and aluminum gate metals/aluminum nitride/silicon balanced capacitors for selective hydrogen sensing, Mater. Res. Soc. Symp. Proc. 693 (2002) 687-692.

[3] A. Tibuzzi, B. Margesin, M. Decarli, C. D. Natale, M. Zen, A. D'Amico, G. Soncini, MOS-junction-based nanostructures by thermal oxidation of silicon wires for hydrogen detection, IEEE Trans. Nanotech. 3 (2004) 287-292.

[4] L. Zhang, E. F. McCullen, M. H. Rahmanb, J. S. Thakur, L. Rimai, R. J. Baird, R. Naik, G. Newaz, G. W. Auner, K.Y. Ng, Response to hydrogen of a metal/AlN/Si thin film structure: Effects of composition and structure of a combination Pd-Cr gate, Sens. Actuators B 113 (2006) 843–851.

[5] L. G. Petersson, H. M. Dannetun, J. Fogelberg, I. Lundstrom, Hydrogen adsorption states at the external and internal palladium surfaces of a palladium-silicon dioxide-silicon structure, J. Appl. Phys. 58 (1985) 404-413.

[6] I. Lundstrom, L. G. Petersson, Chemical sensors with catalytic metal gates, J. Vac. Sci. Tech. A 14 (1996) 1539-1545.

[7] J. H. Swisher, E. D. Johnson, Hydrides versus competing options for storing hydrogen in energy systems, J. Less-Common Metals 74 (1980) 301-320.

[8] H. Buchner, Perspectives for metal hydride technology, Prog. Energy Combustion Sci. 6 (1980) 331-346.

[9] M. H. Armbruster, The Solubility of Hydrogen at Low Pressure in Iron, Nickel and Certain Steels at 400 to 600°, J. Amer. Chem. Soc. 65 (1943) 1043-1054.

[10] F. N. Simon, D. Lichtman, T. R. Kirst, Study of the binding states of the hydrogen-100 nickel system, Surf. Sci. 12 (1968) 299-307.

[11] A. Stroka, B. Baranowski, Penetration Depth of Nickel Hydride into Nickel at Different Activities of Gaseous Hydrogen, Defect and Diffusion Forum 129-130 (1996) 305-307.

[12] J. Fogelberg, M. Eriksson, H. M. Dannetun, L. G. Petersson, Kinetic modeling of hydrogen adsorption/absorption in thin films on hydrogen-sensitive field-effect devices: Observation of large hydrogen-induced dipoles at the Pd-SiO2 interface, J. Appl. Phys. 78 (1995) 988-996.

[13] M. Eriksson, L. G. Ekedahl, The influence of CO on the response of hydrogen sensitive Pd-MOS devices, Sens. Actuators B 42 (1997) 217-223.

[14] M. Lofdahl, C. Utaiwasin, A. Carlsson, I. Lundstrom, M. Eriksson, Gas response dependence on gate metal morphology of field-effect devices, Sens. Actuators B 80 (2001) 183-192.

[15] Y. Morita, K. Nakamura, C. Kim, Langmuir analysis on hydrogen gas response of palladium-gate FET, Sens. Actuators B 33 (1996) 96-99.

[16] T. Eklov, H. Sundgren, I. Lundstrom, Distributed chemical sensing, Sens. Actuators B 45 (1997) 71-77.

[17] R. C. Hughes, R. Bastasz, W. P. Ellis, Hydrogen sensing in vacuum systems with catalytic field plate MNOS capacitors, Appl. Surf. Sci. 115 (1997) 74-79.

[18] K. Dobos, M. Armgarth, G. Zimmer, I. Lundstrom, The influence of different insulators on palladium-gate metal-insulator-semiconductor hydrogen sensors, IEEE Trans. Electron Devices ED-31 (1984) 508-510.

[19] I. Lundstrom, M. Armgarth, L. G. Petersson, Physics with catalytic metal gate chemical sensors, CRC Critical Rev. in Solid State Mater. Sci. 15 (1989) 201-278.

[20] H. M. Dannetun, L. G. Petersson, D. Soderberg, I. Lundstrom, A hydrogen sensitive Pd-MOS structure working over a wide pressure range, Appl. Surf. Sci. 17 (1984) 259-264.

[21] J. Fogelberg, L. G. Petersson, Kinetic modeling of the H_2-O_2 reaction on Pd and of its influence on the hydrogen response of a hydrogen sensitive Pd metal-oxide-semiconductor device, Surf. Sci. 350 (1996) 91-102.

[22] M. Formoso, G. Maclay, The effect of hydrogen and carbon monoxide on the interface state density in MOS gas sensors with ultra-thin palladium gates, Sens. Actuators B 2 (1990) 11-12.

[23] K. Ito, Hydrogen-induced interface traps in a palladium/very thin oxide/silicon structure, Sens. Mater. 11 (1999) 041-050.

Note: The substantial part of this chapter was published as a peer-reviewed journal paper:

Chi Lu, Zhi Chen, and Kozo Saito, Hydrogen sensors based on Ni/SiO_2/Si MOS capacitors, Sensors and Actuators B: Chemical, 122 (2007) 556-559.

Chapter 4 - High-temperature resistive hydrogen sensor based on thin nanoporous rutile TiO_2 film on anodic aluminum oxide

4.1 Introduction:

The sensing and monitoring of hydrogen leakage is an indispensable issue for hydrogen fuel cells [1]. Durable hydrogen sensors working at elevated temperatures with high sensitivity and fast response are always desired, while appropriate compatibility to micro-fabrication is also highly preferred.

During the past few years, hydrogen sensors based on the n-type titanium oxide (TiO_2) films with the thickness of microns or sub-microns have been studied extensively [2-14]. Among these reported devices, films composed of either self-organized TiO_2 nanotube arrays [8-12] or nano-scaled TiO_2 porous structures [6-7, 13-14] are proved to have much higher sensitivities over bulk films. The sensing principle is always based on the significant and abrupt change in resistance [6-14]. Most of such nano-porous devices are fabricated on Ti metal plate or foil, and the top TiO_2 is prepared by anodisation followed by sintering at elevated temperatures. The major or functional component of the TiO_2 films obtained by this method is anatase, a meta-stable phase of TiO_2, which gradually converts into rutile, the preferred polymorph of TiO_2, at above 430°C for nanotubes [15] or 465°C~525°C for nano-crystallites growing over the size of 14 nm [16]. Doping inhibitors into the anatase phase (e.g., P_2O_5 [17]) is only able to reduce the rate of the transformation. Due to this reason, most of the TiO_2 nanotube sensors were characterized

at below 400°C [8-12]. Therefore, for hydrogen detections at temperatures over the onset point of the anatase-to-rutile transformation, the durability becomes a problem. Furthermore, the metal substrate (Ti foil) is not a durable material due to its high chemical activity at elevated temperatures.

Although it had been found that porous films with rutile as the major phase are sensitive to hydrogen [6], the sensitivity was quite low [14] or even null [4], especially at above 400°C [4, 6, 14]. Jun et. al. [18] reported rutile-phased sensors prepared by thermal oxidation, with high sensitivity and swift response. However, the substrate was still a titanium metal plate, which can be further oxidized or electrically shorted. The operating temperature was also limited to less than 300°C. Therefore, the advantage of the rutile-phased sensor (thermal stability) was not demonstrated.

Another major disadvantage of the above Ti-metal-based devices is the difficulty in size-shrinking, due to the millimeter-scaled metal substrate. In addition, the oxide/metal interface is vulnerable to stress. Cracks are easily formed, causing mechanical failure. On considering these problems, fabrication of a nanometer-thick TiO_2 film on a stiff and durable substrate with good adhesion, which is resistant to thermal and/or mechanical stress, is very important for robust hydrogen-detection devices operating at high temperatures.

In the last fifty years of the past century, anodic aluminum oxide (AAO) under certain preparation conditions was found to have a nano-sized, self-organized, hexagonal porous

structure [19-24], and the preparation methods of AAO on non-conductive substrates (e.g., silicon wafer with a native/thermal oxide layer on top) have been refined during the last ten years [25-27]. AAO films prepared by anodization of aluminum metal films coated on durable substrates were used as supporting substrates in H_2 gas detection [28-30] due to their large specific surface area. With a thick barrier layer at the bottom of the pores, the AAO porous structure and AAO/substrate interface are almost invincible to thermal or even mechanical shocks. In addition, the process for AAO is quite compatible to micro-fabrication, and therefore has little difficulty for applications in integrated optic and electronic technologies [31-32]. All the advantages of AAO make it possible to be used as a platform for thin film sensors [28].

In this study, we will present fabrication, characterization, and performance of hydrogen sensors based on very thin rutile-phased TiO_2 films supported by porous AAO and plain silicon oxide, operating at 500°C. The effect of film thickness and the selectivity over other reducing gases than hydrogen will be investigated. Also, possible sensing mechanism will be discussed.

4.2 Experimental:

The preparation of AAO started from a commercial (100) silicon wafer with a 300 nm-thick thermal silicon oxide on the surface, which was coated with a 2.2 μm aluminum metal layer through e-beam evaporation. A two-step anodization procedure was used, in which anodization was performed on an Al metal layer in a 0.3 M oxalic aqueous

solution under a bias voltage of 40 V, with a platinum plate served as the cathode. The anodization details were described in several previous studies and reviews [23, 26, 33-34]. Until the Al metal layer was completely converted into porous Al_2O_3, the sample was rinsed by de-ionized water and then immersed in a 0.6 M phosphoric acid solution for 25 min. at room temperature for pore widening [35].

After rinsing in de-ionized water again and drying, the AAO samples, along with the bare thermal oxide substrates (300 nm-thick, grown on commercial (100) silicon wafers), were both coated with 25 nm, 50 nm, and 100 nm titanium metal layer through e-beam evaporation. Then the samples were oxidized and sintered at 600ºC for 6 h in oxygen with a flow rate of 200 ml/min. After sintering, the crystal phase of the oxidized layer was examined by a Siemens D500 X-ray diffactometer (Source: Cu-Kα). A Hitachi S-9300 scanning electron microscope was used to study the surface morphology of the samples.

Platinum was used as the electrode material of the samples, due to its chemical inertia. Two Pt electrodes arranged in an interdigit configuration were fabricated on the oxidized and sintered TiO_X film for all the samples. The spacing between digits of the two electrodes is 5 μm, as shown in Fig. 4-1. All the samples were equipped with the same number of digits by photolithography. However, the electrodes and digits of the samples based on plain SiO_2 substrates experienced sizeable damages (peeling-off) during the lift-off of the photoresist (will be mentioned later).

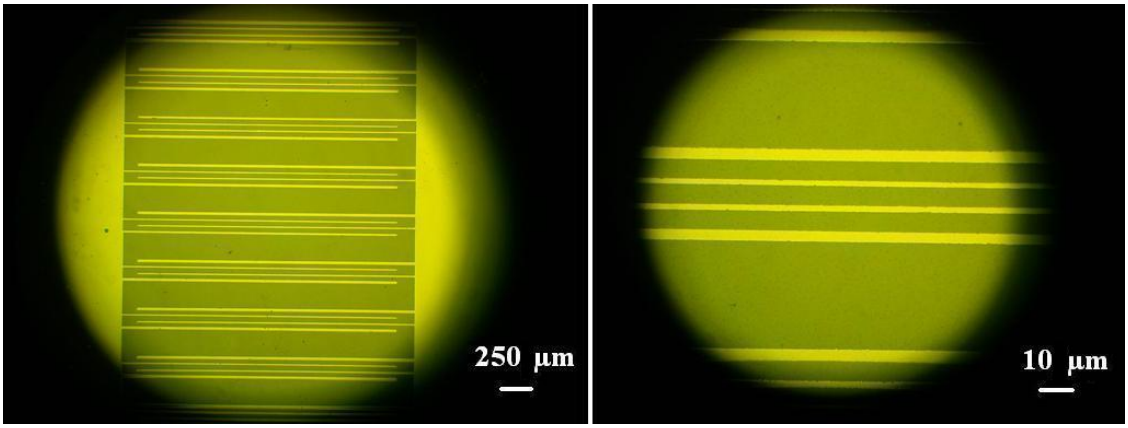

Fig. 4-1 Photos of a finalized sample with the TiO_X film converted from 25 nm-thick Ti on top of the porous AAO substrate, under an optical microscope. The shining regions are the coated platinum. Two large Pt areas were connected to the digits in order to make electrical contacts. The distance between these two large contact areas is about 2 mm, while the spacing between two neighboring digits is only 5μm. The right one has a higher magnification.

The entire procedure for fabricating the samples based on porous AAO substrates is illustrated in Fig. 4-2. For the samples based on plain SiO_2 substrates, the preparation procedures just include the last three steps of that in Fig. 4-2.

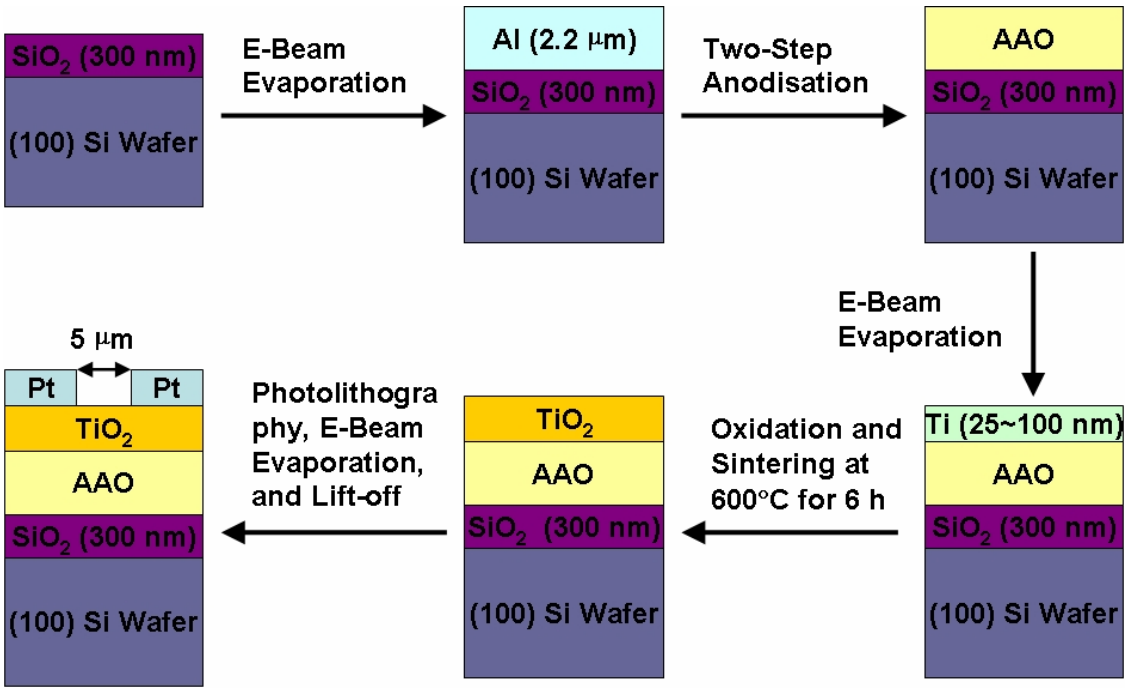

Fig. 4-2 Fabrication steps for preparation of porous AAO, thin TiO_2 film, and Pt electrodes.

Resistance measurements at different hydrogen concentration levels (5 ppm-500 ppm), as well as 50 ppm carbon monoxide and 2000 ppm methane, were performed using an MASTECH M3900 multimeter at elevated temperatures. Nitrogen was used as the background gas. Both of the absolute change of conductance ($\Delta G=G_g-G_0$, where G_0 is the conductance in pure nitrogen ambient, G_g is the stabilized conductance at an applied hydrogen concentration level) and the relative change of conductance ($\Delta G/G_0$) at different hydrogen concentration levels will be used to define the sensor responses in this presentation.

4.3 Results and discussion:

The surface morphologies of the titanium oxide films on all processed substrates were shown in Fig. 4-3, as well as the original substrates. It is noticeable that the oxidized layers from the e-beam-evaporated titanium have been shaped by the porous AAO substrates (Fig 3 (b) to and Fig. 4-3 (c)). Considering that the sample of Fig. 4-3(b) has the same initial thickness of titanium (25 nm) as the sample of Fig. 4-3 (f), it is reasonable to speculate that the oxidized film on the porous AAO from 25 nm-thick Ti holds much larger specific surface area than that based on the plain SiO_2 substrate. Same assumption can be drawn by comparing Fig 3 (c) to Fig. 4-3 (g), samples with identical thickness of Ti (50 nm) before oxidation but on different substrates. Another substantial feature of the morphologies of samples based on porous AAO is the influence of thickness on the specific surface area. From Fig. 4-3 (b) to Fig. 4-3 (d), as the oxide becomes thicker, the diameter of the pores shaped by the AAO underneath shrinks,

reducing the specific surface area. For the oxidized film from 100 nm-thick Ti on AAO (Fig. 4-3 (d)), the pores are completely blocked from the top. However, the rough shape of the AAO substrate is still visible in Fig. 4-3d and the surface morphology is quite different from those based on plain SiO_2 (Fig. 4-3 (f) to Fig. 4-3 (h)). Fig. 4-3 (f), Fig. 4-3 (g), and Fig. 4-3 (h) show similar surface morphology although the thicknesses are different.

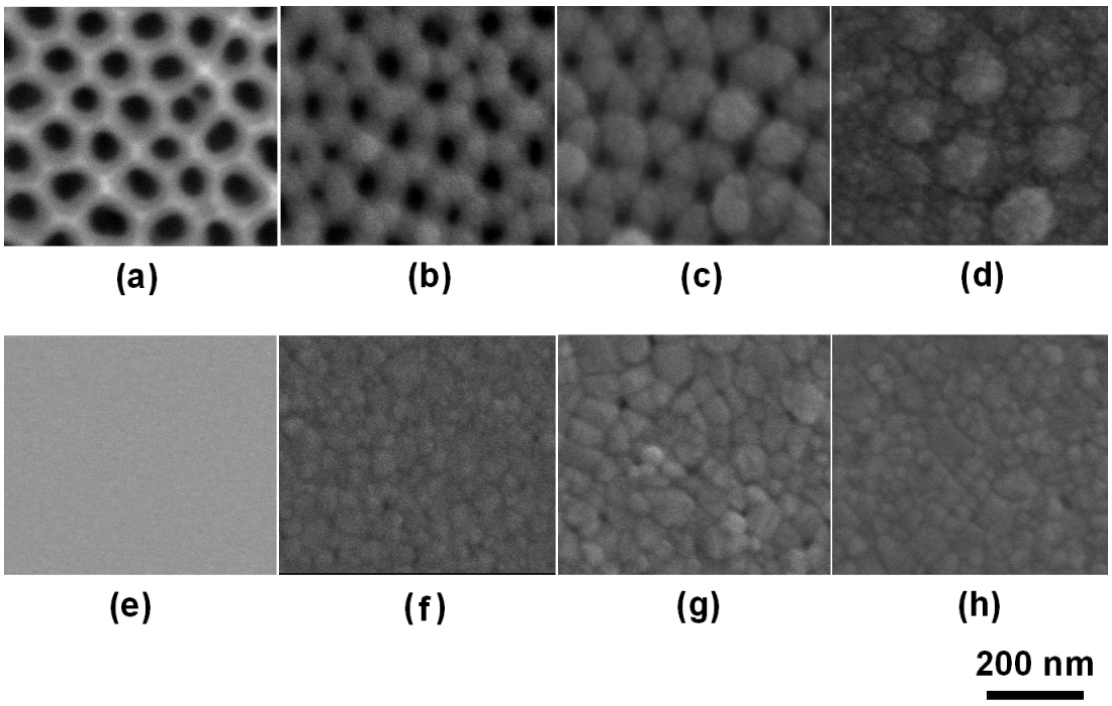

Fig. 4-3 SEM images of surface morphologies: (a) the original porous AAO substrate, (b) oxidized from 25 nm Ti on AAO, (c) oxidized from 50 nm Ti on AAO, (d) oxidized from 100 nm Ti on AAO, (e) the original plain SiO_2 substrate, (f) oxidized from 25 nm Ti on SiO_2 (g) oxidized from 50 nm Ti on SiO_2, and (h) oxidized from 100 nm Ti on SiO_2. All the samples are sintered at 600°C for 6 h in flowing oxygen.

Fig. 4-4 shows the XRD spectra for the oxide films prepared by oxidizing Ti metal layers with thicknesses of 25 nm, 50 nm and 100 nm on porous AAO substrates at 600ºC for 6 h in oxygen with a flow rate of 200 ml/min. There are two significant peaks at about 27.5° and 36° and one wide peak around 33.5° in all the three samples, as well as an additional significant peak at about 54.5° for the thickest oxide film only. Considering the wavelength of the incident X-ray is 1.54 Å (Cu-Kα), we can figure out through Bragg's Law by referring to the lattice constants of all possible crystals on the surface [36]. All the peaks, but the wide one around 33.5° that represents the silicon (200) plane (because the porous AAO layer is based on a commercial (100) Si wafer), are corresponding to the lattice planes of rutile. Therefore, the metallic Ti layers were completely transformed into TiO_2 and rutile was the only observable phase in the TiO_2 films. This is in agreement with previous studies [18, 37, 38, 39], in which rutile was the main product of high-temperature thermal oxidization of Ti metal. It is believed that nano-crystalline anatase with a size smaller than ~14 nm is thermodynamically more stable than rutile under the same size limit [40]. However, the coarsening of anatase is a fast process at elevated temperatures and the anatase crystallites convert to rutile rapidly as long as the size exceeds ~14 nm [16, 40]. Although anatase may have existed during the initial stage of the oxidation process at 600°C, the long-time sintering (6 h) made the crystalline grains grow and no anatase was detected in the final product.

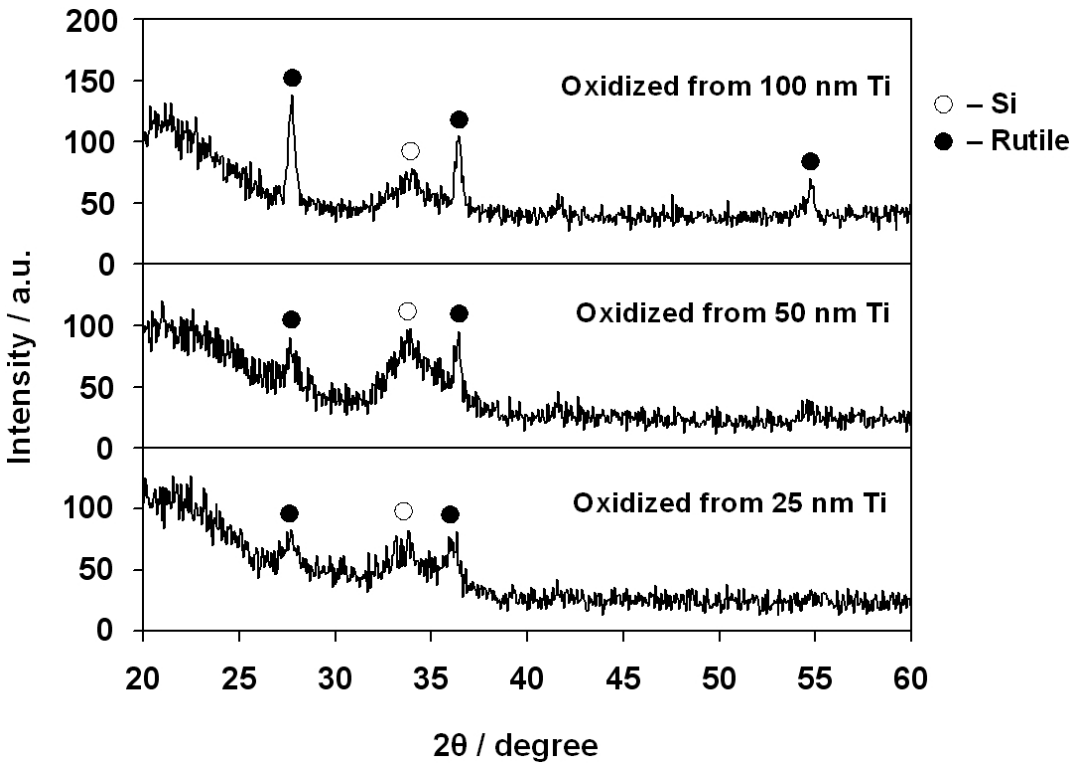

Fig. 4-4 XRD spectra of TiO_2 films that were converted from 25 nm, 50 nm, and 100 nm Ti metal layers on porous AAO substrates. The as-deposited metal layers were processed at 600°C for 6 h in oxygen with a flow rate of 200 ml/min.

Response transients of the TiO_2 film oxidized from 25 nm Ti on AAO at 500°C are shown in Fig. 4-5, the H_2 concentration ranges from 5 ppm to 500 ppm. The baseline conductance, at which no hydrogen was introduced but only pure nitrogen was in the ambient, was found to be ~7 μS or ~142 KΩ. This means the resistivity of the TiO_2 film oxidized from 25 nm-thick Ti on AAO at 500°C in pure N_2 can be roughly estimated to be 12.2 KΩ·cm, assuming the device accommodates 90 TiO_2 strips with the width of 5 μm and the length of 0.19 cm among the Pt digits and the volume expansion from Ti to TiO_2 can be neglected (the density for Ti is 4.51 g/cm^{-3} and 4.23 g/cm^{-3} for TiO_2 single crystal). However, this is a quite sketchy approximation of the resistivity of the converted TiO_2 thin film, the volume expansion resulting from the oxidation, the dimension of the Pt/TiO_2 contacts (not point contacts but strips with the width of 1.5~3 μm, as shown in Fig. 4-1), the porous shape of the film, and the loose texture of the polycrystalline TiO_2 should be carefully considered in order to compute an accurate value.

According to Fig. 4-5, the conductance change due to the introduction of 5 ppm-500 ppm hydrogen is about 25~90 times. For example, at a hydrogen concentration level of 50 ppm, the stabilized conductance is ~0.35 mS, thus the change from the baseline is around 50 times (see Fig. 4-6 for details). Although it is less than that of some reported anatase-phased TiO_2 sensors with a resistance drop of 10^3~10^4 times upon introduction of 100 ppm H_2 [9, 14], this sensitivity is large enough. More importantly, the data in Fig. 4-5 was obtained from a rutile-phased sample, supported by an insulating substrate which is more robust and durable. The conductance increased rapidly upon the introduction of hydrogen. For all the H_2 concentration levels measured in Fig. 4-5, the time delay to

reach 50% of the platform conductance ($t_{50\%}$) was always about 5~10 s. The recovery was quicker than the response ($t_{50\%}$≤5 s) for all concentration levels, indicating a quite fast removal of hydrogen from the device.

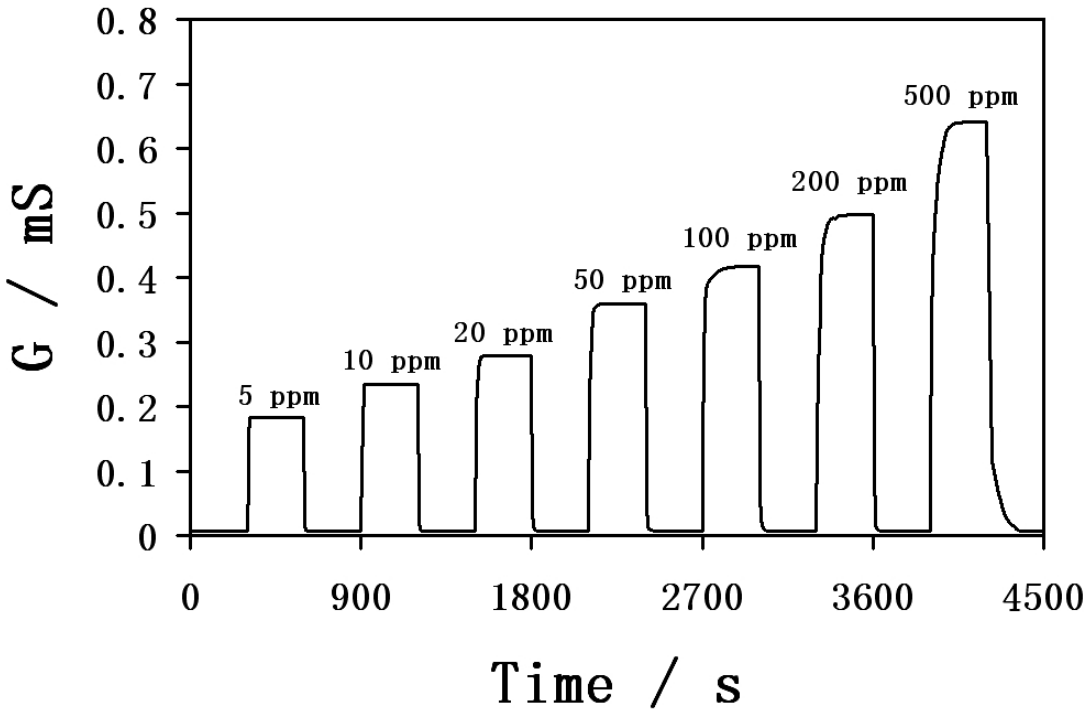

Fig. 4-5 Response transients to 5 ppm, 10 ppm, 20 ppm, 50 ppm, 100 ppm, 200 ppm, and 500 ppm H_2 of the TiO_2 film oxidized from 25 nm Ti supported on AAO. The operating temperature was 500°C.

The influence of specific surface area on H_2 response can be demonstrated by comparing Fig. 4-6 with Fig. 4-3. Since the TiO_2 film converted from 25 nm Ti on AAO (Fig. 4-3 (b)) has the thinnest thickness and largest pores among all the TiO_2 films shown in Fig. 4-3, it is no doubt that this thin film holds the largest specific surface area. In Fig. 4-6, the relative change of conductance ($\Delta G/G_0$) of this sample (TiO_2 film converted from 25 nm Ti on AAO) is also the largest. The $\Delta G/G_0$ of the TiO_2 film oxidized from 50 nm Ti (surface morphology shown in Fig. 4-3 (c)) on AAO is weaker than that of the film converted from 25 nm Ti on AAO, indicating a reduction in specific surface due to the increasing thickness and the shrinkage in the diameter of the nano-sized pores on the film. As the original Ti film becomes even thicker (100 nm), the pores on the TiO_2 film shaped by the AAO substrate are totally blocked (Fig. 4-3 (d)), and the specific surface area drops significantly, resulting in a much weaker $\Delta G/G_0$ to hydrogen than the previous two samples mentioned in this paragraph. Therefore, the surface morphology plays an important role in the response magnitude of the rutile-phase TiO_2 thin film on AAO. This is in agreement with previous studies, in which surface area is a major factor that determines the response magnitude to gases of metal-oxide films, such as TiO_2 [6], SnO_2 [41], ZrO_2 [42], and, WO_3 [43].

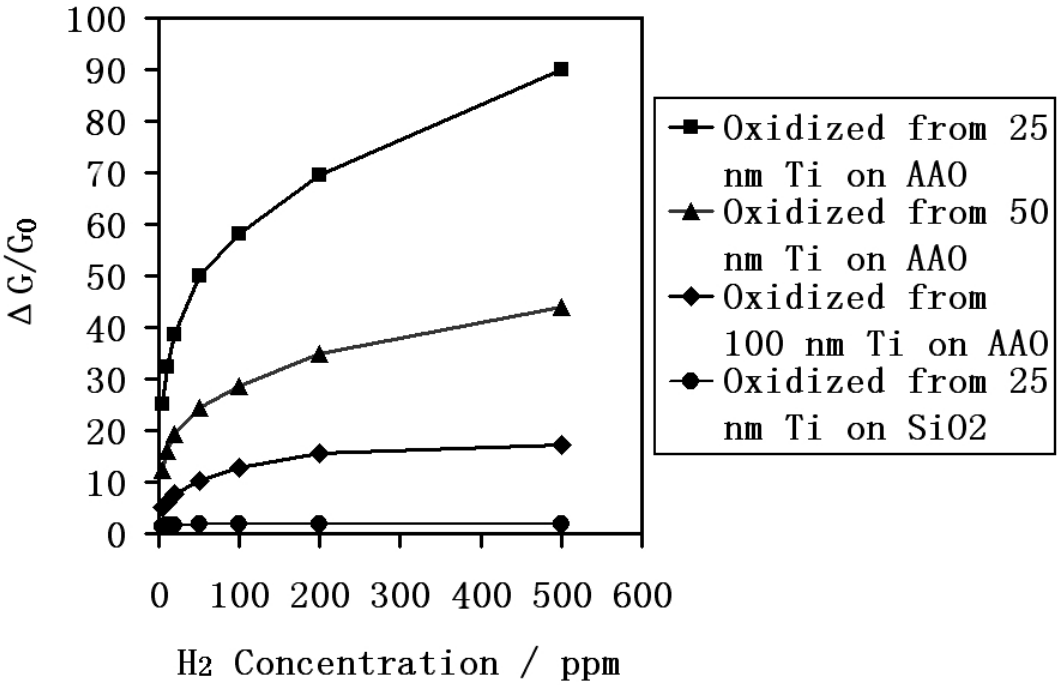

Fig. 4-6 Relative changes of conductance ($\Delta G/G_0$) to 5 ppm-500 ppm hydrogen gas of samples based on various TiO_2 thicknesses as well as different substrates. The operating temperature was 500°C for all the samples.

The very weak response of the film oxidized from 25 nm Ti based on plain SiO_2 should be attributed to both the lack of surface area (Fig. 4-3 (f)) and the partial peeling-off of the Pt electrodes during the fabrication. Actually the Pt electrodes on this sample suffered more peeling-off in the high-temperature (500°C) measurement environment. This destruction of the already damaged electrodes had further degraded the performance. The very weak response and the vulnerability of the electrodes suggest that TiO_2 oxidized directly on a plain SiO_2 surface, is not suitable for high-temperature hydrogen detection. The relative changes of conductance of thicker oxide films (converted from 50 nm and 100 nm Ti) supported by the plain SiO_2 are even weaker than that of the film oxidized from 25 nm Ti on SiO_2.

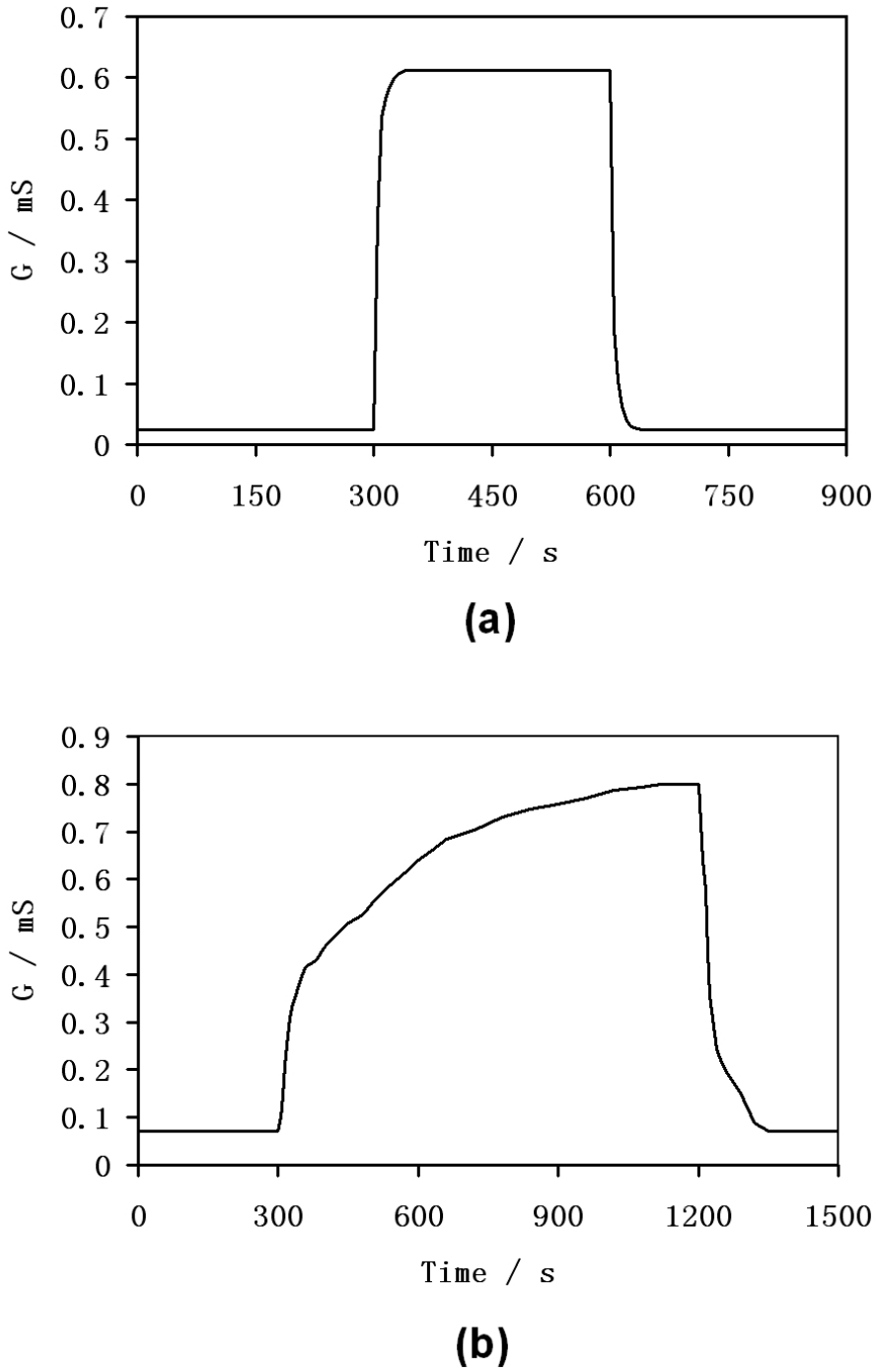

Fig. 4-7 Transient responses to 50 ppm H_2 for AAO-based samples with different TiO_2 thickness: (a) converted from 50 nm Ti, (b) converted from 100 nm Ti. Operating temperature: 500°C.

Typical response transients of the AAO-based TiO_2 film converted from 50 nm and 100 nm Ti are shown in Fig. 4-7. The sample based on the film oxidized from 100 nm Ti on AAO showed not only quite weak response magnitude (Fig. 4-6), but also slow transient rates. As summarized in Fig. 4-8, in response to 50 ppm H_2, the time delay to reach 50% of the platform conductance ($t_{50\%}$) after the introduction of hydrogen of this sample is as long as 84 s, which is several times of those of the thinner films (5 s). The recovery time (time delay to retreat to 50% of the platform conductance after the shut-off of hydrogen) of the thickest film (100 nm-Ti-converted) is 21 s, which is also much longer than those of the thinner films (3 s for the film oxidized from 25 nm Ti, 4 s for that from 50 nm Ti). This phenomenon, in which TiO_2 surfaces with poor specific surface area show slow transient rates, has been noticed in previous studies [18, 44]. A reasonable explanation is that the nano-scaled geometrical flaws on the TiO_2 surface produce an enhanced catalysis effect that accelerates the adsorption of H_2 or derivatives of H_2. According to the theory constructed for surface chemical reactions long time ago [45], the reaction rate is directly determined by the surface density of active sites, which increases with the specific surface area. Therefore, large specific surface area results in fast response.

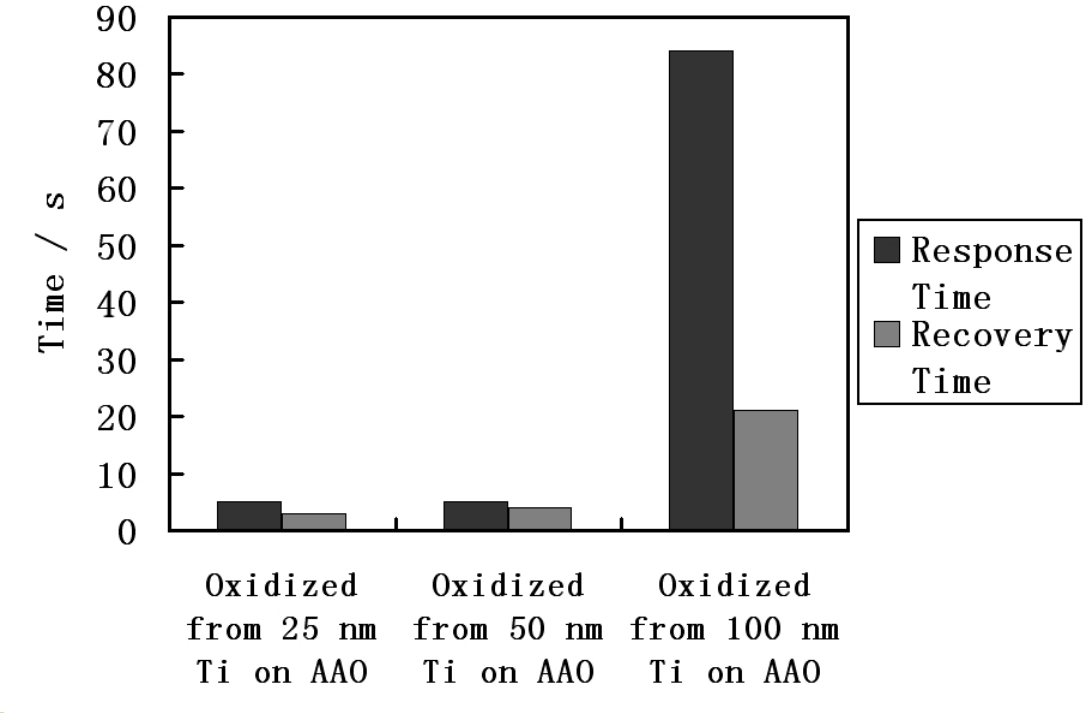

Fig. 4-8 Response and recovery times in terms of $t_{50\%}$ for TiO_2 films with different thicknesses supported by AAO.

The response transients of the sample based on oxidizing 25 nm-thick Ti on AAO to 50 ppm carbon monoxide and 2000 ppm methane are shown in Fig. 4-9. By summarizing the relative changes of conductance in Fig. 4-10, it can be seen straightforwardly that the sample is also very sensitive to carbon monoxide. At 50 ppm CO, the relative change of conductance is about 23 times, nearly half of the $\Delta G/G_0$ in response to H_2 at the same concentration level (around 50 times, see Fig. 4-5 and Fig. 4-6). Whereas the selectivity to methane is quite high, the relative conductance change in response to 2000 ppm CH_4 is approximately as low as 3 times.

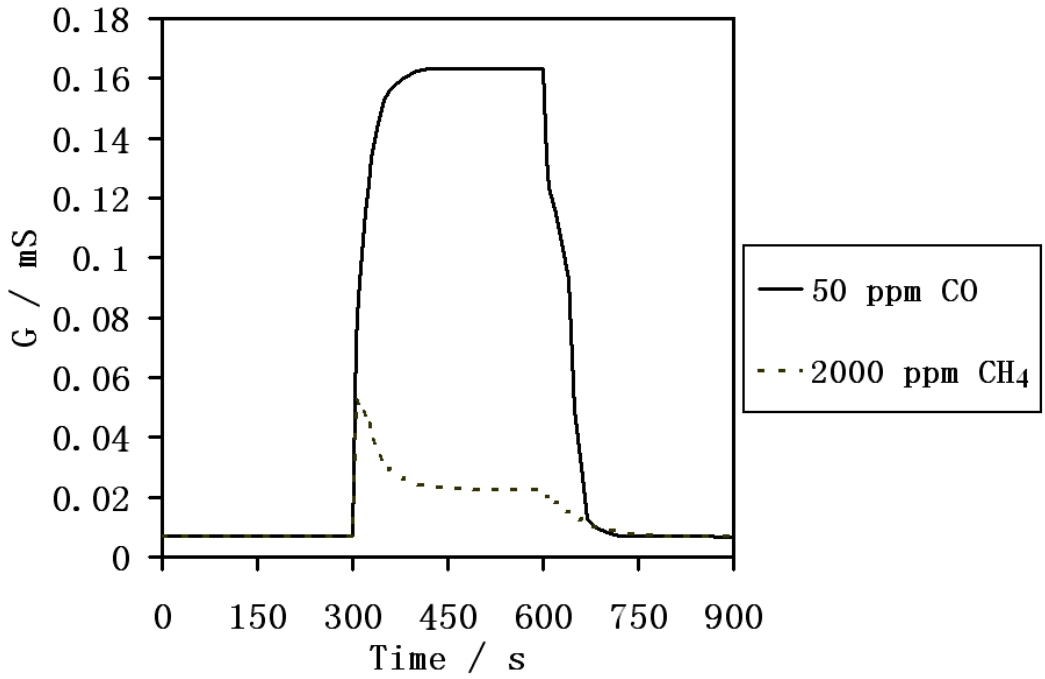

Fig. 4-9 Response transients to 50 ppm CO and 2000 ppm CH_4 of the AAO-based TiO_2 film converted from 25 nm Ti. Operating temperature was 500°C and the background gas was N_2.

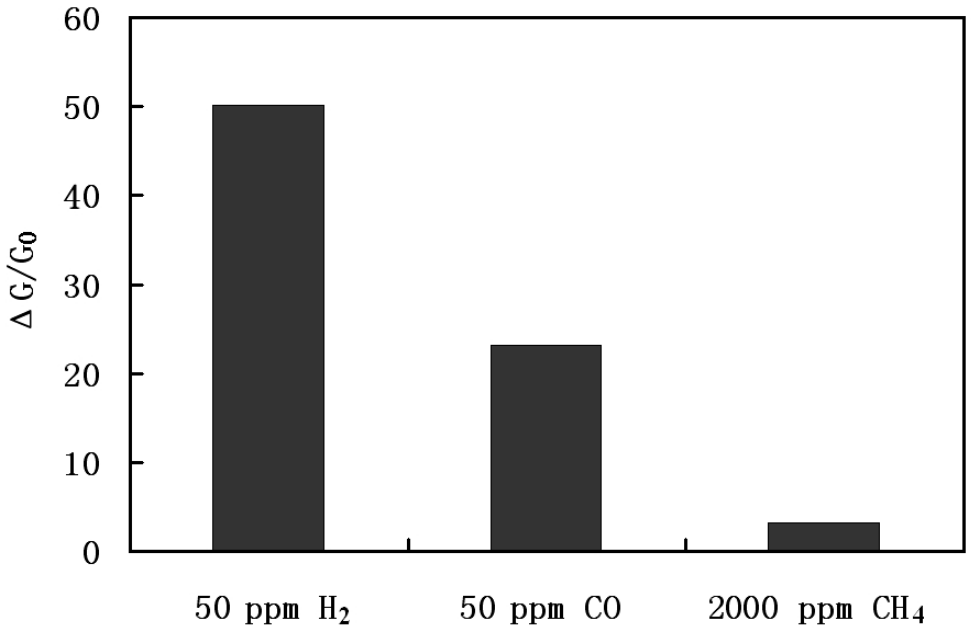

Fig. 4-10 Relative changes of conductance of the TiO_2 film oxidized from 25 nm Ti on AAO in response to 50 ppm H_2, 50 ppm CO, and 2000 ppm CH_4.

The resistance of the TiO_2 films fabricated in this presentation increased upon the introduction of oxygen, and the recovery took very long time (up to hours) after the shut-off of oxygen. With synthetic air as the background gas, all the samples showed null response to hydrogen. This phenomenon has been observed in previous studies [8, 18].

The sensing mechanism of anatase-phased TiO_2 nanotube has been studied rather thoroughly [8, 9]. The large, fast, and reversible response is attributed to a "spill-over" mechanism, in which hydrogen molecules are adsorbed onto the platinum electrodes, dissociating into atoms or even protons, and finally spill out of the Pt, diffusing into the surface layer of the TiO_2. Once the active hydrogen atom is chemically adsorbed at the interstitial positions in the oxide lattice structure, partial electron charge is transferred to the n-type TiO_2 and the conductance increases rapidly [46]. Also, the adsorption of hydrogen atoms is enhanced by the large specific surface area [9].

It is reasonable to consider the sensing principle of the sensors presented in this paper as a spill-over mechanism as well, due to the considerable resistance drop and the swift response transients (Fig. 4-5), as well as the enhanced relative change of conductance (Fig. 4-6) and accelerated transient rates (Fig. 4-7, Fig. 4-8) by the enlarged specific surface area. The swiftness of the transients indicates that the change of conductance is primarily from the partial charge transfer from/to the chemically adsorbed hydrogen atoms but not electrons transfer from/to the totally ionized hydrogen atoms (protons), which causes severe hysteresis due to the slow ionization process. Since the background gas is pure nitrogen and the conductance reaches full recovery, the "oxygen-removal"

mechanism [47], involving desorption of the oxygen adsorbates on the oxide surface by combination with hydrogen to form water ($O_{ad}+2H_{ad}\rightarrow H_2O$), is definitely not applicable. Furthermore, the fast and reversible response has ruled out the possibility of hydrogen reduction of Ti^{4+} into Ti^{3+} [48].

The null response in air was ascribed to the re-oxidation of the TiO_2 lattice by Varghese, et al [8]. Furthermore, the Pt thin-film electrode itself is a catalyst for hydrogen-oxygen combination [49], since the hydrogen concentration is quite low (ppm levels) and the background gas is 20% O_2 (synthetic air), it is very likely that the platinum surface is covered with adsorbed oxygen and hydrogen atoms or molecules are consumed very quickly before the spill-over occurs.

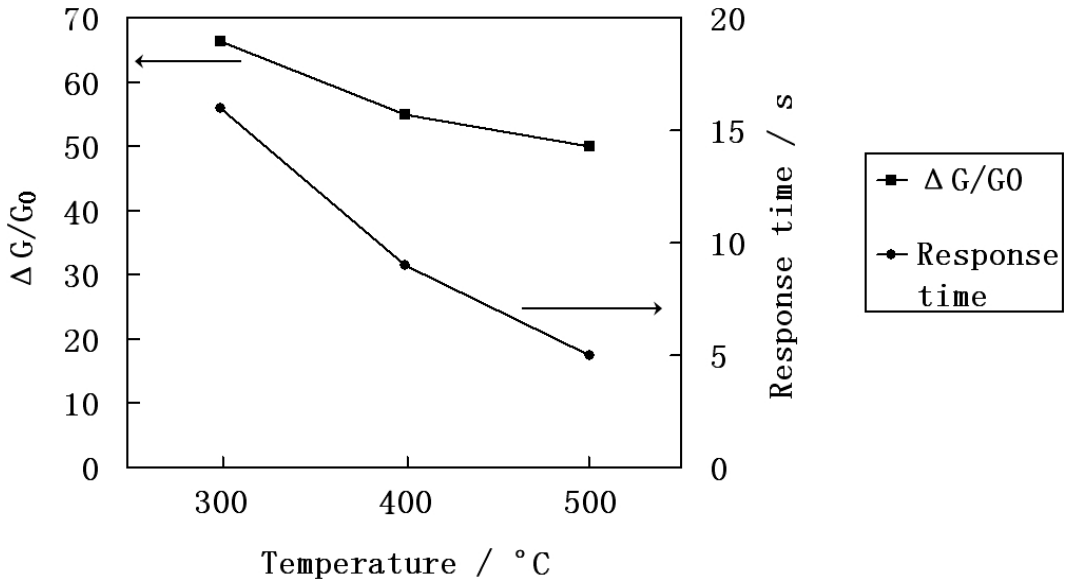

Fig. 4-11 Relative change of conductance and response time in terms of $t_{50\%}$ of the TiO_2 film oxidized from 25 nm-thick Ti at different operating temperatures, in response to 50 ppm H_2.

Fig. 4-11 shows the performance of the device based on the TiO_2 film converted from 25 nm-thick Ti in response to 50 ppm H_2 at 300°C, 400°C, and 500°C. It is found out that the magnitude of the response ($\Delta G/G_0$) is enhanced slightly as the operating temperature drops. In the upper curve in Fig. 4-11, $\Delta G/G_0$ increases about 30% as the operating temperature falls from 500°C to 300°C. However, the response rate becomes much slower at lower temperatures. At 300°C, $t_{50\%}$ is more than 3 times of that at 500°C (see the lower curve in Fig. 4-11). The enchantment in $\Delta G/G_0$ can be considered as a result of increased degree of hydrogen adsorption on the TiO_2 surface at low temperatures, while in the meantime, the surface reactions are severely retarded due to higher activation energies required at low temperatures and therefore $t_{50\%}$ is substantially prolonged. Based on the results in Fig. 4-11, higher operating temperatures are preferred for the device based on the TiO_2 film oxidized from 25 nm-thick Ti. The 30% decrement in response magnitude becomes trivial when comparing to the 3-time faster response rate, as the temperature increases from 300°C to 500°C.

4.4 Conclusions:

Hydrogen sensors based on TiO_2 films oxidized from e-beam-evaporated thin layers of metallic titanium on AAO were prepared through regular micro-fabrication steps. The specific surface area plays a key role in the sensing. Expanded specific surface not only significantly improves the relative change of conductance, but sharply increases the transient rates of response and recovery. The stable rutile phase, as well as the chemical stability and mechanical stiffness of the AAO, make it possible to fabricate durable high-

temperature hydrogen sensors, which are chemically and mechanically stable. The porous AAO surface also helps the adhesion of thin-film metal electrodes.

References for Chapter 4:

[1] J. Larminie, A. Dicks, Fuel Cell Systems Explained, 2nd Edition, John Wiley & Sons, Chichester, West Sussex, UK, 2003.

[2] L. D. Birkefeld, A. M. Azad, S. A. Akbar, Carbon Monoxide and Hydrogen Detection by Anatase Modification of Titanium Dioxide, J. Am. Ceram. Soc. 75 (1992), 2964-2968.

[3] H. Tang, K. Prasad, R. Sanjines, F. Levy, TiO_2 anatase thin films as gas sensors, Sens. Actuators B 26 (1995) 71-75.

[4] V. Guidi, M. C. Carotta, M. Ferroni, G. Martinelli, L. Paglialonga, E. Comini, G. Sberveglieri, Preparation of nanosized titania thick and thin films as gas-sensors, Sens. Actuators B 57 (1999) 197-200.

[5] I. Hayakawa, Y. Iwamoto, K. Kikuta, S. Hirano, Gas sensing properties of platinum dispersed-TiO_2 thin film derived from precursor, Sens. Actuators B 62 (2000) 55-60.

[6] Y. Shimizu, N. Kuwano, T. Hyodo, M. Egashira, High H_2 sensing performance of anodically oxidized TiO_2 film contacted with Pd, Sens. Actuators B 83 (2002) 195-201.

[7] H. Miyazakia, T. Hyodob, Y. Shimizua, M. Egashira, Hydrogen-sensing properties of anodically oxidized TiO_2 film sensors Effects of preparation and pretreatment conditions, Sens. Actuators B 108 (2005) 467-472.

[8] O. K. Varghese, D. Gong, M. Paulose, K. G. Ong, C. A. Grimes, Hydrogen sensing using titania nanotubes, Sens. Actuators B 93 (2003) 338-344.

[9] O. K. Varghese, D. Gong, M. Paulose, K. G. Ong, E. C. Dickey, C. A. Grimes, Extreme changes in the electrical resistance of titania nanotubes with hydrogen exposure, Adv. Mater. 15 (2003) 624-627.

[10] G. K. Mor, M. A. Carvalho, O. K. Varghese, M. V. Pishko, C. A. Grimes, A room-temperature TiO_2-nanotube hydrogen sensor able to self-clean photoactively from environmental contamination, J. Mater. Res. 19 (2004) 628-634.

[11] M. Paulose, O. K Varghese, G. K. Mor, C. A. Grimes, K. G. Ong, Unprecedented ultra-high hydrogen gas sensitivity in undoped titania nanotubes, Nanotechnology 17 (2006) 398-402.

[12] C. A. Grimes, Synthesis and application of highly ordered arrays of TiO_2 nanotubes, J. Mater. Chem. 17 (2007) 1451-1457.

[13] T. Mukherjee, S. K. Hazra, S. Basu, Porous titania thin films grown by anodic oxidation for hydrogen sensors, Mater. Manuf. Processes 21 (2006) 247-251.

[14] H. Kim, W. Moon, Y. Jun, S. Hong, High H_2 sensing performance in hydrogen trititanate-derived TiO_2, Sens. Actuators B 120 (2006) 63-68.

[15] O. K. Varghese, D. Gong, M. Paulose, C. A. Grimes, E. C. Dickey, Crystallization and high-temperature structural stability of titanium oxide nanotube arrays, J. Mater. Res. 18 (2003) 156-165.

[16] A. A. Gribb, J. F. Banfield, Particle size effects on transformation kinetics and phase stability in nanocrystalline TiO_2, Am. Mineral. 82 (1997) 717-728.

[17] B. Grzmil, B. Kic, M. Rabe, Inhibition of the anatase-rutile phase transformation with addition of K_2O, P_2O_5, and Li_2O, Chem. Pap. 58 (2004) 410-414.

[18] Y. Jun, H. Kim, J. Lee, S. Hong, High H_2 sensing behavior of TiO_2 films formed by thermal oxidation, Sens. Actuators B 107 (2005) 264-270.

[19] F. Keller, M. S. Hunter, D. L. Robinson, Structural features of oxide coatings on aluminum, J. Electrochem. Soc. 100 (1953) 411-419.

[20] C. J. L. Booker, J. L. Wood, A. Walsh, Electron micrographs from thick oxide layers on aluminium, Br. J. Appl. Phys. 8 (1957) 347-352.

[21] J. P. O'Sullivan, C. G. Wood, Morphology and mechanism of formation of porous anodic films on aluminum, Proc. R. Soc. London, Ser. A, Math. Phys. Eng. Sci. 317 (1970) 511-543.

[22] L. J. Lanzerotti, W. L. Brown, J. M. Poate, W. M. Augustyniak, Nucleation and growth of porous anodic films on aluminium, Nature 272 (1978) 433-435.

[23] H. Masuda and K. Fukuda, Ordered metal nanohole arrays made by a two-step replication of honeycomb structures of anodic alumina, Science 268 (1995) 1466-1468.

[24] A. P. Li, F. Muller, A. Birner, K. Nielsch, U. Gosele, Hexagonal pore arrays with a 50–420 nm interpore distance formed by self-organization in anodic alumina, J. Appl. Phys. 84 (1998) 6023-6026.

[25] T. Iwasaki, T. Motoi, T. Den, Multiwalled carbon nanotubes growth in anodic alumina nanoholes, Appl. Phys. Lett. 75 (1999) 2044-2046.

[26] W. Hu, D. Gong, Z. Chen, Growth of well-aligned carbon nanotube arrays on silicon substrates using porous alumina film as a nanotemplate, Appl. Phys. Lett. 79 (2001) 3083-3085.

[27] W. Hu, L. M. Yuan, Z. Chen, D. W. Gong, K. Saito, Fabrication and characterization of vertically aligned carbon nanotubes on silicon substrates using porous alumina nanotemplates, J. Nanosci. Nanotechnol. 2 (2002) 203-207.

[28] D. Ding, Z. Chen, C. Lu, Hydrogen sensing of nanoporous palladium films supported by anodic aluminum oxides, Sens. Actuators B 120 (2006) 182-186.

[29] D. Ding, Z. Chen, Volume-expansion-enhanced pinning of nanoporous Pd films for detection of high-concentration hydrogen, Sensor Letters 4 (2006) 331-333.

[30] D. Ding, Z. Chen, A Pyrolytic, Carbon-Stabilized, Nanoporous Pd film for wide-range H_2 sensing, Adv. Mater. 19 (2007) 1996-1999.

[31] P. Chen, C. Kuo, T. Tsai, B. Wu, C. Hsu, F. Pan, Self-organized titanium oxide nanodot arrays by electrochemical anodization, Appl. Phys. Lett. 82 (2003) 2796-2798.

[32] W. Yu, Y. Cho, G. Choi, D. Kim, Patterned carbon nanotube field emitter using the regular array of an anodic aluminium oxide template, Nanotechnology 16 (2005) S291-S295.

[33] H. Masuda, M. Satoh, Fabrication of gold nanodot array using anodic porous alumina as an evaporation mask, Jpn. J. Appl. Phys. 35 (1996) L126-L129.

[34] C. Lu, Z. Chen, Anodic aluminum oxide-based nanostructures and nanodevices in Encyclopedia of Nanoscience and Nanotechnology, H. S. Nalwa (Ed.), American Scientific Publishers, Stevenson Ranch, CA, US, 2009, in press, proof received.

[35] D. A. Mawlawi, N. Coombs, M. Moskovits, Magnetic properties of Fe deposited into anodic aluminum oxide pores as a function of particle size, J. Appl. Phys. 70 (1991) 4421-4425.

[36] W. F. McClune (Ed.), Powder Diffraction File: Inorganic Phases, Alphabetical Index, JCPDS International Center for Diffraction Data, Swarthmore, PA, US, 1987

[37] Y. Katsuta, R. Akahane, K. Yahagi, Electrical properties of rutile (TiO_2) thin film, Jpn. J. Appl. Phys. 10 (1971) 976-986.

[38] C. Ting, S. Chen, D. Liu, Structural evolution and optical properties of TiO_2 thin films prepared by thermal oxidation of sputtered Ti films, J. Appl. Phys. 88 (2000) 4628-4633.

[39] E. Lenarduzzi, P. Bounie, C. Schuman, M. J. Philippe, D. Petelot, Titanium oxidation during thermal treatment: inhibiting role of nitrogen and epitaxial orientation relations evidenced by EBSD, Adv. Eng. Mater. 5 (2003) 587-593.

[40] H. Zhang, J. F. Banfield, Thermodynamic analysis of phase stability of nanocrystalline titania, J. Mater. Chem. 8 (1998) 2073-2076

[41] G. -J. Li, X. -H. Zhang, S. Kawi, Relationships between sensitivity, catalytic activity, and surface areas of SnO_2 gas sensors, Sens. Actuators B 60 (1999) 64-70.

[42] T. Kida, K. Kawasaki, K. Iemura, K. Teshima, M. Nagano, Gas sensing properties of a stabilized zirconia-based sensor with a porous MoO_3 electrode prepared from a molybdenum polyoxometallate–alkylamine hybrid film, Sens. Actuators B 119 (2006) 562-569.

[43] G. Xie, J. Yu, X. Chen, Y. Jiang, Gas sensing characteristics of WO_3 vacuum deposited thin films, Sens. Actuators B 123 (2007) 909-914.

[44] S. V. Patel, K. D. Wise, J. L. Gland, M. Zanini-Fisherd, J. W. Schwank, Characteristics of silicon-micromachined gas sensors based on Pt/TiO_X thin films, Sens. Actuators B 42 (1997) 205-215.

[45] P. W. Atkins, Physical Chemistry, 7th Edition, W. H. Freeman, New York, NY, US, 2002.

[46] U. Roland, R. Salzer, T. Braunschweig, F. Roessner, H. Winkler, Investigations on hydrogen spillover: Part 1 - Electrical conductivity studies on titanium dioxide, J. Chem. Soc., Faraday Trans. 91 (1995) 1091-1095.

[47] G. C. Mather, F. M. B. Marques, J. R. Frade, Detection Mechanism of TiO_2-based Ceramic H_2 Sensors, J. Eur. Ceram. Soc. 19 (1999) 887-891.

[48] R. M. Walton, D. J. Dwyerc, J. W. Schwank, J. L. Glan, Gas sensing based on surface oxidation/reduction of platinum-titania thin films I. Sensing film activation and characterization, Appl. Surf. Sci. 125 (1998) 187-198.

[49] R. Dus, F. C. Tompkins, Mechanism of the hydrogen-oxygen reaction on platinum films from surface potential measurements, Proc. B. Soc. Lond. A. 343 (1975) 477-488.

Note: The substantial part of this chapter was published as a peer-reviewed journal paper:

Chi Lu and Zhi Chen, High-temperature resistive hydrogen sensor based on thin nanoporous rutile TiO_2 film on anodic aluminum oxide, Sensors and Actuators B: Chemical, 140 (2009) 109-115.

Chapter 5 - Highly hydrogen-sensitive SnO_2 nanoscale grain films with platinum electrodes

5.1 Introduction:

Use of tin dioxide (SnO_2) in detection of reactive gases can be traced back to 1960s [1]. Due to its high sensitivity and low operating temperature [2-3], SnO_2-based gas-sensing devices are more preferable over those based on other metal oxides (e. g., ZnO [4], WO_3 [5]), and in the last two decades of the 20th century there were abundant studies of SnO_2 gas-sensors [6-9].

Since early 1990s, nano-crystalline SnO_2 (doped or un-doped) has become a focus in gas-sensing studies due to its highly improved sensitivity [10-11]. Various shapes of nano-structured SnO_2, including nano-particle-based films [12-16], nano-wires [17-19], nano-belts [20-21], nano-rods [22], and self-assembled or pattern-transferred nano-porous structures [23-24], were fabricated and studied for their gas-sensing properties. Currently there are several fabrication approaches for preparation of nano-structured SnO_2 for gas detections, such as sol-gel [12-13, 15, 25-27], pyrolysis [28-30], sputtering [14, 31], chemical vapor deposition [32], rheotaxial growth and thermal oxidation (RGTO) [33-42], etc. Among these processes, RGTO, in which SnO_2 is formed by oxidizing metallic tin films deposited on certain substrates in dry environments, has an advantage in obtaining high aspect-ratio nano-structures [33, 42] and controlling the grain size distribution [35]. Since the SnO_2 particles obtained from the sub-micron-thick Sn film by RGTO are

distributed on almost a uniform plane [36] ("two dimensional"), the irreversible coarsening of the crystallites at elevated temperatures, which causes fast aging for those nano-particle-composed SnO_2 thick films ("three dimensional") [23], is substantially inhabited. Furthermore, the RGTO approach holds good compatibility to MEMS processes as well as industrial microelectronic technologies because no wet-chemical processes are used.

However, most of the reported SnO_2 devices prepared through RGTO were focused on NO_x or CO detection [33-34, 36-38, 40-41]. Although there were some studies concerning about H_2-sensing by RGTO-fabricated SnO_2 thin films, either the response magnitude was too low [42] as comparing to the micron-thick un-doped SnO_2 films consisting of nano-particles prepared by sol-gel or pyrolysis [25, 28], or the operation temperature is too high (e.g., 450°C-530°C [33]), or detailed sensing properties were absent [33, 35].

VIII group metals, especially platinum (Pt) and palladium (Pd), have been used as electrodes for hydrogen detectors for a long time due to their adsorption of hydrogen and capability of dissociating H_2 into atoms [43-46]. H_2 molecules adsorbed on the Pt or the Pd electrode surface are believed to break into hydrogen atoms which migrate into the metal bulk or even to the metal-oxide (*n*-type) contact, reducing the work function of the metal and therefore lowering the Schottky barrier height (SBH) at the metal/oxide interface. This effect has been studied and applied to develop hydrogen sensors based on Pd (or Pt)/SiO_2 MOS structures [47], as well as those based on Pd (or Pt)/TiO_2 (or SnO_2)

Schottky diodes [48-54]. Although fabrication of Pd (or Pt)/TiO_2 Schottky devices and their sensing properties to reactive gases were thoroughly investigated during the last two decades [49-51, 53-54], gas-sensing studies on Pt/SnO_2 diodes were much less frequently reported than the former. The research of gas-sensitive Pt/SnO_2 devices is focused on varistors [55-56], in which the sensing mechanism is not the reduction of the barrier height at the Pt/SnO_2 interface but the lowering of barriers between SnO_2 grains. In this paper, we present a novel Pt/SnO_2 Schottky junction-based hydrogen sensor with high sensitivity, fast response, and good selectivity at low concentrations of hydrogen. The thin films are composed of nano-sized SnO_2 grains converted from the electron-beam-evaporated metallic tin films on thermally oxidized silicon wafers.

5.2 Experimental:

The fabrication procedures are illustrated in Fig. 5-1. A (100) commercial silicon wafer was used as the substrate. Dry oxidation was performed on the wafer following a standard RCA cleaning, and the final thickness of the silicon oxide (SiO_2) was about 100 nm. The wafer was then cut into small pieces. Five pieces with approximately the same sizes were used as samples. Tin (purity 99.99%) was deposited on the samples with thicknesses of 5 nm, 10 nm, 20 nm, 50 nm, and 100 nm using electron-beam (e-beam) evaporation. The evaporation rate was kept in the range of 0.4 - 1.0 Å/s, and the chamber pressure was less than 5×10^{-6} torr. Thermal oxidation was performed on the evaporated Sn films at 200ºC for 2 h, then 400ºC for 2 h, and finally 600ºC for 8 h in pure oxygen with a constant flow rate of 200 ml/min. The ramp rate was 5ºC/min for all temperature

switches. The surface morphologies of the as-deposited Sn films and the oxidized films were studied using a Hitachi S-4300 field emission scanning electron microscope (FE-SEM) and a TI A-35 atomic force microscope (AFM). The crystalline phase of the oxidized films was determined by a Siemens D500 X-ray diffractometer. The source of the X-ray is Cu-Kα (λ=1.54Å).

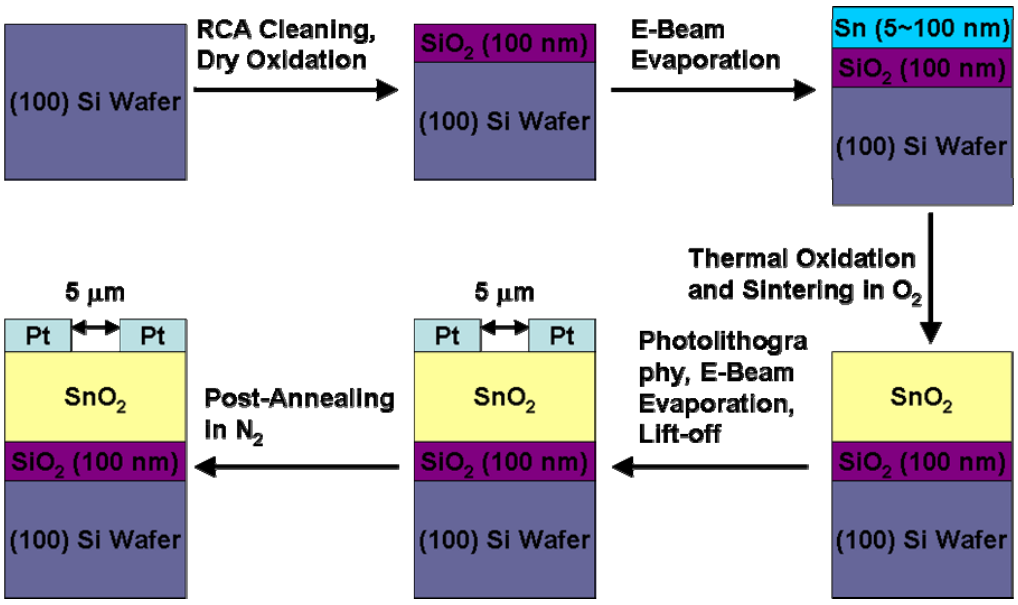

Fig. 5-1 Process flow of the fabrication procedure.

Interdigital platinum electrodes were fabricated on all the samples using e-beam evaporation and photolithography (Fig. 5-2). The thickness of the Pt layer was 60 nm and the electrode separation was 5 μm. The samples were annealed in pure nitrogen at 500ºC for 1 h before any sensing measurements were conducted. Fig. 5-2 shows a device under an optical microscope, for which the thickness of the as-deposited Sn film is 20 nm.

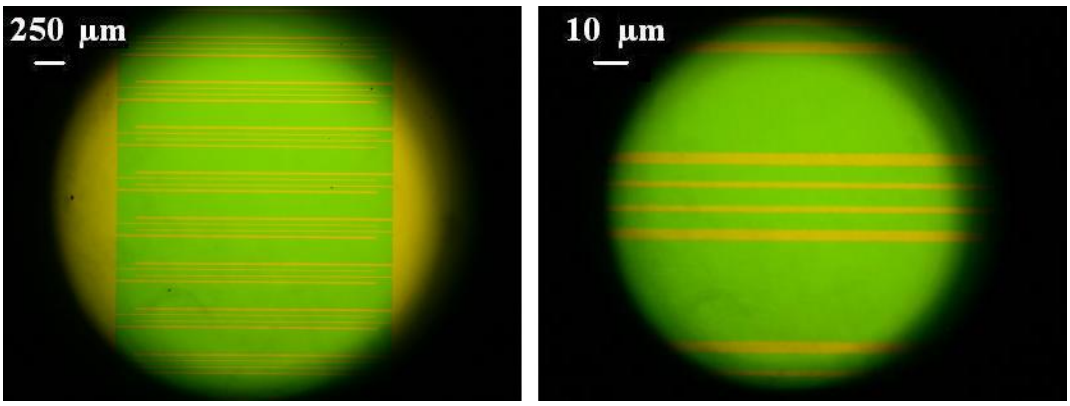

Fig. 5-2 Photos of devices with SnO_x film obtained from oxidation of a 20 nm-thick Sn film. Shining regions are Pt electrodes. The separation between neighboring Pt fingers is 5 µm. Higher magnification is applied to photo on the right.

Current-voltage (I-V) measurements at different H_2 concentration levels (10 ppm - 1000 ppm, balanced by nitrogen or synthetic air) were performed at 300ºC. Bias voltage levels ranging from ±0.2V to ±1.2V were applied to the Pt electrodes in Fig. 5-2 by a Hewlett Packard 6236B triple outlet power supply and the resulted current values were measured by a Mastech M3900 digital multimeter. Since both electrodes were Pt, the bias polarity was assigned arbitrarily. Cross-sensitivities of 100 ppm CO and 2000 ppm CH_4 were also tested. The relative response to H_2 is evaluated by I/I_0, where I_0 is the current intensity in pure N_2 and I is the current intensity in the tested gases under a certain bias voltage. The response/recovery transient rates are represented by $t_{50\%}$, which is the time delay to reach or retreat to half of the stable signal.

5.3 Results and discussion:

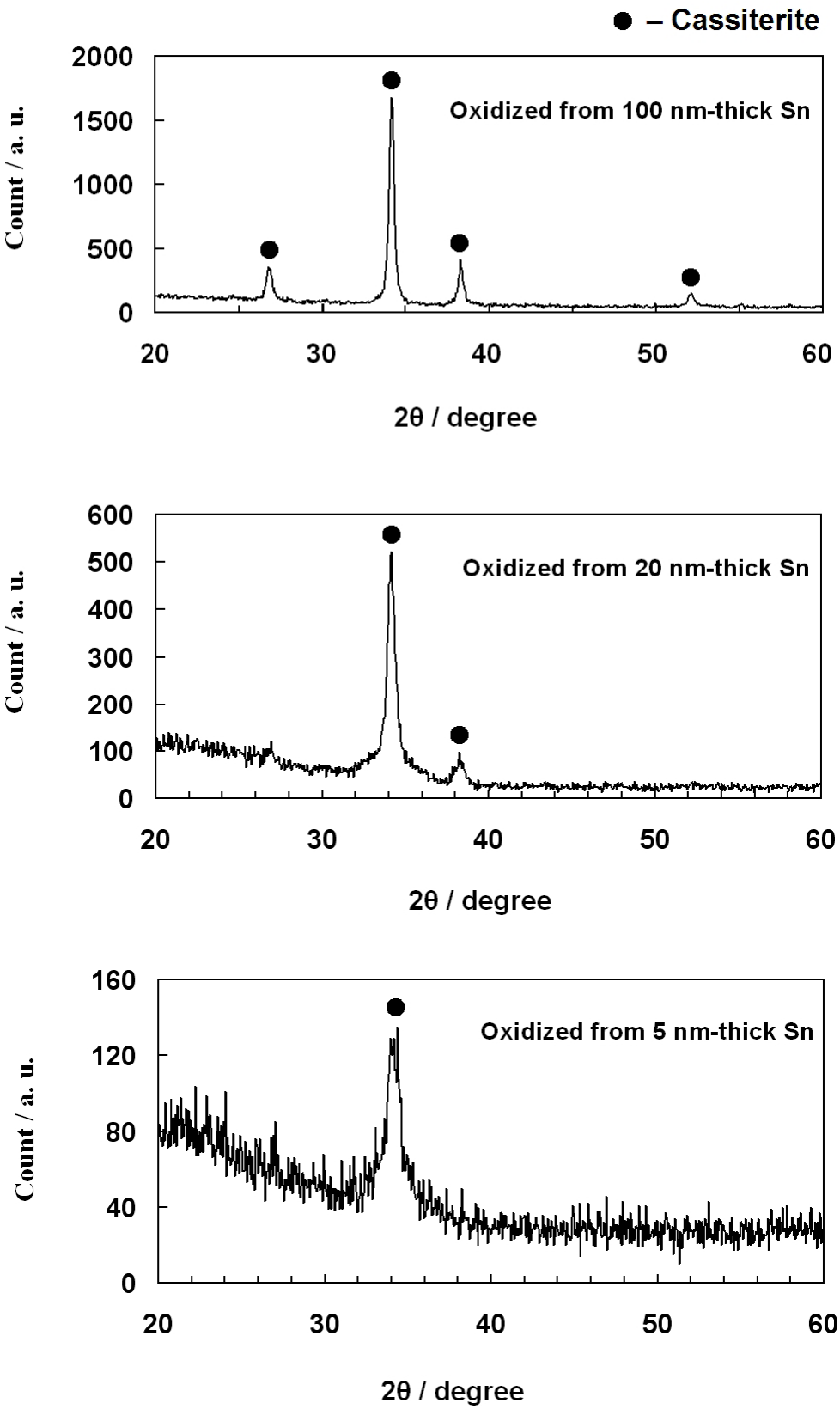
● – Cassiterite
Oxidized from 100 nm-thick Sn
Count / a. u.
2θ / degree
Oxidized from 20 nm-thick Sn
Count / a. u.
2θ / degree
Oxidized from 5 nm-thick Sn
Count / a. u.
2θ / degree

Fig. 5-3 XRD patterns of oxidized Sn films. The thickness of the as-deposited Sn film is 100 nm, 20 nm, 5 nm, respectively.

The X-ray diffraction (XRD) pattern of the oxidized Sn films is shown in Fig. 5-3. It can be seen that all peaks belong to cassiterite, a rutile-structured crystal phase of tin dioxide [57]. Therefore we may conclude that the e-beam deposited metallic Sn films were completely converted to SnO_2, and cassiterite is the only detectable crystal phase. Detailed studies on the thermal oxidation of evaporated Sn films showed that heating in oxygen at 600ºC for 8h is sufficient for oxidation of the entire 100 nm-thick Sn film [58-59]. Since the intensity of the peak of the silicon (200) plane (2θ value is around 33.5°, as we have seen Fig. 4-4) is very weak and the position is quite close to the large and strong cassiterite peak around 34°, the peak observed for Si in the XRD spectra of the TiO_2 films in Chapter 4 is indistinguishable in Fig. 5-3.

Fig. 5-4 shows the SEM images of both as-deposited Sn metal films and the SnO_2 films. Since the melting point of Sn is as low as 232°C [57], and the substrate holder was mounted very close to the evaporation source, the condensed thin layer grew predominantly in liquid-phase, agglomerating into nano-sized grains on the ultra-smooth silicon wafer substrate due to surface tension. It is also observed that under the same evaporation conditions, the Sn grain size shrinks as the film thickness decreases. Furthermore, for thicker films, there were observable small particles in the intergranular regions (Fig. 5- 4 (d) and (e)).

This film-growth mechanism is believed to be a typical Volmer-Weber mode suggested by previous researchers [42, 60, 61]. The dependence of grain size on film thickness and

the formation of the small particles between large grains have also been confirmed using computer simulations [62].

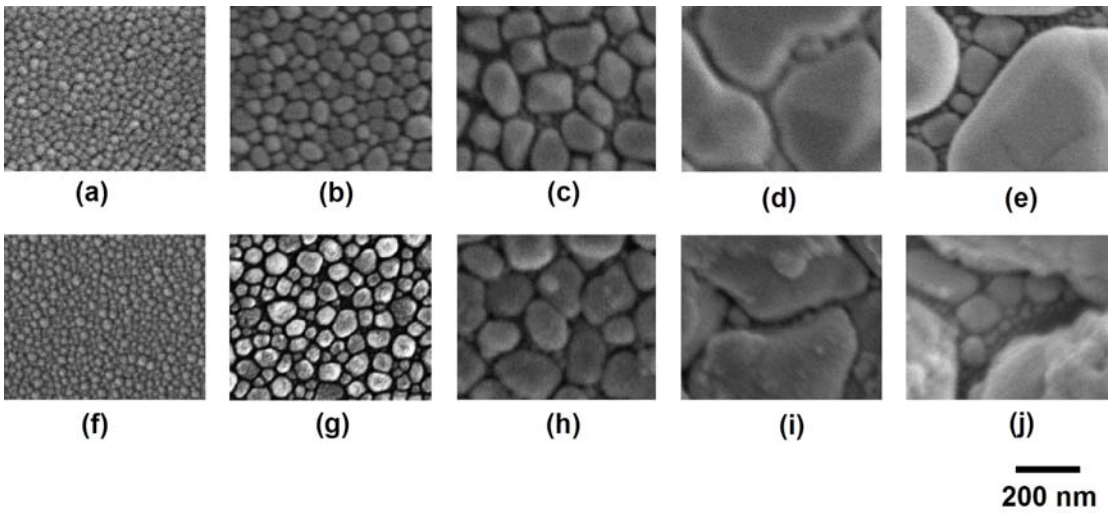

Fig. 5-4 SEM images of the surface morphologies of Sn and SnO_2 films with different thicknesses. (a) 5 nm-thick as deposited Sn film; (b) 10 nm-thick as deposited Sn film; (c) 20 nm-thick as deposited Sn film; (d) 50 nm-thick as deposited Sn film; (e) 100 nm-thick as deposited Sn film; (f) SnO_2 oxidized from 5 nm-thick Sn film; (g) SnO_2 oxidized from 10 nm-thick Sn film; (h) SnO_2 oxidized from 20 nm-thick Sn film; (i) SnO_2 oxidized from 50 nm-thick Sn film; (j) SnO_2 oxidized from 100 nm-thick Sn film. The oxidation-sintering procedure was described in the Experimental section. Note that any one image in the lower row is the oxidized morphology of the sample in the upper row in the same column, e.g., (f) is oxidized from (a).

During the thermal oxidation that started at a slow temperature ramping rate (5ºC/min), the agglomerated morphology of the deposited Sn was transformed from metal into oxide. According to the two-dimensional morphologies in Fig. 5-4, the change of particle size and surface roughness due to the Sn-SnO_2 transformation is not very significant. However, AFM images (Fig. 5-5) do demonstrate raised particle height and therefore increased roughness as a result of oxidation. Comparing the two images in Fig. 5, the particle height is considerably enlarged after oxidation and sintering (200ºC for 2 h, then 400ºC for 2 h, and finally 600ºC for 8 h). This indicates that the volume expansion caused by oxidation is mostly on the direction normal to the substrate plane (*z*-axis), while little volume change occurs on the directions parallel to the substrate plane (*x*- and *y*-axis) due to the confinement of the wafer substrate beneath the Sn or SnO_2 film.

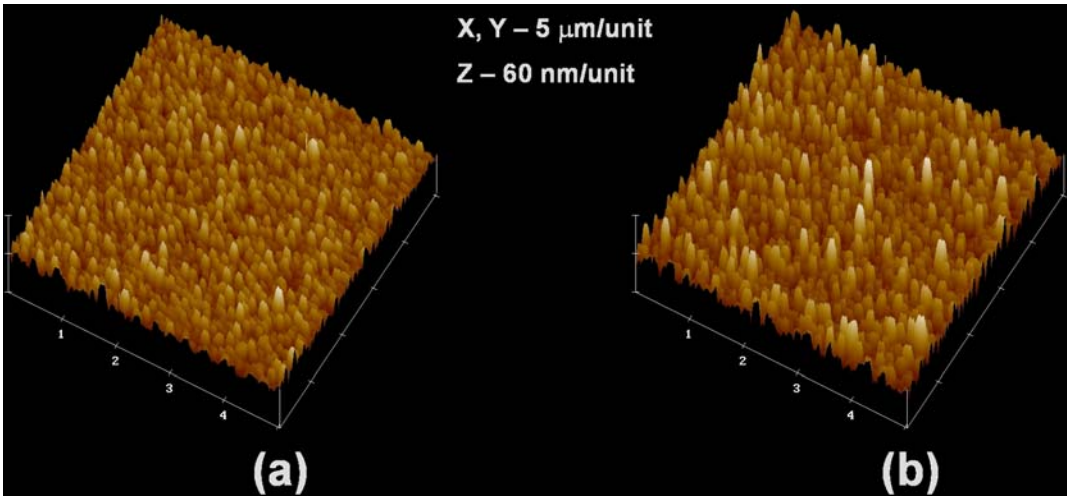

Fig. 5-5 AFM images of the 20 nm-thick as-deposited Sn film (a) and the SnO_2 film produced by oxidation of the former (b).

The results of the I-V measurements for devices with different SnO_2 thicknesses in pure N_2 and 100 ppm H_2 (balanced by N_2) are shown in Fig. 5-6. It can be seen that all of the I-V curves in 100 ppm hydrogen are primarily ohmic, while in pure nitrogen the curves look like from reversely biased Schottky junctions in varying degrees. For thicker oxide films, such as the samples converted from 50 nm- and 100 nm-thick as-deposited Sn film, the I-V curves are more like ohmic than Schottky. For the thinner oxide films (oxidized from 5 nm-, 10 nm-, 20 nm-thick as-deposited Sn), however, the details of the I-V curves in pure N_2 is not clearly displayed due to the scale of the plots. Therefore, these three curves are re-plotted in Fig. 5-7.

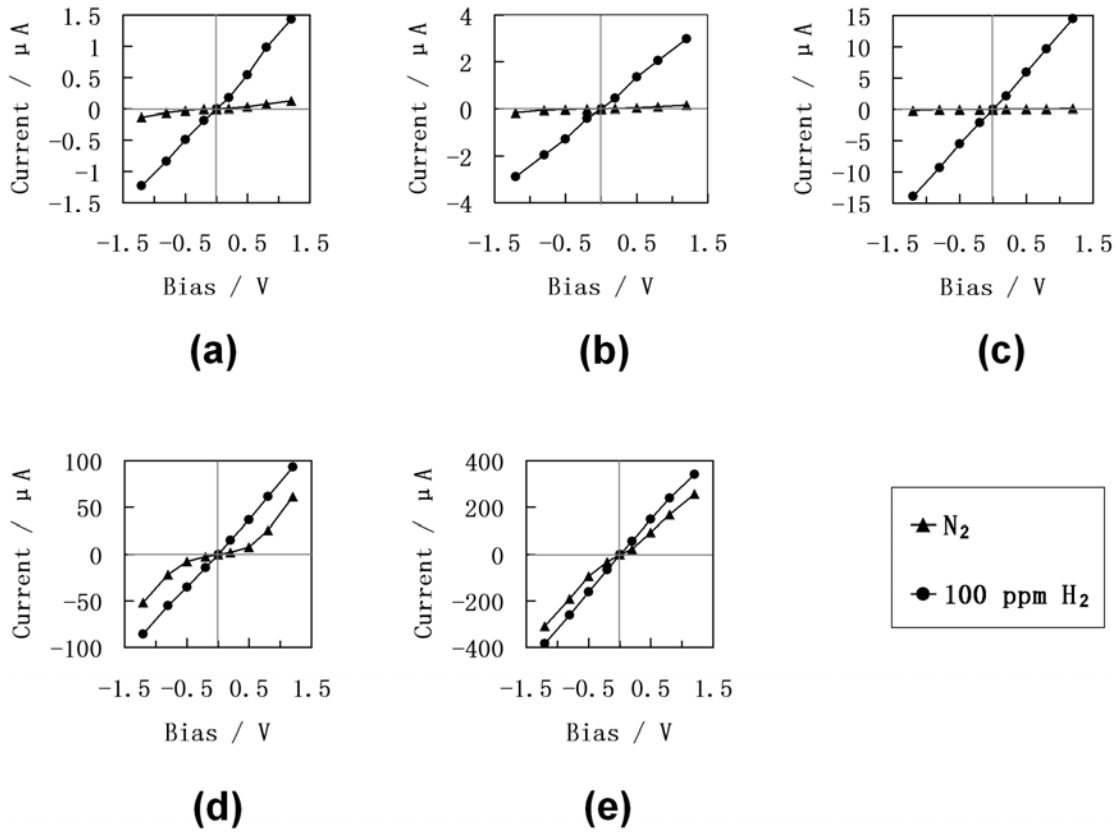

Fig. 5-6 I-V curves of devices based on SnO_2 films with different thicknesses: (a) oxidized from 5 nm-thick as-deposited Sn; (b) oxidized from 10 nm-thick as-deposited Sn; (c) oxidized from 20 nm-thick as-deposited Sn; (d) oxidized from 50 nm-thick as-deposited Sn; (e) oxidized from 100 nm-thick as-deposited Sn. All the measurements were processed at 300°C.

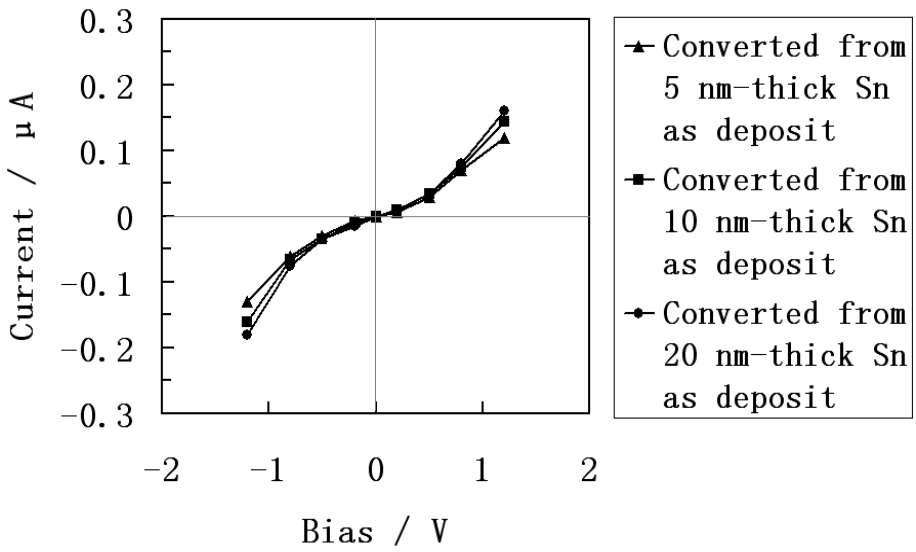

Fig. 5-7 I-V curves for the devices based on the three thinner SnO_2 films (oxidized from 5 nm-, 10 nm-, 20 nm-thick as-deposited Sn films) in pure N_2.

In Fig. 5-7, very weak currents were observed at the bias voltage ranging from 0.2V to 1.2V, although the current increases slightly and non-linearly with the voltage, for either polarity. Based on the results displayed in Fig. 5-6 and Fig. 5-7, it is reasonable to speculate that Schottky barriers exist at the Pt/SnO_2 interfaces as long as the ambient atmosphere is pure nitrogen. The whole device can be considered as two Schottky diodes connected back-to-back (or head-to-head). The overall Pt/SnO_2 interface can be regarded as a kind of "mixed phased contact" [63-64] that consists of both Schottky and ohmic. As the SnO_2 film is thicker than that converted from 20 nm as-deposited Sn film, ohmic contact becomes dominant (Fig. 5-6 (d) and (e)). Therefore, the currents in pure N_2 in Fig. 5-6 (d) and (e) are much larger than their counterparts in thinner films (Fig. 5-7).

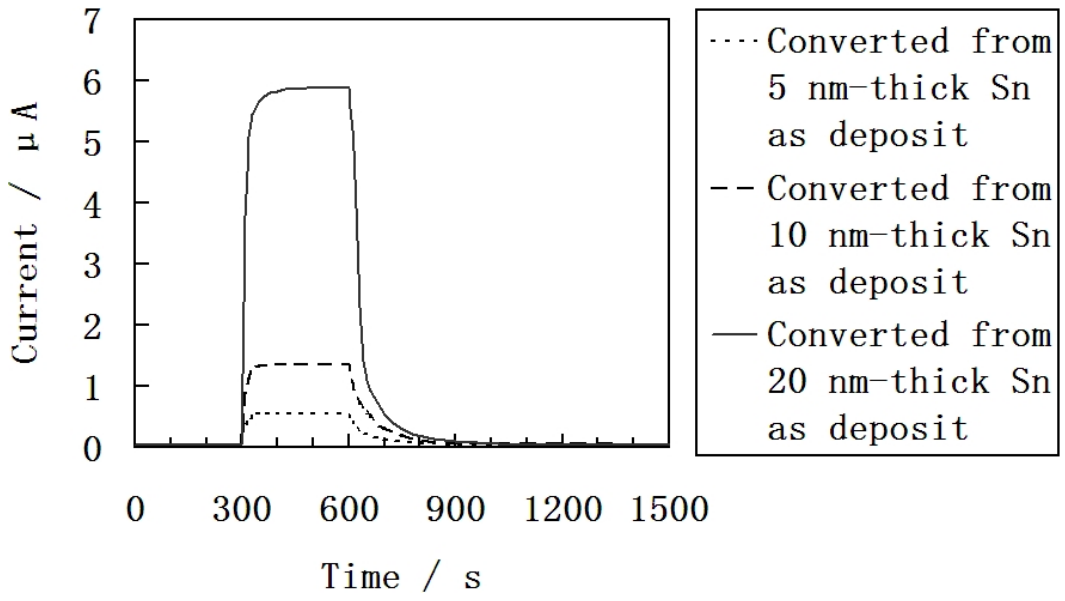

Fig. 5-8 Transient curves in response to 100 ppm H_2 in N_2 for devices based on SnO_2 films oxidized from 5 nm-, 10 nm-, and 20 nm-thick as-deposited Sn films. Bias voltage: 0.5V. Operating temperature: 300°C.

In the presence of 100 ppm H_2, the Schottky barrier height (SBH) is lowered to such extent that electrons can easily cross the barrier at low voltage and the I-V curve becomes approximately linear. This is observed on all devices with various SnO_2 thicknesses. Fig. 5-8 shows the reversible response/recovery transient curves to 100 ppm H_2 on SnO_2 films oxidized from 5 nm-, 10 nm-, and 20 nm-thick as-deposited Sn films (the reversible transient curves for thicker oxide films (converted from 50 nm- and 100 nm-thick as-deposited Sn films) is not plotted in Fig. 5-8 due to their large absolute current values and low relative responses (I/I_0)). The response/recovery times to 100 ppm H_2 of SnO_2 films oxidized from 5 nm-, 10 nm-, and 20 nm-thick as-deposited Sn films are summarized in Fig. 5-9. The response times are all around 7 s. Regarding the delay of the gas delivery system, the reaction of the sensor to H_2 should be considered as a fast process.

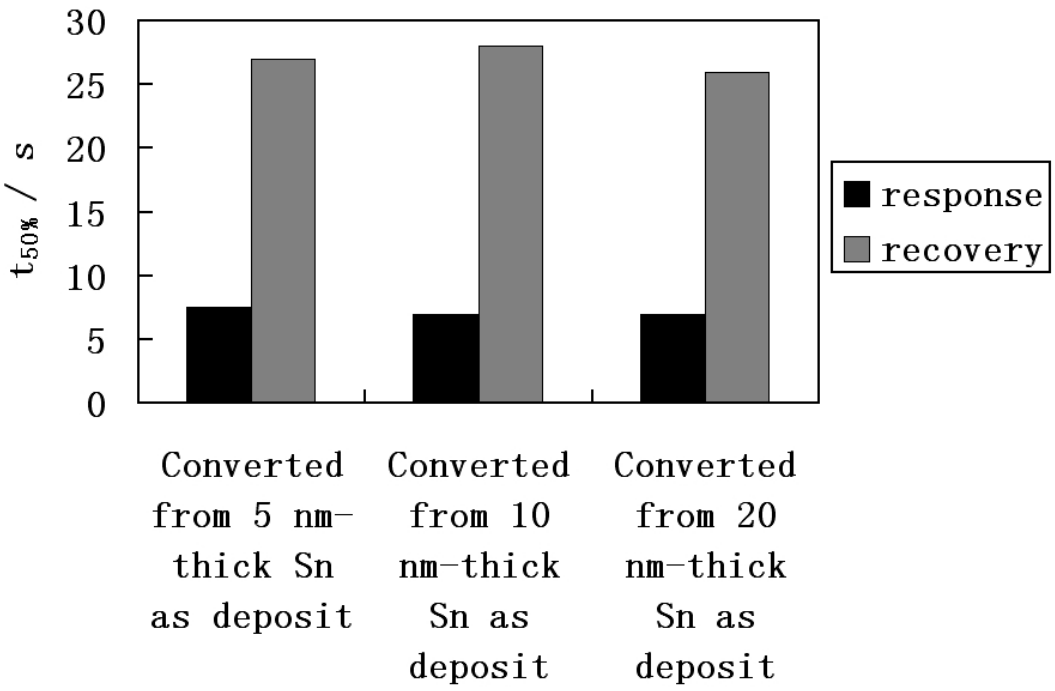

Fig. 5-9 Response/recovery times ($t_{50\%}$) for devices based on SnO_2 films oxidized from 5 nm-, 10 nm-, and 20 nm-thick as-deposited Sn films.

The mechanism of this interface phase-conversion can be ascribed to the following sequential processes: (1) H_2 adsorbs on the Pt electrode surface; (2) H_2 dissociates into atomic hydrogen (H), which is an electron donor; (3) H migrates into Pt, reaching the Pt/SnO_2 interface, causing reduction of work function of the Pt in proximity to the interface and the SBH is lowered down. This mechanism has been demonstrated in several previous studies [49-50, 52, 54]. Fig. 5-10 illustrates the reduction of the SBH caused by hydrogen introduction. The uniformity in the response or recovery rates regardless of the film thickness (Fig. 5-9) also supports the mechanism proposed above. Since the sensing (change of current) results from the reduction of the SBH at the Pt/SnO_2 interface, major kinetic processes of H_2 adsorption (response) or desorption (recovery) occurs only on the electrode (Pt) surface and in the bulk, and thus the thickness of the SnO_2 film has little influence on the transient rate.

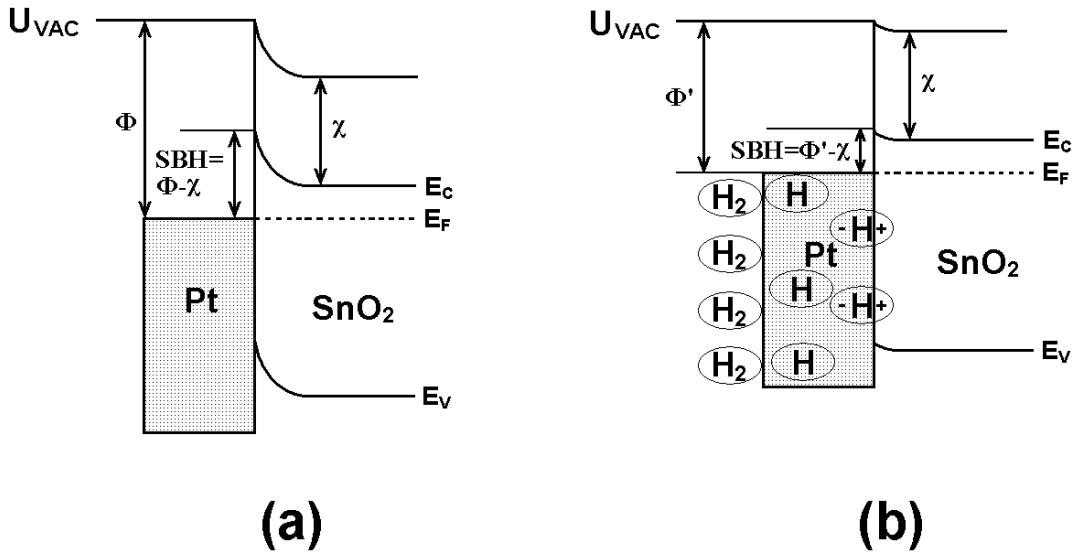

Fig. 5-10 Energy phase diagrams of the fabricated Pt/SnO_2 interface (a Schottky junction) under zero bias: (a) in pure N_2; (b) after exposure to H_2. Φ is the work function of platinum in pure nitrogen (5.64 eV in vacuum [57]), Φ' is the modified work function due to the introduction of hydrogen, and Φ>Φ'. χ is the electron affinity of SnO_2 in pure nitrogen (around 4.50 eV in vacuum, as calculated in [65]). U_{VAC} is the energy in vacuum level. E_c, E_F, and E_V represent the energies at the conduction band, the Fermi level, and valence band of the SnO_2 nano-grain film, respectively.

Although the SBH reduction mechanism illustrated in Fig. 5-10 is supported by I-V curves and transient rates, the magnitudes of relative responses (I/I_0) of SnO_2 films with different thicknesses, as shown in Fig. 5-11, does not suggest a simple model. Due to large absolute currents in pure N_2 (Fig. 5-6 (d) and (e)), I/I_0 values of the two thicker films (oxidized from 50 nm- and 100 nm-thick as-deposited Sn) are much lower than those of the thinner films. The large current in pure N_2 is apparently from the significant content of ohmic contact existing at the Pt/SnO_2 interface [63-64], which can be confirmed by the "poor linear" shapes of the I-V curves in pure N_2 in Fig. 5-6 (d) and (e).

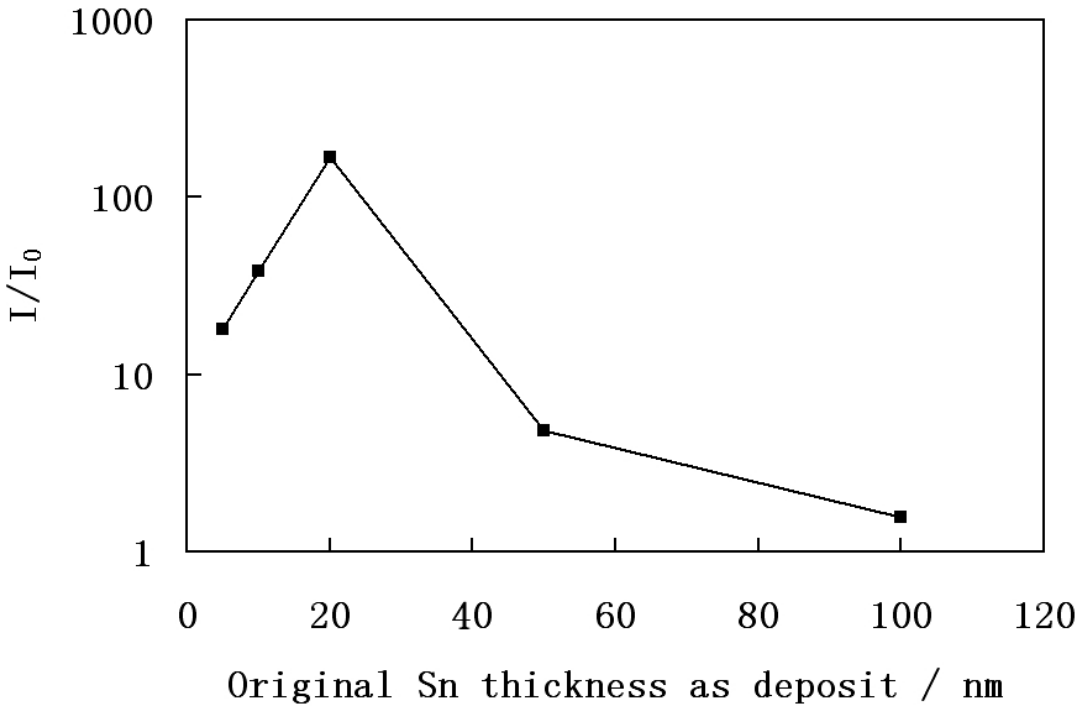

Fig. 5-11 Relative response (I/I_0) of SnO_2 films with different thicknesses under the bias voltage of 0.5V. The *x*-axis represents the thickness of the as-deposited Sn films before oxidation.

As a polycrystalline semiconductor, SnO_2 has high densities of defects at the grain boundaries [66]. Although most of the Pt-SnO_2 contact regions have high SBH values as verified by X-ray photoelectron spectroscopy (XPS) [66], minority contact patches with low SBH dominate the I-V characteristics, just like a set of parallel resistors for which the total resistance is primarily decided by the small ones. This phenomenon has also been frequently observed and verified by computer simulations on other defect-rich semiconductors [63-64, 67]. In this research, we believe that the significant ohmic components on the samples with as-deposited Sn thickness of 50 nm and 100 nm are caused by the local low SBH Pt/SnO_2 contact patches at the grain boundaries. However, for the samples with thin SnO_2 films (converted from 5 nm, 10 nm, and 20 nm-thick as-deposited Sn), the low SBH contact patches are "pinched off" by the depletion regions created by the high SBH metal/semiconductor patches that surround the formers [63-64, 68]. It is reasonable to assume that the size of the grain boundary, at which low SBH exists, is roughly proportional to the grain size. Therefore a pinch-off model to explain the discrepancy in the Pt/SnO_2 contact phases (good Schottky or Schottky-ohmic mixed) between the thin SnO_2 films with small grain sizes and the thick films with large grains can be shown in Fig. 5-12.

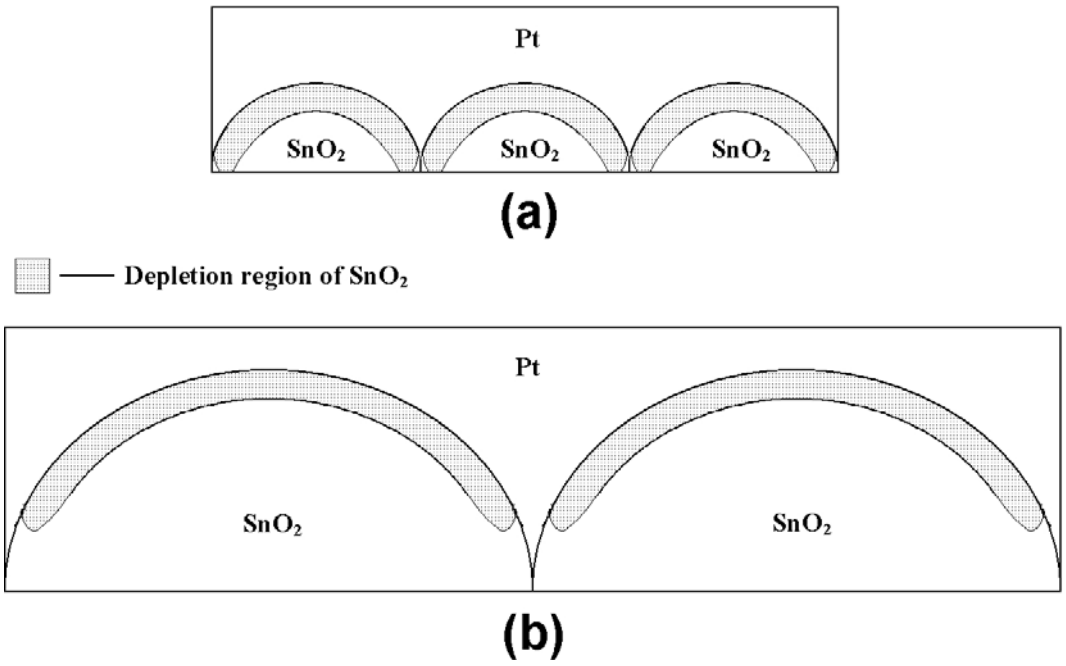

Fig. 5-12 Pinch-off model for (a) small (converted from thin Sn film as-deposited) and (b) large SnO_2 grains (converted from thick Sn film as-deposited). The depletion depths (shown as the "thickness" of the shadowed regions) in (a) and (b) are identical. Large grains in (b) and small grains in (a) are assumed to be in the same shape (geometrically similar).

In Fig. 5-12 (a), even if any low SBH contact exists locally at a grain boundary between the small grains, it is electrically confined to the boundary by the depletion regions that penetrate throughout the grains to the SnO_2/SiO_2 interface. In Fig. 5-12 (b), since the grain is so large and thick, the depletion depth, which is independent of the grain size or thickness, stops far beyond the SnO_2/SiO_2 interface, and the low-SBH contacts at the grain boundaries cannot be pinched off.

Although Fig. 5-12 provides a qualitative model that reasonably explicates the grain-size-dependent mixed phase contacts of the presented Pt/SnO_2 devices, details of this model remains not quite clear. The depth of the depletion region drawn in Fig. 5-12 can be regarded as the Debye Length (L_D) of the prepared SnO_2. According to literatures [25], sol-gel produced SnO_2 has a Debye Length of around 3 nm. In Fig. 5-12 (b), if the minimum thickness of the grain (from the grain top to the SnO_2/SiO_2 interface) is 50 nm (significant ohmic characteristic is observed in the I-V curve in pure N_2 of the SnO_2 film converted from 50 nm-thick as-deposited Sn, as shown in Fig. 5-6 (d)), then the L_D should be much less than 50 nm. But this rough analysis cannot solve an exact value of L_D in order to support or weaken the model presented in Fig. 5-12. Further experiments, such as ballistic electron emission microscopy (BEEM) and spectroscopic approaches for local SBH values, high-resolution SEM and TEM for the grain shapes, and Hall measurements for the carrier density (n_c) of the prepared SnO_2 ($L_D \sim n_c^{-0.5}$) are necessary in order to construct a reliable quantitative model for the speculated grain-size-dependent Pt/SnO_2 contacts of the presented devices.

According to Fig. 5-11, the relative response (I/I_0) reached the maximum (168 times) for the SnO_2 film converted from the 20 nm-thick as-deposited Sn film. The small values of I/I_0 for the thicker films (converted from 50 nm- and 100 nm-thick as-deposited Sn films) can be attributed to the poor Schottky contacts (or more ohmic-like contacts) that cause large I_0, as discussed above. Because the Pt/SnO_2 interfaces of thinner films (converted from 5 nm-, 10 nm-, and 20 nm-thick as-deposited Sn films) are much better Schottky contacts, the corresponding leakage currents (I_0) are quite low and thus the I/I_0 ratios are very large (Fig. 5-6 (a), (b), and (c), and Fig. 5-7). However, there should be an extra

mechanism that is responsible for the decrease in I/I_0 as the SnO_2 film becomes thinner than the one converted from the 20 nm-thick as-deposited Sn film (See Figure 5-11).

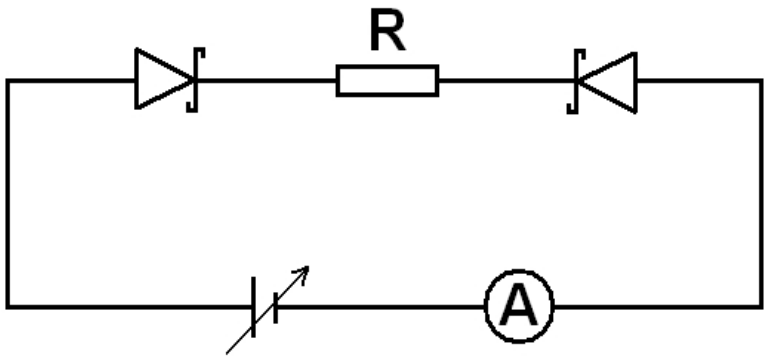

Fig. 5-13 Circuit model of the devices based on SnO_2 films oxidized from 5 nm-, 10 nm-, and 20 nm-thick as-deposited Sn.

The circuit model drawn in Fig. 5-13 simulates the overall device in pure N_2 as long as the Pt/SnO_2 contact is in good Schottky phase with little leakage. The two back-to-back diodes represent the Pt/SnO_2 interfaces beneath the paired electrodes. The resistor (R) represents the whole serial resistance in the loop, in which the resistance of the SnO_2 film between the electrodes is the dominant constituent (other equivalent components, such as the resistors and/or capacitors in parallel to the Schottky diodes, are omitted in Fig. 5-13). Although thinner film bears high resistance, the magnitude of the loop current does not vary too much with the film thickness (Fig. 5-7), due to the much higher resistance at the reverse-biased Schottky junction. Whereas at the presence of 100 ppm H_2 and under a constant bias voltage, the SBH becomes so low that the resistance at Schottky junction is trivial, the loop current is mostly determined by the resistance R, which decreases with the film thickness. Therefore, as the SnO_2 film turns thinner, the resistance R increases so that the loop current drops in the 100 ppm H_2 ambient.

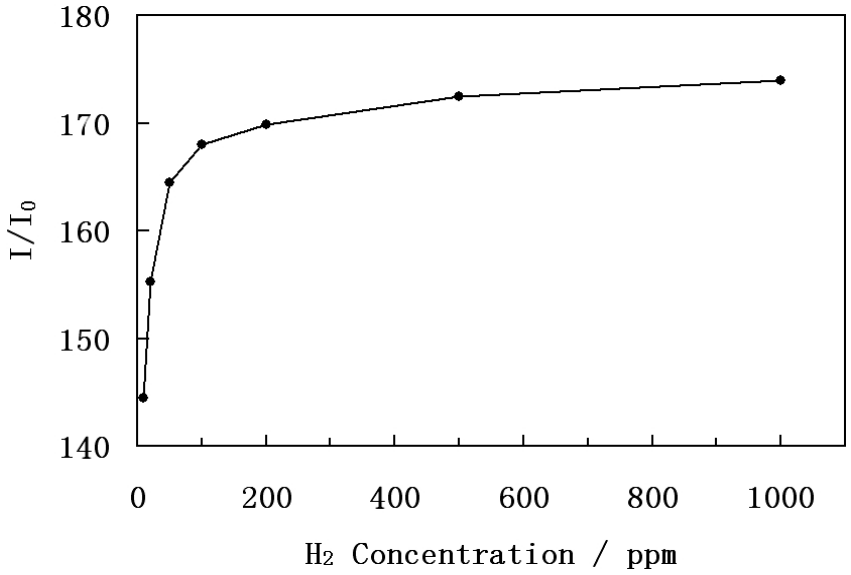

Fig. 5-14 Dependence of relative response (I/I_0) on H_2 concentration for the device based on SnO_2 films oxidized from 20 nm-thick as-deposited Sn.

Under the bias voltage of 0.5 V and at the H_2 concentration of 100 ppm, since the highest I/I_0 was found on the device based on the SnO_2 film converted from 20 nm-thick as-deposited Sn at 300°C, the relationship between I/I_0 and H_2 concentration was further tested, as shown in Fig. 5-14. It was found that the device was quite sensitive to hydrogen, I/I_0 reached about 144 times at the H_2 concentration as low as 10 ppm. However, significant saturation was observed over 100 ppm H_2.

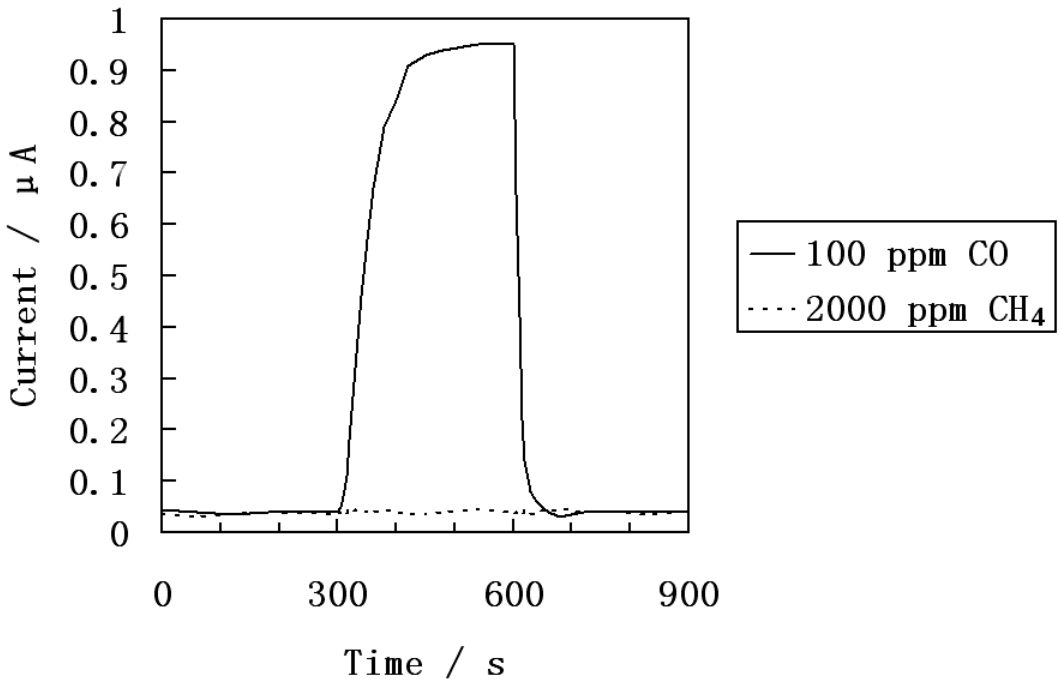

Fig. 5-15 Transient curves in response to 100 ppm CO and 2000 ppm CH_4 for the device based on the SnO_2 film oxidized from 20 nm-thick as-deposited Sn. Bias voltage: 0.5V. Operating temperature: 300°C.

The response transients to 100 ppm carbon monoxide and 2000 ppm methane of the device based on the SnO_2 film converted from the 20 nm-thick as-deposited Sn film are shown in Fig. 5-15. Relative response (I/I_0) values are extracted from Fig. 5-15 and re-plotted in Fig. 5-16. Undoubtedly, the device's response to CO was much less than that to H_2, and no response was found for CH_4 at the concentration as high as 2000 ppm.

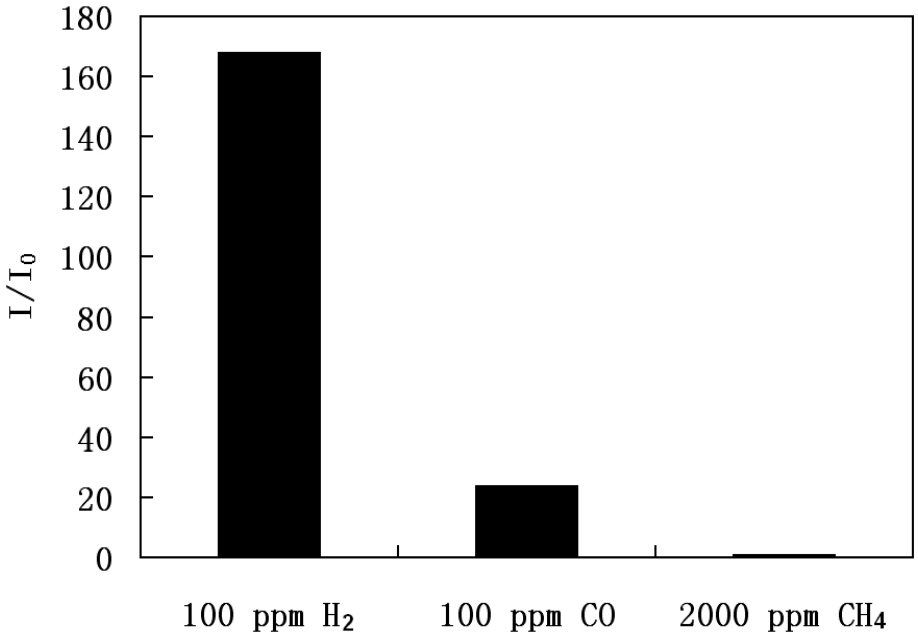

Fig. 5-16 I/I_0 values in response to 100 ppm H_2, 100 ppm CO, and 2000 ppm CH_4 for the device based on the SnO_2 film oxidized from the 20 nm-thick as-deposited Sn film.

Upon introduction of oxygen into the pure nitrogen ambient, the device current decreases and null responses ($I/I_0 \approx 1$) to 10 ppm ~ 1000 ppm H_2 were recorded on all the fabricated devices in synthetic air (80% N_2 + 20% O_2) at 300°C under bias voltages ranging from ±0.2V to ±1.2V. The current drop at O_2 introduction can be attributed to the elevation of SBH due to the chemical adsorption of oxygen molecules (usually electron acceptors) at the electrode/oxide interface [52], as well as due to the increased SnO_2 resistance resulting from the surface depletion caused by the adsorbed oxygen [53]. The null response to H_2 in air should result from the platinum-catalyzed hydrogen-oxygen combination (H_2O formation), which was reported to be 100% complete at the temperature as low as 150°C [69]. Null or very weak H_2 response in air or oxygen for sensors based on SnO_2 or TiO_2 equipped with platinum electrodes has been reported in multiple studies [54, 70-71]. In addition, the null response at the presence of oxygen further excludes the likelihood that the quite high and fast response to hydrogen in pure N_2 is caused by the removal of lattice oxygen in the SnO_2 films.

5.4 Conclusions:

Sn layers with thicknesses from 5 nm to 100 nm were prepared on silicon wafers by e-beam evaporation. After thermal oxidation, SnO_2 films composed of nanoscale grains with thickness-dependent sizes were obtained. Novel hydrogen sensors were formed by coating interdigital Pt electrodes on the nano-grain SnO_2 films. Very high signal and fast responses to H_2 in low concentrations were found on thinner films. A sensing mechanism is proposed, i.e. the H_2-induced reduction of the SBH at the Pt/SnO_2 contact is responsible for hydrogen sensing. An improved model is also proposed to elucidate the discrepancies between the experimental results and the simple SBH-reduction mechanism.

References for Chapter 5:

[1] T. Seiyama, S. Kagawa, Study on a detector for gaseous components using semiconductive thin films, Anal. Chem. 38 (1966) 1069-1073.

[2] W. Hagen, R. E. Lambrich, J. Lagois, Semiconducting gas sensors, Festkörperprobleme (Advances in Solid State Physics) 23 (1983) 259-274.

[3] J. F. McAleer, P. T. Moseley, J. O. W. Norris, D. E. Williams, Tin dioxide gas sensors: Part 1. - Aspects of the surface chemistry revealed by electrical conductance variations, J. Chem. Soc., Faraday Trans. I 83 (1987) 1323-1346.

[4] T. Seiyama, A. Kato, K. Fujiishi, M. Nagatani, A new detector for gaseous components using semiconductive thin films, Anal. Chem. 34 (1962) 1502-1503.

[5] P. J. Shaver, Activated tungsten oxide gas detectors, Appl. Phys. Lett. 11 (1967) 255-257.

[6] S. R. Morrison, Semiconductor gas sensors, Sens. Actuators 2 (1982) 329-341.

[7] J. Watson, Tin oxide gas sensor and its applications, Sens. Actuators 5 (1984) 29-42.

[8] J. Watson, K. Ihokura, G. S. V. Coles, The tin dioxide gas sensor, Meas. Sci. Tech. 4 (1993) 711-719.

[9] K. Ihokura, J. Watson, The stannic oxide gas sensor: principles and applications, CRC Press, Boca Raton, FL, 1994.

[10] C. Xu, J. Tamaki, N. Miura, N. Yamazoe, Grain size effects on gas sensitivity of porous SnO_2-based elements, Sens. Actuators B 3 (1991) 147-155.

[11] N. Yamazoe, New approaches for improving semiconductor gas sensors, Sens. Actuators B 5 (1991) 7-19.

[12] K. H. Song, S. J. Park, Gas sensing characteristics of tin dioxide with small crystallites, J. Mater. Sci.-Mater. El. 4 (1993) 249-253.

[13] S. G. Ansari, P. Boroojerdian, S. R. Sainkar, R. N. Karekar, R. C. Aiyer, S. K. Kulkarni, Grain size effects on H_2 gas sensitivity of thick film resistor using SnO_2 nanoparticles, Thin Solid Films 295 (1997) 271-276.

[14] D. G. Rickerby, M. C. Horrillo, J. P. Santos, P. Serrini, Microstructural characterization of nanograin tin oxide gas sensors, Nanostruct. Mater. 9 (1997) 43-52.

[15] S. Shukla, S. Patil, S. C. Kuiry, Z. Rahman, T. Du, L. Ludwig, C. Parish, S. Seal, Synthesis and characterization of sol-gel derived nanocrystalline tin oxide thin film as hydrogen sensor, Sens. Actuators B 96 (2003) 343-353.

[16] N. Yamazoe, K. Shimanoe, New perspectives of gas sensor technology, Sens. Actuators B 138 (2009) 100-107.

[17] Q. Kuang, C. S. Lao, Z. Li, Y. Z. Liu, Z. X. Xie, L. S. Zheng, Z. L. Wang, Enhancing the photon- and gas-sensing properties of a single SnO_2 nanowire based nanodevice by nanoparticle surface functionalization, J. Phys. Chem. C 112 (2008) 11539-11544.

[18] Y. J. Choi, I. S. Hwang, J. G. Park, K. J. Choi, J. H. Park, J. H. Lee, Novel fabrication of an SnO_2 nanowire gas sensor with high sensitivity, Nanotechnology 19 (2008) 095508/1-095508/4.

[19] Y. Shen, T. Yamazaki, Z. Liu, D. Meng, T. Kikuta, N. Nakatani, M. Saito, M. Mori, Microstructure and H_2 gas sensing properties of undoped and Pd-doped SnO_2 nanowires, Sens. Actuators B 135 (2009) 524-529.

[20] L. H. Qian, K. Wang, Y. Li, H. T. Fang, Q. H. Lu, X. L. Ma, CO sensor based on Au-decorated SnO_2 nanobelt, Mater. Chem. Phys. 100 (2006) 82-84.

[21] X. Han, B. Zhang, S. Guan, J. Liu, X. Zhang, R. Chen, Gas-sensing properties of SnO_2 nanobelts synthesized by thermal evaporation of Sn foil, J. Alloy Compd. 461 (2008) L26-L28.

[22] H. Huang, Y. C. Lee, O. K. Tan, W. Zhou, N. Peng, Q. Zhang, High sensitivity SnO_2 single-nanorod sensors for the detection of H_2 gas at low temperature, Nanotechnology 20 (2009) 115501/1-115501/5.

[23] T. Hyodo, N. Nishida, Y. Shimizu, M. Egashira, Preparation and gas-sensing properties of thermally stable mesoporous SnO_2, Sens. Actuators B 83 (2002) 209-215.

[24] T. Hamaguchi, N. Yabuki, M. Uno, S. Yamanaka, M. Egashira, Y. Shimizu, T. Hyodo, Synthesis and H_2 gas sensing properties of tin oxide nanohole arrays with various electrodes, Sens. Actuators B 113 (2006) 852-856.

[25] N. S. Baik, G.. Sakai, N. Miura, N. Yamazoe, Hydrothermally treated sol solution of tin oxide for thin-film gas sensor, Sens. Actuators B 63 (2000) 74-79.

[26] A. Z. Adamyan, Z. N. Adamyan, V. M. Aroutiounian, A. H. Arakelyan, K. J. Touryan, J. A. Turner, Sol-gel derived thin-film semiconductor hydrogen gas sensor, Int. J. of Hydrogen Energy 32 (2007) 4101-4108.

[27] S. Shukla, P. Zhang, H. J. Cho, L. Ludwig, S. Seal, Significance of electrode-spacing in hydrogen detection for tin oxide-based MEMS sensor, Int. J. of Hydrogen Energy 33 (2008) 470-475.

[28] K. Hieda, T. Hyodo, Y. Shimizu, M. Egashira, Preparation of porous tin dioxide powder by ultrasonic spray pyrolysis and their application to sensor materials, Sens. Actuators B 133 (2008) 144-150.

[29] C. Agashe, R. C. Aiyer, High-yield synthesis of nanocrystalline tin dioxide by thermal decomposition for use in gas sensors, Int. J. Appl. Ceram. Tech., 5 (2008) 181-187.

[30] A. Kock,, A. Tischnera, T. Maier, M. Kast, C. Edtmaier, C. Gspan, G. Kothleitner, Atmospheric pressure fabrication of SnO_2-nanowires for highly sensitive CO and CH_4 detection, Sens. Actuators B 138 (2009) 160-167.

[31] B. K. Min, S. D. Choi, SnO_2 thin film gas sensor fabricated by ion beam deposition, Sens. Actuators B 98 (2004) 239-246.

[32] B. Panchapakesan, D. L. DeVoe, M. R Widmaier, R. Cavicchi, S. Semancik, Nanoparticle engineering and control of tin oxide microstructures for chemical microsensor applications, Nanotechnology 12 (2001) 336-349.

[33] G. Sberveglieri, G. Faglia, S. Groppelli, P. Nelli, A. Camanz, A new technique for growing large surface area SnO_2 thin film (RGTO technique), Semicond. Sci. Tech. 5 (1990) 1231-1233.

[34] G. Sberveglieri, Recent developments in semiconducting thin-film gas sensors, Sens. Actuators B 23 (1995) 103-109.

[35] T. Aste, R. Botter, D. Beruto, Double-layer granular SnO_2 sensors, Sens. Actuators B 25 (1995) 826-829.

[36] L. Sangaletti, L.E. Depero, A. Dieguez, G. Marca, J.R. Morante, A. Romano-Rodriguez, G. Sberveglieri, Microstructure and morphology of tin dioxide multilayer thin film gas sensors, Sens. Actuators B 44 (1997) 268-274.

[37] P. Nelli, G. Faglia, G. Sberveglieri, E. Cereda, G. Gabetta, A. Dieguez, A. Romano-Rodriguez, J. R. Morante, The aging effect on SnO_2 Au thin film sensors: electrical and structural characterization, Thin Solid Films 371 (2000) 249-253.

[38] E. Comini, G. Faglia, G. Sberveglieri, CO and NO_2 response of tin oxide silicon doped thin films, Sens. Actuators B 76 (2001) 270-274.

[39] M. Radecka, J. Przewoznik, K. Zakrzewska, Microstructure and gas-sensing properties of (Sn, Ti)O_2 thin films deposited by RGTO technique, Thin Solid Films 391 (2001) 247-254.

[40] J. Szuber, J. Uljanow, T. Karczewska-Buczek, W. Jakubik, K. Waczynski, M. Kwoka, S. Konczak, On the correlation between morphology and gas sensing properties of RGTO SnO_2 thin films, Thin Solid Films 490 (2005) 54-58.

[41] Elisabetta Comini, Luca Ottini, Guido Faglia, Giorgio Sberveglieri, SnO_2 RGTO UV activation for CO monitoring, IEEE Sens. J. 4 (2004) 17-20.

[42] J. G. Partridge, M. R. Field, J. L. Peng, A. Z. Sadek, K. Kalantar-Zadeh, J Du Plessis, D. G. McCulloch, Nanostructured SnO2 films prepared from evaporated Sn and their application as gas sensors, Nanotechnology 19 (2008) 125504/1-125504/5.

[43] F. A. Lewis, The Palladium Hydrogen System, Academic Press, New York, NY, 1967.

[44] I. Lundström, T. DiStefano, Influence of hydrogen on Pt-SiO_2-Si structures, Solid State Commun. 19 (1976) 871-875.

[45] J. C. Loh, “Gas detector”, U.S. Patent 4045729, Aug. 30, 1977.

[46] M. Armgarth, D. Söderberg, I. Lundström, Palladium and platinum gate metal-oxide-semiconductor capacitors in hydrogen and oxygen mixtures, Appl. Phys. Lett. 41 (1982) 654-655.

[47] I. Lundström, H. Sundgren, F. Winquist, M. Eriksson, C. Krantz-Rülcker, A. Lloyd-Spetz, Twenty-five years of field effect gas sensor research in Linköping, Sens. Actuators B 30 (2007) 247-262.

[48] M. C. Steele, B. A. Maciver, Palladium/cadmium-sulfide Schottky diodes for hydrogen detection, Appl. Phys. Lett. 28 (1976) 687-688.

[49] K. Ito, Hydrogen-sensitive Schottky barrier diodes, Surf. Sci. 86 (1979) 345-352.

[50] N. Yamamoto, S. Tonomura, T. Matsuoka, H. Tsubomura, A study on a palladium-titanium oxide Schottky diode as a detector for gaseous components, Surf. Sci. 92 (1980) 400-406.

[51] U. Kirner, K.D. Schierbaum, W. Göpel, B. Leibold, N. Nicoloso, W. Weppner, D. Fischer, W. F. Chu, Low and high temperature TiO_2 oxygen sensors, Sens. Actuators B 1 (1990) 103-107.

[52] K. D. Schierbaum, U. K. Kirner, J. F. Geiger, W. Göpel, Schottky-barrier and conductivity gas sensors based upon Pd/SnO_2 and Pt/TiO_2, Sens. Actuators B 4 (1991) 87-94.

[53] K. D. Schierbaum, Engineering of oxide surfaces and metal/oxide interfaces for chemical sensors: recent trends, Sens. Actuators B 24 (1995) 239-247.

[54] Y. Shimizu, N. Kuwano, T. Hyodo, M. Egashira, High H_2 sensing performance of anodically oxidized TiO_2 film contacted with Pd, Sens. Actuators B 83 (2002) 195-201.

[55] M. Egashira, Y. Shimizu, Y. Takao, S. Sako, Variations in I-V characteristics of oxide semiconductors induced by oxidizing gases, Sens. Actuators B 35-36 (1996) 62-67.

[56] T. Hyodo, Y. Baba, K. Wada, Y. Shimizu, M. Egashira, Hydrogen sensing properties of SnO2 varistors loaded with SiO_2 by surface chemical modification with diethoxydimethylsilane, Sens. Actuators B 64 (2000) 175-181.

[57] D. R. Lide (Ed.), CRC Handbook of Chemistry and Physics, Internet Version 2008, <http://www.hbcpnetbase.com>, CRC Press, Boca Raton, FL, 2008.

[58] W. Hellmich, Ch. Bosch-v. Braunmuhl, G. Muller, G. Sberveglieri, M. Bertih, C. Perego, The kinetics of formation of gas-sensitive RGTO-SnO_2 films, Thin Solid Films 263 (1995) 231-237.

[59] L. Sangaletti, L. E. Depero, B. Allieri, F. Pioselli, E. Comini, G. Sberveglieri, M. Zocchi, Oxidation of Sn thin films to SnO_2. Micro-Raman mapping and x-ray diffraction studies, J. Mater. Res. 13 (1998) 2457-2460.

[60] E. Søndergård, R. Kofman, P. Cheyssac, A. Stella, Production of nanostructures by self-organization of liquid Volumer-Weber films, Surf. Sci. 364 (1996) 467-476.

[61] M. Zinke-Allmang, L. C. Feldman, M. H. Grabow, Clustering on surfaces, Surf. Sci. Rep. 16 (1992) 377-463.

[62] S. Ulrich, S. Stoll, E. Pefferkorn, Computer simulations of homogeneous deposition of liquid droplets, Langmuir 20 (2004) 1763-1771.

[63] J. L. Freeouf, T. N. Jackson, S. E. Laux, J. M. Woodall, Effective barrier heights of mixed phase contacts: size effects, Appl. Phys. Lett. 40 (1982) 634-636.

[64] J. L. Freeouf, T. N. Jackson, S. E. Laux, J. M. Woodall, Size dependence of "effective" barrier heights of mixed-phase contacts, J. Vac. Sei. Technol. 21 (1982) 570-573.

[65] M. A. Butler, D. S. Ginley, Prediction of flatband potentials at semiconductor-electrolyte interfaces from atomic electronegativities, J. Electrochem. Soc. 125 (1978) 228-232.

[66] C. Kober, S. P. Harvey, T. O. Mason, A. Klein, Barrier heights at the SnO_2/Pt interface: in situ photoemission and electrical properties, Surf. Sci. 602 (2008) 3246-3252.

[67] H. J. Im, Y. Ding, J. P. Pelz, W. J. Choyke, Nanometer-scale test of the Tung model of Schottky-barrier height inhomogeneity, Phys. Rev. B 64 (2001) 075310/1-075310/9.

[68] R. T. Tung, Electron transport at metal-semiconductor interfaces: general theory, Phys. Rev. B 45 (1992) 13509-13523.

[69] Jr. W. H. King, The monitoring of hydrogen, methane, and hydrocarbons in the atmosphere, Environ. Sci. Technol. 4 (1970) 1136-1141.

[70] Y. Jun, H. Kim, J. Lee, S. Hong, High H_2 sensing behavior of TiO_2 films formed by thermal oxidation, Sens. Actuators B 107 (2005) 264-270.

[71] C. Lu, Z. Chen, High-temperature resistive hydrogen sensor based on thin nanoporous rutile TiO_2 film on anodic aluminum oxide, Sens. Actuators B 140 (2009) 109-115.

Note: The substantial part of this chapter has been sent to a journal as a research paper for reviewing.

Chapter 6 - Summary and future works

6.1 Summary of the research:

Three types of H_2 sensors operating at elevated temperatures were developed based on micro-fabrication technologies. Significant improvements were achieved as comparing to previously reported devices. The sensing mechanisms were investigated and verified to be consistent with existing theories. The structural features of the devices were studied by micro-to-nano scale materials characterization approaches. Detailed conclusions for each device can be found in Section 3.4, 4.4, and 5.4.

6.2 Future works:

The research presented in this dissertation can be extended to the following directions:

(1) Construction of quantitative models for devices presented in Chapter 4 and 5. Although the mechanisms have been proposed and supported by the experimental data, detailed numerical models will help better understand the sensing properties and improve the performances.

(2) H_2 microsensors operating at ultra-high temperatures (600 - 800°C). Above 600°C, sub-micron-thick Pt film strips off the substrate, in spite of the material or surface roughness of the substrate. Inserting adhesive layers, such as chromium (Cr) and titanium

(Ti), between the Pt film and the substrate would not provide remarkable improvement. Due to this, lifetimes of microfabricated gas sensors for ultra-high temperature applications were always short [1] and long-term stable devices were rarely reported [2]. Durable H_2 sensors operating at over 600°C were usually electrochemical devices equipped with macroscale Pt electrode, i. e., millimeter-to-centimeter-sized bulky Pt sintered from Pt ink or paste [3, 4]. The development of micro-sized H_2 sensors tolerant to ultra-high temperatures will be a noteworthy topic for the next-step research.

(3) High temperature H_2 sensors operating in both nitrogen and air ambients. Although the operation environment of the devices presented in this research is limited to oxygen-free ambients, O_2 gravely interferes with the hydrogen sensing of all these devices. Therefore improved sensors with good sensing performances in oxygen-rich ambients are necessary in case the existence of oxygen is unavoidable. SiO_2 thin films have been developed as a type of filters for O_2 and other large gas molecules on H_2 sensors [4]. Thin film filters may also be applied to the devices presented in this dissertation in order to minimize the interference from oxygen.

References for Chapter 6:

[1] A. L. Spetz, P. Tobias, L. Unéus, H. Svenningstorp, L. G. Ekedahl, I. Lundström, High temperature catalytic metal field effect transistors for industrial applications, Sens. Actuators B 70 (2000) 67-76.

[2] I. Lundström, H. Sundgren, F. Winquist, M. Eriksson, C. Krantz-Rülcker, A. Lloyd-Spetz, Twenty-five years of field effect gas sensor research in Linköping, Sens. Actuators B 30 (2007) 247-262.

[3] N. Taniguchi, T. Kuroha, C. Nishimura, K. Iijima, Characteristics of novel $BaZr_{0.4}Ce_{0.4}In_{0.2}O_3$ proton conducting ceramics and their application to hydrogen sensors, Solid State Ionics 176 (2005) 2979-2983.

[4] T. Weh, J. Frank, M. Fleischer, H. Meixner, On the mechanism of hydrogen sensing with SiO_2 modificated high temperature Ga_2O_3 sensors, Sens. Actuators B 78 (2001) 202-207.

References

A. Stwertka, A Guide to the Elements, 2nd Edition, Oxford University Press, New York, NY, 2002.

National Research Council and National Academy of Engineering, The Hydrogen Economy: Opportunities, Costs, Barriers, and R&D Needs, National Academies Press, Washington, DC, 2004.

R. Archbold, Hindenburg: An Illustrated History, Toronto: Viking Studio/Madison Press, Toronto, Canada, 1994.

S. Capone, A. Forleo, L. Francioso, R. Rella, P. Siciliano, J. Spadavecchia, D. S. Presicce, A. M. Taurino, Solid state gas sensors: state of the art and future activities, Journal of Optoelectronics and Advanced Materials 5 (2003) 1335-1348.

P. T. Moseley, Solid state gas sensors, Meas. Sci. Technol. 8 (1997) 223-237.

K. M. Goeders, J. S. Colton, L. A. Bottomley, Microcantilevers: Sensing chemical interactions via mechanical motion, Chem. Rev. 108 (2008) 522-542.

G. Korotcenkov, S. D. Han, J. R. Stetter, Review of electrochemical hydrogen sensors, Chem. Rev. 109 (2009) 1402–1433.

Z. Chen, C. Lu, Humidity sensors: a review of materials and mechanisms, Sensor Letters 3 (2005) 274-295.

I. Lundström, H. Sundgren, F. Winquist, M. Eriksson, C. Krantz-Rülcker, A. Lloyd-Spetz, Twenty-five years of field effect gas sensor research in Linköping, Sensors and Actuators B 30 (2007) 247-262.

G. Korotcenkov, Metal oxides for solid-state gas sensors: What determines our choice? Materials Science and Engineering B 139 (2007) 1-23.

J. Janata, R. J. Huber (Ed.), Solid State Chemical Sensors, Academic Press, New York, NY, 1985.

D. R. Lide (Ed.), CRC Handbook of Chemistry and Physics, Internet Version 2008, <http://www.hbcpnetbase.com>, CRC Press, Boca Raton, FL, 2008.

N. Lopez, Z. Lodziana, F. Illas, M. Salmeron, When Langmuir is too simple: H_2 dissociation on Pd (111) at high coverage, Physical Review Letters 93 (2004) 146103/1-146103/4.

C. Christofides, A. Mandelis, Solid-state sensors for trace hydrogen gas detection, J. Appl. Phys. 68 (1990) R1-R30.

F. Favier, E. C. Walter, M. P. Zach, T. Benter, R. M. Penner, Hydrogen sensors and switches from electrodeposited palladium mesowire arrays, Science 293 (2001) 2227-2231.

T. Xu, M. P. Zach, Z. L. Xiao, D. Rosenmann, U. Welp, W. K. Kwok, G. W. Crabtree, Self-assembled monolayer-enhanced hydrogen sensing with ultrathin palladium films, Appl. Phys. Lett. 86 (2005) 203104/1-203104/3.

Kitco Inc., Monthly Palladium Chart, Retrieved 08/25, 2009.

London Metal Exchange, Primary Nickel Price Graph, Retrieved 08/25, 2009.

D. C. Harris, L. J. Cabri, Nomenclature of platinum-group-element alloys: review and revision, The Canadian Mineralogist 29 (1991) 231-237.

K. Potje-Kamloth, Semiconductor junction gas sensors, Chem. Rev. 108 (2008) 367-399.

N. Barsan, D. Koziej, U. Weimar, Metal oxide-based gas sensor research: How to? Sensors and Actuators B 121 (2007) 18-35.

G. Korotcenkov, The role of morphology and crystallographic structure of metal oxides in response of conductometric-type gas sensors, Materials Science and Engineering R 61 (2008) 1-39.

U. Roland, R. Salzer, T. Braunschweig, F. Roessner, H. Winkler, Investigations on hydrogen spillover: Part 1 - Electrical conductivity studies on titanium dioxide, J. Chem. Soc., Faraday Trans. 91 (1995) 1091-1095.

O. K. Varghese, D. Gong, M. Paulose, K.G. Ong, E.C. Dickey, C.A. Grimes, Extreme changes in the electrical resistance of titania nanotubes with hydrogen exposure, Adv. Mater. 15 (2003) 624-627.

Jr. W. C. Conner, G. M. Pajonk, S. J. Teichner, Spill over of sorbed species, in: D. D. Eley, H. Pines, P. B. Weisz (Ed.), Advances in Catalysis, Academic Press, NY, New York, 1986, vol. 34, 1-74.

W. Buttner, Today's commercial hydrogen sensors, DOE Hydrogen Sensor Workshop, April 4, 2007.

K. A. Reinhardt, W. Kern, Handbook of Silicon Wafer Cleaning Technology, 2nd Edition, William Andrew Publishing, Norwich, NY, 2008.

R. C. Jaeger, Introduction to Microelectronic Fabrication, 2nd Edition, Prentice Hall, Upper Saddle River, NJ, 2001.

S. A. Campbell, The Science and Engineering of Microelectronic Fabrication, 2nd Edition, Oxford University Press, New York, NY, 2001.

M. Mulder, Basic Principles of Membrane Technology, 2nd Edition, Kluwer Academic Publishers, New York, NY, 1996.

C. Giacovazzo, H. L. Monaco, G. Artioli, D. Viterbo, G. Ferraris, G. Gilli, G. Zanotti, M. Catti, Fundamentals of Crystallography, 2nd Edition, Oxford University Press, New York, NY, 2002.

I. Lundstrom, S. Shivaraman, C. Svensson, L. Lundkvist, A hydrogen-sensitive MOS field-effect transistor, Appl. Phys. Lett. 26 (1975) 55-57.

H. E. Prakasam, F. Serina, C. Huang, G. W. Auner, L. Rimai, S. Ng, R. Naik, Palladium and aluminum gate metals/aluminum nitride/silicon balanced capacitors for selective hydrogen sensing, Mater. Res. Soc. Symp. Proc. 693 (2002) 687-692.

A. Tibuzzi, B. Margesin, M. Decarli, C. D. Natale, M. Zen, A. D'Amico, G. Soncini, MOS-junction-based nanostructures by thermal oxidation of silicon wires for hydrogen detection, IEEE Trans. Nanotech. 3 (2004) 287-292.

L. Zhang, E. F. McCullen, M. H. Rahmanb, J. S. Thakur, L. Rimai, R. J. Baird, R. Naik, G. Newaz, G. W. Auner, K.Y. Ng, Response to hydrogen of a metal/AlN/Si thin film structure: Effects of composition and structure of a combination Pd-Cr gate, Sens. Actuators B 113 (2006) 843–851.

L. G. Petersson, H. M. Dannetun, J. Fogelberg, I. Lundstrom, Hydrogen adsorption states at the external and internal palladium surfaces of a palladium-silicon dioxide-silicon structure, J. Appl. Phys. 58 (1985) 404-413.

I. Lundstrom, L. G. Petersson, Chemical sensors with catalytic metal gates, J. Vac. Sci. Tech. A 14 (1996) 1539-1545.

J. H. Swisher, E. D. Johnson, Hydrides versus competing options for storing hydrogen in energy systems, J. Less-Common Metals 74 (1980) 301-320.

H. Buchner, Perspectives for metal hydride technology, Prog. Energy Combustion Sci. 6 (1980) 331-346.

M. H. Armbruster, The Solubility of Hydrogen at Low Pressure in Iron, Nickel and Certain Steels at 400 to 600°, J. Amer. Chem. Soc. 65 (1943) 1043-1054.

F. N. Simon, D. Lichtman, T. R. Kirst, Study of the binding states of the hydrogen-100 nickel system, Surf. Sci. 12 (1968) 299-307.

A. Stroka, B. Baranowski, Penetration Depth of Nickel Hydride into Nickel at Different Activities of Gaseous Hydrogen, Defect and Diffusion Forum 129-130 (1996) 305-307.

J. Fogelberg, M. Eriksson, H. M. Dannetun, L. G. Petersson, Kinetic modeling of hydrogen adsorption/absorption in thin films on hydrogen-sensitive field-effect devices: Observation of large hydrogen-induced dipoles at the Pd-SiO2 interface, J. Appl. Phys. 78 (1995) 988-996.

M. Eriksson, L. G. Ekedahl, The influence of CO on the response of hydrogen sensitive Pd-MOS devices, Sens. Actuators B 42 (1997) 217-223.

M. Lofdahl, C. Utaiwasin, A. Carlsson, I. Lundstrom, M. Eriksson, Gas response dependence on gate metal morphology of field-effect devices, Sens. Actuators B 80 (2001) 183-192.

Y. Morita, K. Nakamura, C. Kim, Langmuir analysis on hydrogen gas response of palladium-gate FET, Sens. Actuators B 33 (1996) 96-99.

T. Eklov, H. Sundgren, I. Lundstrom, Distributed chemical sensing, Sens. Actuators B 45 (1997) 71-77.

R. C. Hughes, R. Bastasz, W. P. Ellis, Hydrogen sensing in vacuum systems with catalytic field plate MNOS capacitors, Appl. Surf. Sci. 115 (1997) 74-79.

K. Dobos, M. Armgarth, G. Zimmer, I. Lundstrom, The influence of different insulators on palladium-gate metal-insulator-semiconductor hydrogen sensors, IEEE Trans. Electron Devices ED-31 (1984) 508-510.

I. Lundstrom, M. Armgarth, L. G. Petersson, Physics with catalytic metal gate chemical sensors, CRC Critical Rev. in Solid State Mater. Sci. 15 (1989) 201-278.

H. M. Dannetun, L. G. Petersson, D. Soderberg, I. Lundstrom, A hydrogen sensitive Pd-MOS structure working over a wide pressure range, Appl. Surf. Sci. 17 (1984) 259-264.

J. Fogelberg, L. G. Petersson, Kinetic modeling of the H_2-O_2 reaction on Pd and of its influence on the hydrogen response of a hydrogen sensitive Pd metal-oxide-semiconductor device, Surf. Sci. 350 (1996) 91-102.

M. Formoso, G. Maclay, The effect of hydrogen and carbon monoxide on the interface state density in MOS gas sensors with ultra-thin palladium gates, Sens. Actuators B 2 (1990) 11-12.

K. Ito, Hydrogen-induced interface traps in a palladium/very thin oxide/silicon structure, Sens. Mater. 11 (1999) 041-050.

J. Larminie, A. Dicks, Fuel Cell Systems Explained, 2nd Edition, John Wiley & Sons, Chichester, West Sussex, UK, 2003.

L. D. Birkefeld, A. M. Azad, S. A. Akbar, Carbon Monoxide and Hydrogen Detection by Anatase Modification of Titanium Dioxide, J. Am. Ceram. Soc. 75 (1992), 2964-2968.

H. Tang, K. Prasad, R. Sanjines, F. Levy, TiO_2 anatase thin films as gas sensors, Sens. Actuators B 26 (1995) 71-75.

V. Guidi, M. C. Carotta, M. Ferroni, G. Martinelli, L. Paglialonga, E. Comini, G. Sberveglieri, Preparation of nanosized titania thick and thin films as gas-sensors, Sens. Actuators B 57 (1999) 197-200.

I. Hayakawa, Y. Iwamoto, K. Kikuta, S. Hirano, Gas sensing properties of platinum dispersed-TiO_2 thin film derived from precursor, Sens. Actuators B 62 (2000) 55-60.

Y. Shimizu, N. Kuwano, T. Hyodo, M. Egashira, High H_2 sensing performance of anodically oxidized TiO_2 film contacted with Pd, Sens. Actuators B 83 (2002) 195-201.

H. Miyazakia, T. Hyodob, Y. Shimizua, M. Egashira, Hydrogen-sensing properties of anodically oxidized TiO_2 film sensors Effects of preparation and pretreatment conditions, Sens. Actuators B 108 (2005) 467-472.

O. K. Varghese, D. Gong, M. Paulose, K. G. Ong, C. A. Grimes, Hydrogen sensing using titania nanotubes, Sens. Actuators B 93 (2003) 338-344.

G. K. Mor, M. A. Carvalho, O. K. Varghese, M. V. Pishko, C. A. Grimes, A room-temperature TiO_2-nanotube hydrogen sensor able to self-clean photoactively from environmental contamination, J. Mater. Res. 19 (2004) 628-634.

M. Paulose, O. K Varghese, G. K. Mor, C. A. Grimes, K. G. Ong, Unprecedented ultra-high hydrogen gas sensitivity in undoped titania nanotubes, Nanotechnology 17 (2006) 398-402.

C. A. Grimes, Synthesis and application of highly ordered arrays of TiO_2 nanotubes, J. Mater. Chem. 17 (2007) 1451-1457.

T. Mukherjee, S. K. Hazra, S. Basu, Porous titania thin films grown by anodic oxidation for hydrogen sensors, Mater. Manuf. Processes 21 (2006) 247-251.

H. Kim, W. Moon, Y. Jun, S. Hong, High H_2 sensing performance in hydrogen trititanate-derived TiO_2, Sens. Actuators B 120 (2006) 63-68.

O. K. Varghese, D. Gong, M. Paulose, C. A. Grimes, E. C. Dickey, Crystallization and high-temperature structural stability of titanium oxide nanotube arrays, J. Mater. Res. 18 (2003) 156-165.

A. A. Gribb, J. F. Banfield, Particle size effects on transformation kinetics and phase stability in nanocrystalline TiO_2, Am. Mineral. 82 (1997) 717-728.

B. Grzmil, B. Kic, M. Rabe, Inhibition of the anatase-rutile phase transformation with addition of K_2O, P_2O_5, and Li_2O, Chem. Pap. 58 (2004) 410-414.

Y. Jun, H. Kim, J. Lee, S. Hong, High H_2 sensing behavior of TiO_2 films formed by thermal oxidation, Sens. Actuators B 107 (2005) 264-270.

F. Keller, M. S. Hunter, D. L. Robinson, Structural features of oxide coatings on aluminum, J. Electrochem. Soc. 100 (1953) 411-419.

C. J. L. Booker, J. L. Wood, A. Walsh, Electron micrographs from thick oxide layers on aluminium, Br. J. Appl. Phys. 8 (1957) 347-352.

J. P. O'Sullivan, C. G. Wood, Morphology and mechanism of formation of porous anodic films on aluminum, Proc. R. Soc. London, Ser. A, Math. Phys. Eng. Sci. 317 (1970) 511-543.

L. J. Lanzerotti, W. L. Brown, J. M. Poate, W. M. Augustyniak, Nucleation and growth of porous anodic films on aluminium, Nature 272 (1978) 433-435.

H. Masuda and K. Fukuda, Ordered metal nanohole arrays made by a two-step replication of honeycomb structures of anodic alumina, Science 268 (1995) 1466-1468.

A. P. Li, F. Muller, A. Birner, K. Nielsch, U. Gosele, Hexagonal pore arrays with a 50–420 nm interpore distance formed by self-organization in anodic alumina, J. Appl. Phys. 84 (1998) 6023-6026.

T. Iwasaki, T. Motoi, T. Den, Multiwalled carbon nanotubes growth in anodic alumina nanoholes, Appl. Phys. Lett. 75 (1999) 2044-2046.

W. Hu, D. Gong, Z. Chen, Growth of well-aligned carbon nanotube arrays on silicon substrates using porous alumina film as a nanotemplate, Appl. Phys. Lett. 79 (2001) 3083-3085.

W. Hu, L. M. Yuan, Z. Chen, D. W. Gong, K. Saito, Fabrication and characterization of vertically aligned carbon nanotubes on silicon substrates using porous alumina nanotemplates, J. Nanosci. Nanotechnol. 2 (2002) 203-207.

D. Ding, Z. Chen, C. Lu, Hydrogen sensing of nanoporous palladium films supported by anodic aluminum oxides, Sens. Actuators B 120 (2006) 182-186.

D. Ding, Z. Chen, Volume-expansion-enhanced pinning of nanoporous Pd films for detection of high-concentration hydrogen, Sensor Letters 4 (2006) 331-333.

D. Ding, Z. Chen, A Pyrolytic, Carbon-Stabilized, Nanoporous Pd film for wide-range H_2 sensing, Adv. Mater. 19 (2007) 1996-1999.

P. Chen, C. Kuo, T. Tsai, B. Wu, C. Hsu, F. Pan, Self-organized titanium oxide nanodot arrays by electrochemical anodization, Appl. Phys. Lett. 82 (2003) 2796-2798.

W. Yu, Y. Cho, G. Choi, D. Kim, Patterned carbon nanotube field emitter using the regular array of an anodic aluminium oxide template, Nanotechnology 16 (2005) S291-S295.

H. Masuda, M. Satoh, Fabrication of gold nanodot array using anodic porous alumina as an evaporation mask, Jpn. J. Appl. Phys. 35 (1996) L126-L129.

C. Lu, Z. Chen, Anodic aluminum oxide-based nanostructures and nanodevices in Encyclopedia of Nanoscience and Nanotechnology, H. S. Nalwa (Ed.), American Scientific Publishers, Stevenson Ranch, CA, US, 2009, in press, proof received.

D. A. Mawlawi, N. Coombs, M. Moskovits, Magnetic properties of Fe deposited into anodic aluminum oxide pores as a function of particle size, J. Appl. Phys. 70 (1991) 4421-4425.

W. F. McClune (Ed.), Powder Diffraction File: Inorganic Phases, Alphabetical Index, JCPDS International Center for Diffraction Data, Swarthmore, PA, US, 1987

Y. Katsuta, R. Akahane, K. Yahagi, Electrical properties of rutile (TiO_2) thin film, Jpn. J. Appl. Phys. 10 (1971) 976-986.

C. Ting, S. Chen, D. Liu, Structural evolution and optical properties of TiO_2 thin films prepared by thermal oxidation of sputtered Ti films, J. Appl. Phys. 88 (2000) 4628-4633.

E. Lenarduzzi, P. Bounie, C. Schuman, M. J. Philippe, D. Petelot, Titanium oxidation during thermal treatment: inhibiting role of nitrogen and epitaxial orientation relations evidenced by EBSD, Adv. Eng. Mater. 5 (2003) 587-593.

H. Zhang, J. F. Banfield, Thermodynamic analysis of phase stability of nanocrystalline titania, J. Mater. Chem. 8 (1998) 2073-2076

G. -J. Li, X. -H. Zhang, S. Kawi, Relationships between sensitivity, catalytic activity, and surface areas of SnO_2 gas sensors, Sens. Actuators B 60 (1999) 64-70.

T. Kida, K. Kawasaki, K. Iemura, K. Teshima, M. Nagano, Gas sensing properties of a stabilized zirconia-based sensor with a porous MoO_3 electrode prepared from a molybdenum polyoxometallate–alkylamine hybrid film, Sens. Actuators B 119 (2006) 562-569.

G. Xie, J. Yu, X. Chen, Y. Jiang, Gas sensing characteristics of WO_3 vacuum deposited thin films, Sens. Actuators B 123 (2007) 909-914.

S. V. Patel, K. D. Wise, J. L. Gland, M. Zanini-Fisherd, J. W. Schwank, Characteristics of silicon-micromachined gas sensors based on Pt/TiO_X thin films, Sens. Actuators B 42 (1997) 205-215.

P. W. Atkins, Physical Chemistry, 7th Edition, W. H. Freeman, New York, NY, US, 2002.

G. C. Mather, F. M. B. Marques, J. R. Frade, Detection Mechanism of TiO_2-based Ceramic H_2 Sensors, J. Eur. Ceram. Soc. 19 (1999) 887-891.

R. M. Walton, D. J. Dwyerc, J. W. Schwank, J. L. Glan, Gas sensing based on surface oxidation/reduction of platinum-titania thin films I. Sensing film activation and characterization, Appl. Surf. Sci. 125 (1998) 187-198.

R. Dus, F. C. Tompkins, Mechanism of the hydrogen-oxygen reaction on platinum films from surface potential measurements, Proc. B. Soc. Lond. A. 343 (1975) 477-488.

T. Seiyama, S. Kagawa, Study on a detector for gaseous components using semiconductive thin films, Anal. Chem. 38 (1966) 1069-1073.

W. Hagen, R. E. Lambrich, J. Lagois, Semiconducting gas sensors, Festkörperprobleme (Advances in Solid State Physics) 23 (1983) 259-274.

J. F. McAleer, P. T. Moseley, J. O. W. Norris, D. E. Williams, Tin dioxide gas sensors: Part 1. - Aspects of the surface chemistry revealed by electrical conductance variations, J. Chem. Soc., Faraday Trans. I 83 (1987) 1323-1346.

T. Seiyama, A. Kato, K. Fujiishi, M. Nagatani, A new detector for gaseous components using semiconductive thin films, Anal. Chem. 34 (1962) 1502-1503.

P. J. Shaver, Activated tungsten oxide gas detectors, Appl. Phys. Lett. 11 (1967) 255-257.

S. R. Morrison, Semiconductor gas sensors, Sens. Actuators 2 (1982) 329-341.

J. Watson, Tin oxide gas sensor and its applications, Sens. Actuators 5 (1984) 29-42.

J. Watson, K. Ihokura, G. S. V. Coles, The tin dioxide gas sensor, Meas. Sci. Tech. 4 (1993) 711-719.

K. Ihokura, J. Watson, The stannic oxide gas sensor: principles and applications, CRC Press, Boca Raton, FL, 1994.

C. Xu, J. Tamaki, N. Miura, N. Yamazoe, Grain size effects on gas sensitivity of porous SnO_2-based elements, Sens. Actuators B 3 (1991) 147-155.

N. Yamazoe, New approaches for improving semiconductor gas sensors, Sens. Actuators B 5 (1991) 7-19.

K. H. Song, S. J. Park, Gas sensing characteristics of tin dioxide with small crystallites, J. Mater. Sci.-Mater. El. 4 (1993) 249-253.

S. G. Ansari, P. Boroojerdian, S. R. Sainkar, R. N. Karekar, R. C. Aiyer, S. K. Kulkarni, Grain size effects on H_2 gas sensitivity of thick film resistor using SnO_2 nanoparticles, Thin Solid Films 295 (1997) 271-276.

D. G. Rickerby, M. C. Horrillo, J. P. Santos, P. Serrini, Microstructural characterization of nanograin tin oxide gas sensors, Nanostruct. Mater. 9 (1997) 43-52.

S. Shukla, S. Patil, S. C. Kuiry, Z. Rahman, T. Du, L. Ludwig, C. Parish, S. Seal, Synthesis and characterization of sol-gel derived nanocrystalline tin oxide thin film as hydrogen sensor, Sens. Actuators B 96 (2003) 343-353.

N. Yamazoe, K. Shimanoe, New perspectives of gas sensor technology, Sens. Actuators B 138 (2009) 100-107.

Q. Kuang, C. S. Lao, Z. Li, Y. Z. Liu, Z. X. Xie, L. S. Zheng, Z. L. Wang, Enhancing the photon- and gas-sensing properties of a single SnO_2 nanowire based nanodevice by nanoparticle surface functionalization, J. Phys. Chem. C 112 (2008) 11539-11544.

Y. J. Choi, I. S. Hwang, J. G. Park, K. J. Choi, J. H. Park, J. H. Lee, Novel fabrication of an SnO_2 nanowire gas sensor with high sensitivity, Nanotechnology 19 (2008) 095508/1-095508/4.

Y. Shen, T. Yamazaki, Z. Liu, D. Meng, T. Kikuta, N. Nakatani, M. Saito, M. Mori, Microstructure and H_2 gas sensing properties of undoped and Pd-doped SnO_2 nanowires, Sens. Actuators B 135 (2009) 524-529.

L. H. Qian, K. Wang, Y. Li, H. T. Fang, Q. H. Lu, X. L. Ma, CO sensor based on Au-decorated SnO_2 nanobelt, Mater. Chem. Phys. 100 (2006) 82-84.

X. Han, B. Zhang, S. Guan, J. Liu, X. Zhang, R. Chen, Gas-sensing properties of SnO_2 nanobelts synthesized by thermal evaporation of Sn foil, J. Alloy Compd. 461 (2008) L26-L28.

H. Huang, Y. C. Lee, O. K. Tan, W. Zhou, N. Peng, Q. Zhang, High sensitivity SnO_2 single-nanorod sensors for the detection of H_2 gas at low temperature, Nanotechnology 20 (2009) 115501/1-115501/5.

T. Hyodo, N. Nishida, Y. Shimizu, M. Egashira, Preparation and gas-sensing properties of thermally stable mesoporous SnO_2, Sens. Actuators B 83 (2002) 209-215.

T. Hamaguchi, N. Yabuki, M. Uno, S. Yamanaka, M. Egashira, Y. Shimizu, T. Hyodo, Synthesis and H_2 gas sensing properties of tin oxide nanohole arrays with various electrodes, Sens. Actuators B 113 (2006) 852-856.

N. S. Baik, G.. Sakai, N. Miura, N. Yamazoe, Hydrothermally treated sol solution of tin oxide for thin-film gas sensor, Sens. Actuators B 63 (2000) 74-79.

A. Z. Adamyan, Z. N. Adamyan, V. M. Aroutiounian, A. H. Arakelyan, K. J. Touryan, J. A. Turner, Sol-gel derived thin-film semiconductor hydrogen gas sensor, Int. J. of Hydrogen Energy 32 (2007) 4101-4108.

S. Shukla, P. Zhang, H. J. Cho, L. Ludwig, S. Seal, Significance of electrode-spacing in hydrogen detection for tin oxide-based MEMS sensor, Int. J. of Hydrogen Energy 33 (2008) 470-475.

K. Hieda, T. Hyodo, Y. Shimizu, M. Egashira, Preparation of porous tin dioxide powder by ultrasonic spray pyrolysis and their application to sensor materials, Sens. Actuators B 133 (2008) 144-150.

C. Agashe, R. C. Aiyer, High-yield synthesis of nanocrystalline tin dioxide by thermal decomposition for use in gas sensors, Int. J. Appl. Ceram. Tech., 5 (2008) 181-187.

A. Kock,, A. Tischnera, T. Maier, M. Kast, C. Edtmaier, C. Gspan, G. Kothleitner, Atmospheric pressure fabrication of SnO_2-nanowires for highly sensitive CO and CH_4 detection, Sens. Actuators B 138 (2009) 160-167.

B. K. Min, S. D. Choi, SnO_2 thin film gas sensor fabricated by ion beam deposition, Sens. Actuators B 98 (2004) 239-246.

B. Panchapakesan, D. L. DeVoe, M. R Widmaier, R. Cavicchi, S. Semancik, Nanoparticle engineering and control of tin oxide microstructures for chemical microsensor applications, Nanotechnology 12 (2001) 336-349.

G. Sberveglieri, G. Faglia, S. Groppelli, P. Nelli, A. Camanz, A new technique for growing large surface area SnO_2 thin film (RGTO technique), Semicond. Sci. Tech. 5 (1990) 1231-1233.

G. Sberveglieri, Recent developments in semiconducting thin-film gas sensors, Sens. Actuators B 23 (1995) 103-109.

T. Aste, R. Botter, D. Beruto, Double-layer granular SnO_2 sensors, Sens. Actuators B 25 (1995) 826-829.

L. Sangaletti, L.E. Depero, A. Dieguez, G. Marca, J.R. Morante, A. Romano-Rodriguez, G. Sberveglieri, Microstructure and morphology of tin dioxide multilayer thin film gas sensors, Sens. Actuators B 44 (1997) 268-274.

P. Nelli, G. Faglia, G. Sberveglieri, E. Cereda, G. Gabetta, A. Dieguez, A. Romano-Rodriguez, J. R. Morante, The aging effect on SnO_2 Au thin film sensors: electrical and structural characterization, Thin Solid Films 371 (2000) 249-253.

E. Comini, G. Faglia, G. Sberveglieri, CO and NO_2 response of tin oxide silicon doped thin films, Sens. Actuators B 76 (2001) 270-274.

M. Radecka, J. Przewoznik, K. Zakrzewska, Microstructure and gas-sensing properties of (Sn, Ti)O_2 thin films deposited by RGTO technique, Thin Solid Films 391 (2001) 247-254.

J. Szuber, J. Uljanow, T. Karczewska-Buczek, W. Jakubik, K. Waczynski, M. Kwoka, S. Konczak, On the correlation between morphology and gas sensing properties of RGTO SnO_2 thin films, Thin Solid Films 490 (2005) 54-58.

Elisabetta Comini, Luca Ottini, Guido Faglia, Giorgio Sberveglieri, SnO_2 RGTO UV activation for CO monitoring, IEEE Sens. J. 4 (2004) 17-20.

J. G. Partridge, M. R. Field, J. L. Peng, A. Z. Sadek, K. Kalantar-Zadeh, J Du Plessis, D. G. McCulloch, Nanostructured SnO2 films prepared from evaporated Sn and their application as gas sensors, Nanotechnology 19 (2008) 125504/1-125504/5.

F. A. Lewis, The Palladium Hydrogen System, Academic Press, New York, NY, 1967.

I. Lundström, T. DiStefano, Influence of hydrogen on Pt-SiO_2-Si structures, Solid State Commun. 19 (1976) 871-875.

J. C. Loh, "Gas detector", U.S. Patent 4045729, Aug. 30, 1977.

M. Armgarth, D. Söderberg, I. Lundström, Palladium and platinum gate metal-oxide-semiconductor capacitors in hydrogen and oxygen mixtures, Appl. Phys. Lett. 41 (1982) 654-655.

M. C. Steele, B. A. Maciver, Palladium/cadmium-sulfide Schottky diodes for hydrogen detection, Appl. Phys. Lett. 28 (1976) 687-688.

K. Ito, Hydrogen-sensitive Schottky barrier diodes, Surf. Sci. 86 (1979) 345-352.

N. Yamamoto, S. Tonomura, T. Matsuoka, H. Tsubomura, A study on a palladium-titanium oxide Schottky diode as a detector for gaseous components, Surf. Sci. 92 (1980) 400-406.

U. Kirner, K.D. Schierbaum, W. Göpel, B. Leibold, N. Nicoloso, W. Weppner, D. Fischer, W. F. Chu, Low and high temperature TiO_2 oxygen sensors, Sens. Actuators B 1 (1990) 103-107.

K. D. Schierbaum, U. K. Kirner, J. F. Geiger, W. Göpel, Schottky-barrier and conductivity gas sensors based upon Pd/SnO_2 and Pt/TiO_2, Sens. Actuators B 4 (1991) 87-94.

K. D. Schierbaum, Engineering of oxide surfaces and metal/oxide interfaces for chemical sensors: recent trends, Sens. Actuators B 24 (1995) 239-247.

M. Egashira, Y. Shimizu, Y. Takao, S. Sako, Variations in I-V characteristics of oxide semiconductors induced by oxidizing gases, Sens. Actuators B 35-36 (1996) 62-67.

T. Hyodo, Y. Baba, K. Wada, Y. Shimizu, M. Egashira, Hydrogen sensing properties of SnO2 varistors loaded with SiO_2 by surface chemical modification with diethoxydimethylsilane, Sens. Actuators B 64 (2000) 175-181.

W. Hellmich, Ch. Bosch-v. Braunmuhl, G. Muller, G. Sberveglieri, M. Bertih, C. Perego, The kinetics of formation of gas-sensitive RGTO-SnO_2 films, Thin Solid Films 263 (1995) 231-237.

L. Sangaletti, L. E. Depero, B. Allieri, F. Pioselli, E. Comini, G. Sberveglieri, M. Zocchi, Oxidation of Sn thin films to SnO_2. Micro-Raman mapping and x-ray diffraction studies, J. Mater. Res. 13 (1998) 2457-2460.

E. Søndergård, R. Kofman, P. Cheyssac, A. Stella, Production of nanostructures by self-organization of liquid Volumer-Weber films, Surf. Sci. 364 (1996) 467-476.

M. Zinke-Allmang, L. C. Feldman, M. H. Grabow, Clustering on surfaces, Surf. Sci. Rep. 16 (1992) 377-463.

S. Ulrich, S. Stoll, E. Pefferkorn, Computer simulations of homogeneous deposition of liquid droplets, Langmuir 20 (2004) 1763-1771.

J. L. Freeouf, T. N. Jackson, S. E. Laux, J. M. Woodall, Effective barrier heights of mixed phase contacts: size effects, Appl. Phys. Lett. 40 (1982) 634-636.

J. L. Freeouf, T. N. Jackson, S. E. Laux, J. M. Woodall, Size dependence of "effective" barrier heights of mixed-phase contacts, J. Vac. Sei. Technol. 21 (1982) 570-573.

M. A. Butler, D. S. Ginley, Prediction of flatband potentials at semiconductor-electrolyte interfaces from atomic electronegativities, J. Electrochem. Soc. 125 (1978) 228-232.

C. Kober, S. P. Harvey, T. O. Mason, A. Klein, Barrier heights at the SnO_2/Pt interface: in situ photoemission and electrical properties, Surf. Sci. 602 (2008) 3246-3252.

H. J. Im, Y. Ding, J. P. Pelz, W. J. Choyke, Nanometer-scale test of the Tung model of Schottky-barrier height inhomogeneity, Phys. Rev. B 64 (2001) 075310/1-075310/9.

R. T. Tung, Electron transport at metal-semiconductor interfaces: general theory, Phys. Rev. B 45 (1992) 13509-13523.

Jr. W. H. King, The monitoring of hydrogen, methane, and hydrocarbons in the atmosphere, Environ. Sci. Technol. 4 (1970) 1136-1141.

C. Lu, Z. Chen, High-temperature resistive hydrogen sensor based on thin nanoporous rutile TiO_2 film on anodic aluminum oxide, Sens. Actuators B 140 (2009) 109-115.

A. L. Spetz, P. Tobias, L. Unéus, H. Svenningstorp, L. G. Ekedahl, I. Lundström, High temperature catalytic metal field effect transistors for industrial applications, Sens. Actuators B 70 (2000) 67-76.

N. Taniguchi, T. Kuroha, C. Nishimura, K. Iijima, Characteristics of novel $BaZr_{0.4}Ce_{0.4}In_{0.2}O_3$ proton conducting ceramics and their application to hydrogen sensors, Solid State Ionics 176 (2005) 2979-2983.

T. Weh, J. Frank, M. Fleischer, H. Meixner, On the mechanism of hydrogen sensing with SiO_2 modificated high temperature Ga_2O_3 sensors, Sens. Actuators B 78 (2001) 202-207.

Vita

Author's Name: Chi Lu

Birthplace: Beijing, China

Date of Birth: July 1, 1974

Education:

Master of Science in Materials Science

Thesis: Electrochemical Phosphate Conversion Coating of Rusted Carbon Steel Surface

Beijing University of Chemical Technology

June 1999

Bachelor of Science in Analytical Chemistry/Environmental Engineering

Senior Design: Quantitative Determination of Zinc in Vegetables through Oxygen Flask Combustion Followed by Ultraviolet-Visible Spectrophotometry

Hebei University of Science and Technology

July 1996

Peer Reviewed Journal Papers:

Chi Lu and Zhi Chen, High-temperature resistive hydrogen sensor based on thin nanoporous rutile TiO_2 film on anodic aluminum oxide, Sensors and Actuators B: Chemical, vol. 140, 109-115, 2009.

Ping Yu, Sidong Xiong, Qiuzao He, Yiwei Chu, **Chi Lu**, and Jason Charles Steel, Induction of allogeneic mixed chimerism by immature dendritic cells and bone marrow transplantation leads to prolonged tolerance to MHC disparate allografts, Immunology, vol. 127, 500-511, 2009.

Chi Lu, Zhi Chen, and Kozo Saito, Hydrogen sensors based on $Ni/SiO_2/Si$ MOS capacitors, Sensors and Actuators B: Chemical, vol. 122, 556-559, 2007.

Dongyan Ding, Zhi Chen, and **Chi Lu**, Hydrogen sensing of nanoporous palladium films supported by anodic aluminum oxides, Sensors and Actuators B: Chemical, vol. 120, 182-186, 2006.

Zhi Chen and **Chi Lu**, Humidity sensors: a review of materials and mechanisms, Sensor Letters, vol. 3, 274-295, 2005.

Book Chapters:

Chi Lu and Zhi Chen, "Anodic aluminum oxide-based nanostructures and nanodevices" in Encyclopedia of Nanoscience and Nanotechnology, edited by H. S. Nalwa, American Scientific Publishers, Stevenson Ranch, CA, 2009, in press, proof received.

Conference Presentations/Posters/Abstracts:

Chi Lu, Young-Sik Song, and Zhi Chen, Investigation of hydrogen sensing properties of rutile-phased titanium oxide nanotube thick layer, 14th Annual Kentucky EPSCoR Conference Louisville, KY, Oct. 2008.

Chi Lu and Zhi Chen, A novel hydrogen sensor based on an MOS capacitor with nickel gate, 13th Annual Kentucky EPSCoR Conference, Lexington, KY, Oct. 2007.